Spring 2012

Enabling frequency and voltage regulation in microgrids using wind power plants

Anshuman Shrikant Vaidya

Department:

ENABLING FREQUENCY AND VOLTAGE REGULATION IN MICROGRIDS USING WIND POWER PLANTS

by

ANSHUMAN SHRIKANT VAIDYA

A THESIS

Presented to the Faculty of the Graduate School of the

MISSOURI UNIVERSITY OF SCIENCE AND TECHNOLOGY

In Partial Fulfillment of the Requirements for the Degree

MASTER OF SCIENCE IN ELECTRICAL ENGINEERING

2012

Approved by

Badrul H. Chowdhury, Advisor
Mehdi Ferdowsi,
Mariesa L. Crow

ABSTRACT

Renewable energy sources, like wind can be used to augment the grid-friendly services in the form of additional active and reactive power for control of frequency and voltage regulation. Currently, wind power systems are operated in simple energy supply mode and are not utilized to participate in ancillary power services. With the increase in the installed wind power capacity, limited conventional generation and increasing interest in microgrids, the necessity to implement regulation support from wind energy becomes critical.

This thesis focuses on the effect of enabling frequency and voltage regulation capability in wind power plants in a microgrid environment. This thesis investigates the active and reactive power capability of a wind power plant and a model of the wind turbine with the ability to control the output power is developed in Simulink. A microgrid control model is also developed for distributing the load variations in the system between the conventional and wind power generators according to their rated capacity. The aim of this control strategy is to maintain the system frequency and voltages at critical buses within safe operating limits when the microgrid is operating in islanded mode. The aim of this strategy is also to command the required active and reactive power from wind power plants when operating in parallel with the grid. A comparison of system voltage and frequency is done to show the effectiveness of allowing the participation of wind power plants in regulation mode when compared with the present operating mode where wind power plants must operate at maximum active power. Lastly, a study on determining a suitable generation mix for the microgrid is carried out with the load and wind variation data from two different locations in Texas and California. This study helps to determine the amount of wind power that can be delivered into the system under the new regulating mode without compromising on the reliability and integrity of the system.

ACKNOWLEDGMENTS

I sincerely extend my thanks to my advisor Dr. Badrul Chowdhury for his support and invaluable guidance. This thesis would not have been possible without his patience and firm belief in me. I am also grateful to the Intelligent System Center (ISC) for providing me with a research assistantship during the course of my graduate studies.

I would also like to thank Dr. Mehdi Ferdowsi and Dr. Mariesa Crow for serving on my graduate committee. I am grateful to all my friends and research associates who have made my stay in Rolla a pleasant one.

Finally, I would like to dedicate this thesis to my loving parents Mr Shrikant Anant Vaidya and Mrs Sujata Vaidya; my late grandmother Meera Vaidya, and my sisters Devayani and Swati, who have always been a great source of inspiration and encouragement for my higher education.

TABLE OF CONTENTS

LIST OF ILLUSTRATIONS

Page

LIST OF TABLES

NOMENCLATURE

Symbol	Description
T_{wind}	Torque produced by wind turbine.
ρ	Air Density.
A	Area swept by the wind Turbine.
v	Velocity of the wind.
ω_r	DFIG rotor speed.
ω_s	Synchronous speed.
λ	Tip Speed Ratio.
β	Pitch Angle.
$c(\lambda,\beta)$	Power coefficient for wind turbine.
I_s , I_r	Stator and Rotor current.
R_s , R_r	Stator and Rotor resistance.
V_s , V_r	Stator and Rotor Voltage.
ω	Stator frequency.
Ψ_s	Stator Flux.
Ψ_d , Ψ_q	Flux along the d-q axis.
L_s , L_r	Stator and Rotor inductance.
L_m	Mutual inductance.
V_d	Voltage across the d-axis.
V_q	Voltage across the q-axis.
P_s	Stator active power output.
Q_s	Stator reactive power output.
Z_s , Z_r	Stator and Rotor total impedance.
Z_m	Mutual Impedance.
S_{s_Ir}	Apparent power for rotor current limitation.
S_{s_Vr}	Apparent power for rotor voltage limitation.
S_{s_Is}	Apparent power for stator current limitation.
DFIG	Doubly Fed Induction Generator.
WPP	Wind Power Plant.

SG	Synchronous Generator.
AVR	Automatic Voltage Regulator.
c_{s_Ir}, c_{s_Vr}, c_{s_Is}	Center for three different limitations on DFIG.
r_{s_Ir}, r_{s_Vr}, r_{s_Is}	Radius for three different limitations on DFIG.\
WC	With Control.
NC	No Control.

1. INTRODUCTION

1.1. INTRODUCTION

Wind power generation is considered to be the most rapidly growing renewable energy technology in the world. Installation of wind power in the USA is increasing exponentially; by the year 2009 wind power installation had reached a total capacity of 30 GW, as seen in Figure 1.1.

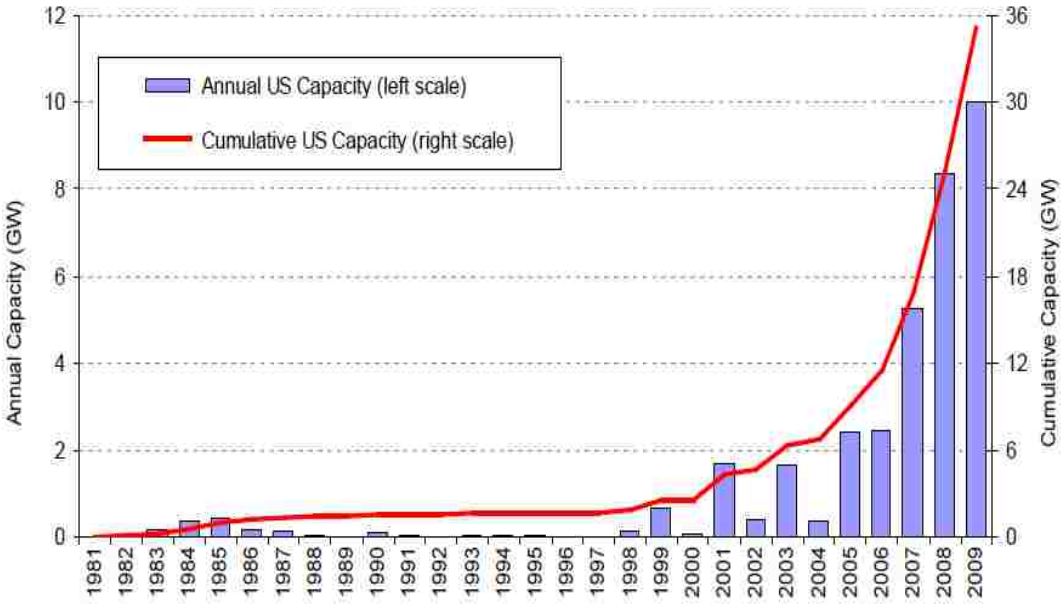

Figure 1.1. Annual and cumulative growth in US wind power capacity [1].

A collaborative effort by the Department of Energy and industry leaders led to a modeled scenario of 20% wind power penetration in the energy market by 2030 to reduce the dependence on conventional energy sources and get some relief on fluctuating energy prices and supply uncertainties. It is estimated that US energy requirements will grow by 39% from 2005 to 2030 reaching a figure of 5.8 billion MWh by 2030. To reach the vision of 20% wind penetration, the wind installation would need to reach at least 300 GW in capacity by 2030. Installation rates of wind capacity in 2007 and 2008 exceed the

conservative growth trajectory (Figure 1.2) by 30%. Presently, the wind industry is on track of growing to a size capable of installing 16 GW/year which exceeds the expectation [1].

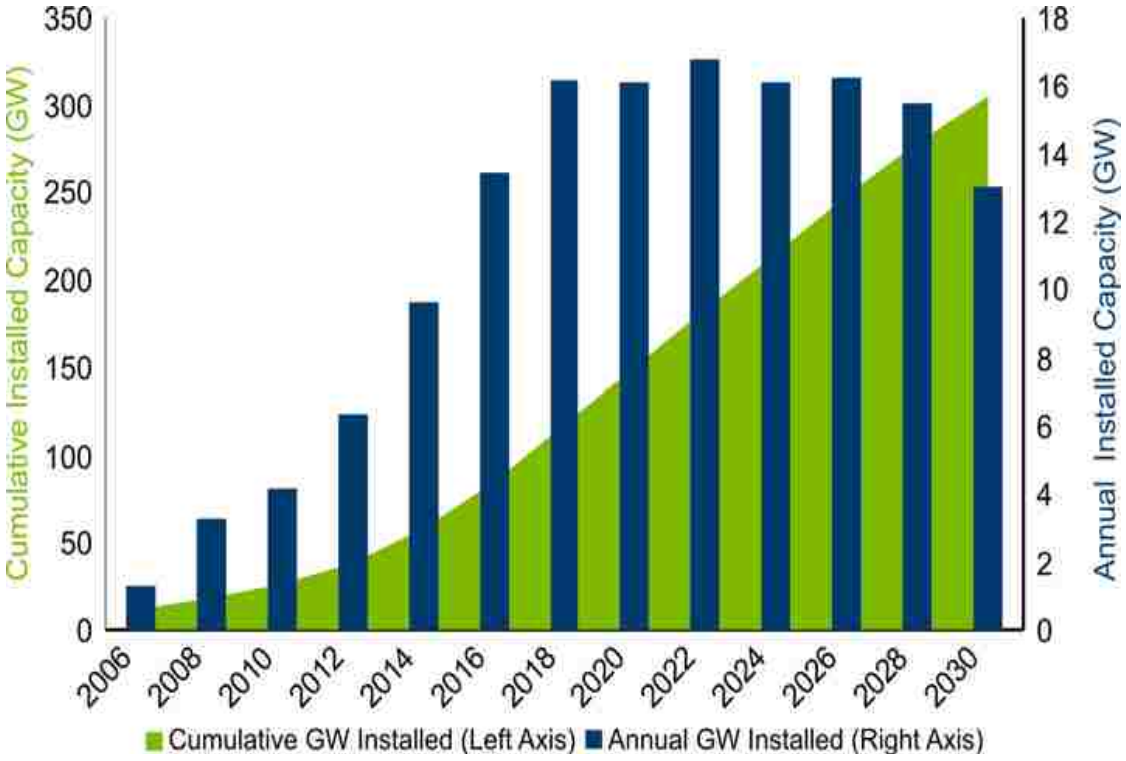

Figure 1.2. :Wind power projections [1].

With such high penetration levels, it would be extremely difficult to maintain grid frequency requirements without wind power participation in regulation.

1.2. OBJECTIVE

Variability and unpredictability in wind power generation has generally kept wind power plants from participating in voltage and frequency regulation. In the typical operating mode, wind power plants are made to operate at the maximum possible generation for a given wind speed. Figure 1.3 shows the general characteristics curve of wind turbine output power with varying rotor speed. This figure shows the variation in

the output power of the wind turbine with wind speeds. It is also apparent that if required, the output of the wind turbine can be changed by varying the rotor speed at a given wind speed.

In a small scale autonomous system such as a microgrid, the scenario of comparable wind power capacity with respect to conventional generation in a generation mix may become feasible within a few decades. The present mode of barring the wind power plant from participating in the voltage and frequency regulation could lead to greater frequency excursions or even blackouts.

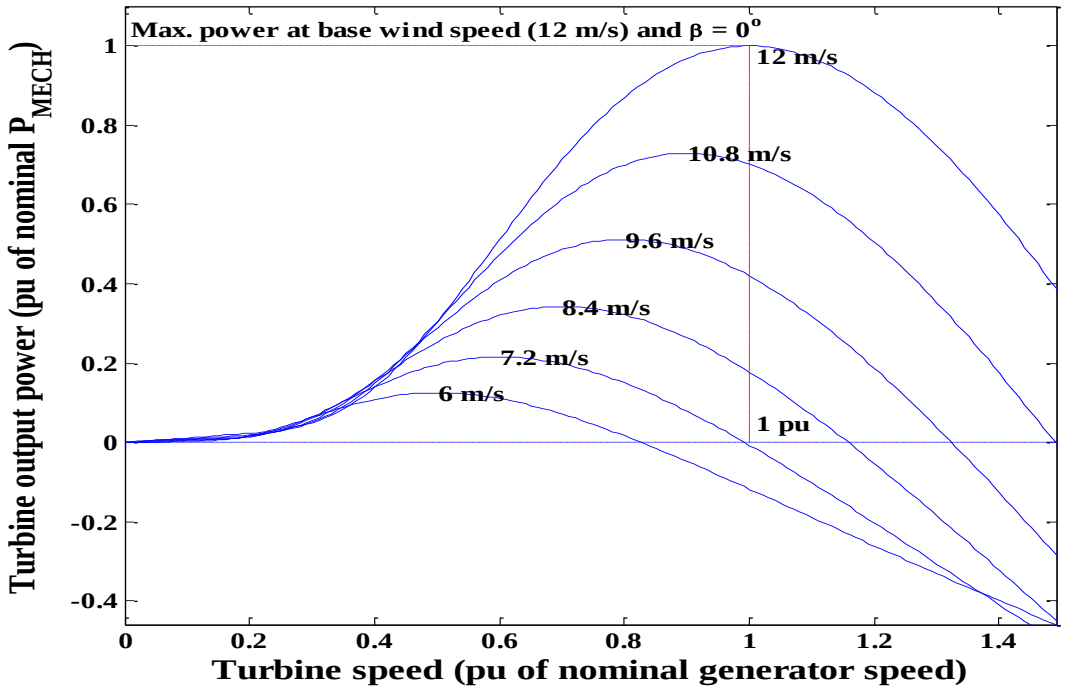

Figure 1.3. Wind turbine power characteristics for 0*· pitch angle.

The most commonly used type of wind generator is a variable speed generator consisting of doubly fed induction generator (DFIG) with both a stator-side and a rotor side power electronic converter [2]. In this topology, the converter has around 30% rating of the whole generator. The power electronic converter has different functions; the generator side converter controls the real and reactive power output from the wind

generator and the grid side converter maintains the DC link voltage at the set point which supports the generator side converter. To control the wind power output, the feedback command from the generator side converter can be manipulated to get the desired output by varying the DFIG rotor speed. Another approach to control the active power output is to control the pitch angle of the wind turbine. The pitch angle is the angle between the turbine blade and the wind direction. Maximum power is extracted from the wind turbine when the pitch angle is close to zero. This control is only employed in the case of high wind speeds to protect the wind turbine from getting damaged.

In this thesis, the output of the rotor/generator side converter is manipulated to control the output power of the wind power plant. This model is used in a microgrid system with a generation mix consisting of conventional generators and wind power plants in different configurations of the generation capacity. This system allows wind generation to participate in voltage and frequency regulation. The system is used to study the impact of voltage and frequency regulation participation by the wind power plant.

A novel hysteresis droop controller would be utilized in this thesis for the wind power plants to control the commanded power signal according to the system requirements. This control is required to offset the limitations of droop control when applied to wind power plants.

1.3. LITERATURE REVIEW

The existing literature on wind power integration, DFIG and microgrid are studied in this section along with the literature focusing on integration of wind power in microgrid environment.

An NREL report by Parsons [3] and [4] did a comprehensive analysis of grid ancillary service impact of integrating wind power plants into the US power grid. This study shows that that large penetration of wind power will affect the cost and operation of the grid but the impact will be low for the penetration levels expected in the next several years.

A similar study was performed by DeMeo [5] to analyze issues presented to power system planners and operators with respect to wind power integration. Planning and integration data from different utilities was used to draw some conclusions. The

study concluded that the integration of wind helped in reducing overall energy prices, and that wind forecasting has helped influence the unit commitment decision taken for the day ahead markets. It was also seen the cost arising due to variability depends on the generation mix, fuel cost and the size of the balancing authority.

Driven by the increasing wind energy penetration in the grid, a wide interest in analyzing the capability of wind power plants to support the grid with ancillary services is generated. Fernandez [6] and Shuhui [7] analyzed the capability of PMSG to produce active and reactive power. The mathematical model for the capability of PMSG was developed and the active participation of PMSG wind power plant in grid operations was tested by simulation.

A comprehensive study on the capability of DFIG type variable speed wind turbine was done by Lund [8]. He developed the mathematical model for the DFIG and analyzed the capacity to produce active and reactive power. Also the limitations of the DFIG machine with respect to their variation with slip were discussed in detail. These limitations are also discussed in [9] and [10]. The authors of [9] and [10] also discussed the increase in installation and operational cost due to the added ancillary services and an optimization solution to minimize the real time costs incurred. GE claims that their wind energy management system [11] can provide ancillary services and improve grid stability. It uses pitch control to vary the active power output by around 10%.

Singh [12] discusses the limitations of DFIG based wind turbine model and suggests an improvement in the DFIG topology. This new topology - unified DFIG displayed a considerable improvement in PQ capability of the wind turbine in the low active power production region and improved the range of operating speeds. Cheng [13] also developed a new topology for wind turbines which can achieve superior aerodynamic efficiency over a wide range of wind speeds with better control, fault tolerance and improved reliability. This topology uses a full scale converter and requires self excitation for starting.

The work by Brauner [14] investigates the behavior of wind parks for network faults. It concludes that faults in transmission networks are more severe than short circuit faults at a wind generator terminal with regard to voltage drop and recovery.

Steady improvement in technology is acting as a catalyst for adding increased amounts of renewable energy sources in the grid [15, 16]. The renewable sources are widely spread and are generally small scale power generation units. These distributed energy sources have sparked an increased interest in support of the microgrid concept. With advancements in power electronics and control technologies, effective integration of distributed generation and energy storage technologies into the energy infrastructure may finally become possible and economically feasible[17-20]. Several tests beds are reported for microgrids around the world [21].

Microgrids enjoy some benefits like higher reliability, better quality power supply, and increased efficiency of energy use by utilizing the available waste heat from power generation systems. Also, the ability to use renewable energy with little or no pollution is becoming increasingly attractive for environmental protection. In addition, microgrids can benefit the electric utility industry by reducing congestion on the grid, reducing the need for new generation and transmission capacity, and offering ancillary services such as voltage support and demand response[22]. The microgrid concept also has some disadvantages which can create problems for grid operations as described in [23]. Some of the issues listed in the literature are analysis of voltage profile, stability, harmonics, power quality and imbalances.

A need for some degree of central control or coordination is required between the micro generation elements in order to operate as a system. State variables of the microgrid like phase voltages and currents at the point of common coupling should be regulated. When the microgrid is connected to the grid, the state variables are maintained by the inertia of the large network, but the ability to have an adequate control response during islanding is a challenge. Lasseter [24] lists the various efforts done around the world to evaluate the microgrid concept. Most of these efforts have opted to control the microgrid with a large utility or a storage system. The Kythnos microgrid project in Europe [23], although still dependent on an energy storage system, is operated as an autonomous standalone system and can be identified as a big step towards microgrid success.

To maintain frequency and voltage requirements, a microgrid can employ either the active load sharing techniques or the droop control method [25]. Active load sharing

techniques rely on communication links and employ mostly a centralized approach to control the generating units in the microgrid. This method is computationally expensive for large interconnected units. Droop control is another method discussed in the literature which facilitates microgrid control by allowing the individual generating units to adjust their power output according to the changes in the frequency and terminal voltage[26-29].

The addition of wind power to the microgrid equation raises serious technical challenges due to intermittency and variability of wind speeds. These challenges can be solved by using FATCS devices and energy storage systems [30-32]. Although wind power plants are capable of supporting the grid for regulation on its own [5-12], these qualities of wind power plants are not exploited for microgrid regulation. It is shown in [33] that inclusion of a variable-speed wind turbine with DFIG in a microgrid participating in the frequency and voltage controls may improve the microgrid system's dynamic performance, reducing the frequency changes following disturbances subsequent to islanding.

The literature review clearly shows the importance of microgrids and the role of wind power plants. It provides enough motivation to find solutions for integration of wind power plants in a microgrid and participation in regulation responsibility.

1.4. THESIS OUTLINE

This thesis comprises of different sections as described in details below. The current section discusses the trend of wind installation growth in the USA and the need for extending the voltage and frequency regulation responsibilities to new installations of renewable energy sources like wind energy. A literature survey is also done in order to highlight the recent progress in wind technology and microgrids evolution. An introduction to wind power generation methodology and the capability of the DFIG wind power plant is discussed in Section 2.

In Section 3, a brief introduction to microgrid is discussed. Also, the different components of the microgrid test system are modeled and simulated in SIMULINK.

Section 4 discusses the control methodology used for making the microgrid autonomous by maintaining its own frequency and voltage requirements in the islanded mode.

Microgrid test system is introduced and a microgrid study for identifying the impact of allowing wind power plants to participate in voltage and frequency regulation is carried out for different generation mix configurations in Section 5. This section will also discuss the simulation results and the various insights gathered from the study. Section 6 contains the conclusions inferred from the simulation study.

2. WIND POWER GENERATION IN POWER SYSTEM

2.1. INTRODUCTION

Wind generation is classified into two major wind power generating units i.e. fixed speed generation and variable speed generation (VSG) [34]. The fixed speed generators operate at a fixed rotor speed to obtain maximum efficiency. Deviation from the pre determined speed causes reduction in efficiency. VSG inherits a wide range of operating speeds for the rotor to match up with prevailing wind for better efficiency. VSG has maximum power tracking capability that extracts maximum available power out of the wind at different wind speeds thereby resulting in more efficient operation. Also VSG reduces mechanical stresses on the turbine thus increasing the lifetime of the turbine. Thus VSG's are more commonly installed.

In both forms of wind power generation the power extraction principle remains the same. The amount of power generated by the turbine can be associated with the torque generated by the wind. The relationship between the torque and the wind can be formulated as below [8].

$$P = \frac{1}{2} * \rho * A * v^3 * c(\lambda, \beta) \tag{2.1}$$

Where,

$$c(\lambda, \beta) = c_1 \left(\frac{c_2}{\lambda_i} - c_3 \beta - c_4 \right) e^{\frac{-c_5}{\lambda_i}} + c_5 \lambda \tag{2.2}$$

$$\frac{1}{\lambda_i} = \frac{1}{\lambda + 0.08\beta} - \frac{0.035}{\beta^3 + 1} \tag{2.3}$$

$c(\lambda, \beta)$ is the power coefficient for the wind turbine given by the manufacturer and λ is the tip speed ratio or TSR which is the ratio between the linear speed of the tip of the

blade with respect to the wind speed. The coefficients c_1, c_2, c_3, c_4 and c_5 are provided by the manufacturer.

The different variations of extracted wind power level with varying pitch angle and rotor speed can be seen calculated with Equations 2.1 - 2.3 as shown in Figure 2.1.

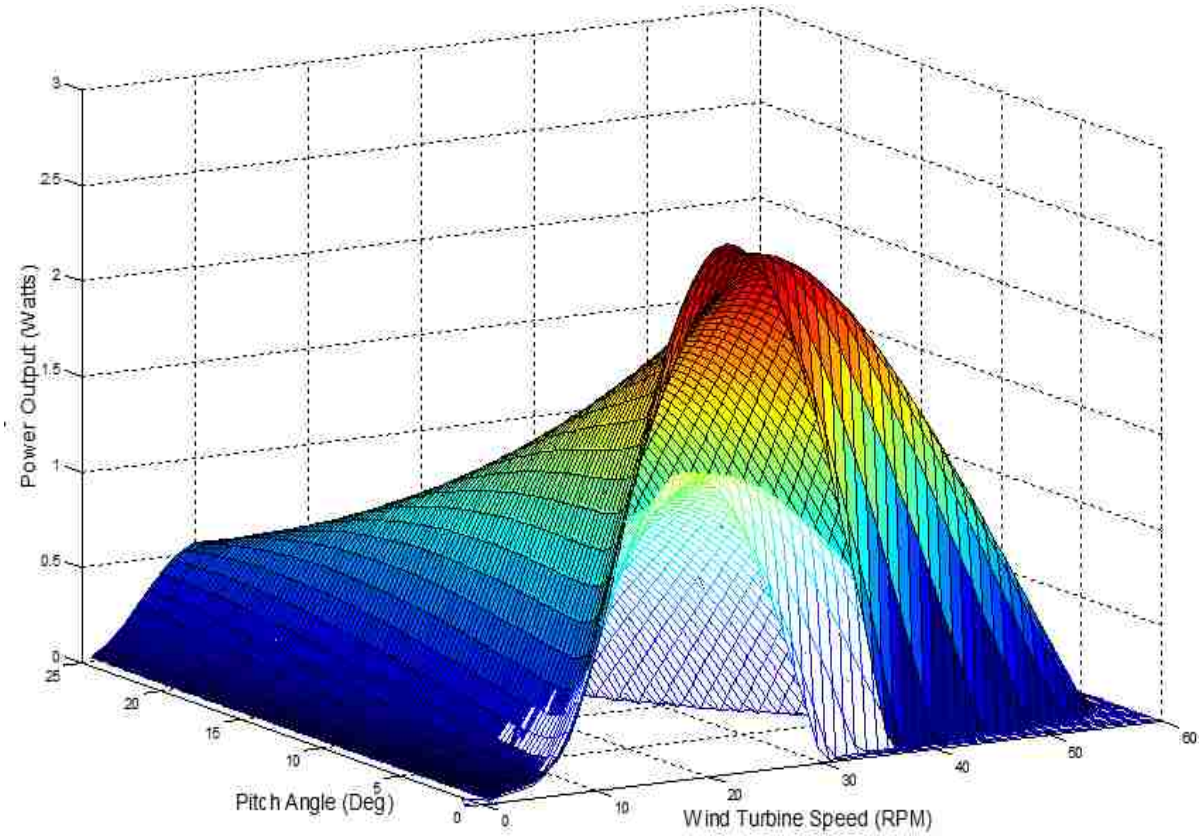

Figure 2.1. Variation of power with respect to the pitch angle and wind turbine speed (wind speeds 10 m/s and 12 m/s).

2.2. DFIG WIND POWER

The doubly fed induction generator consists of a wind turbine connected to the rotor shaft of the induction generator through a gear train. The topology used in this scenario uses a converter capable of supplying and receiving power from the rotor to the grid.

This converter consists of two separate devices with different functions connected to each other via a DC interconnection link i.e. a dc link capacitor. These two devices are separate converters, one connected to the grid and the other connected to the rotor. The converter connected to the generator controls the real and reactive power output of the wind turbine and the grid connected converter maintains the dc link capacitor voltage at the set point. A wind turbine connected to a double fed induction generator equipped with a grid side and a generator side converter is shown in Figure 2.2.

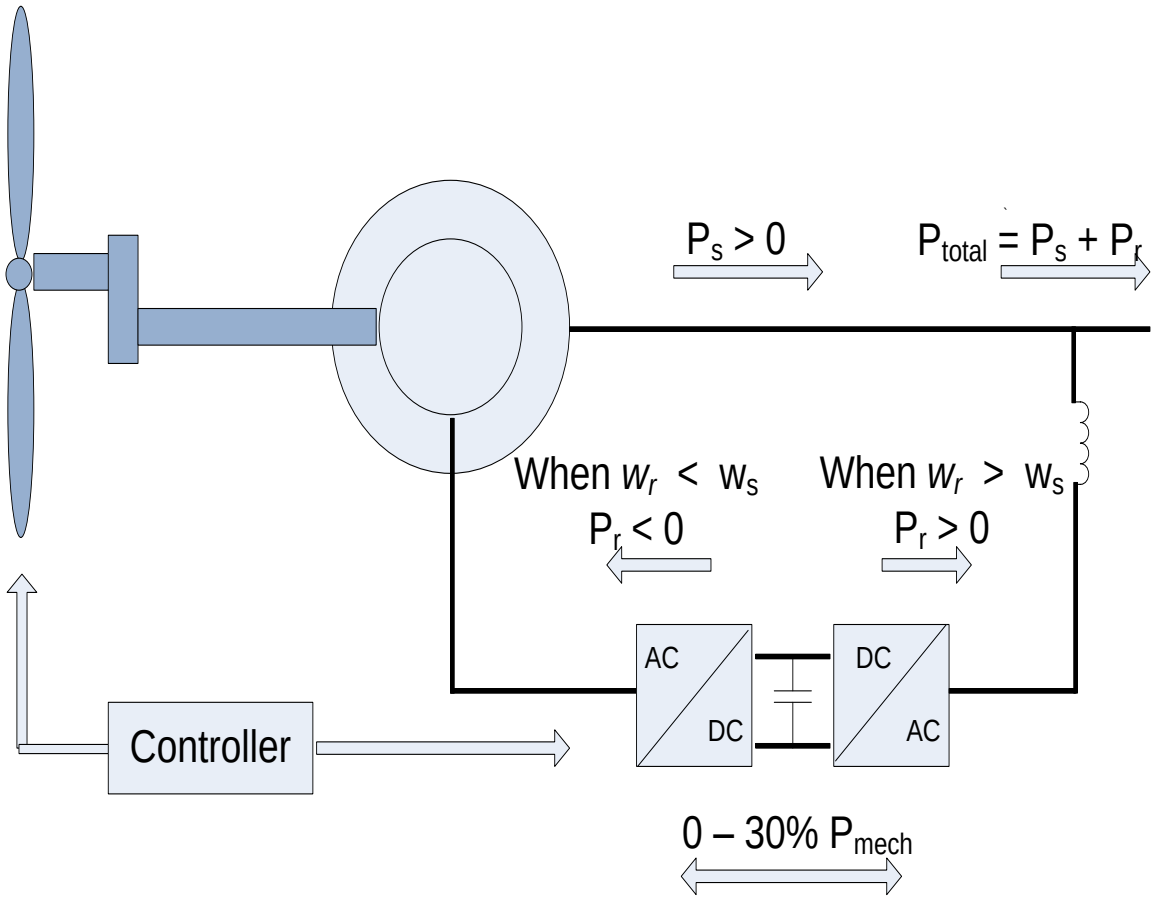

Figure 2.2 Double fed induction generator schematic.

The rotor windings of the three phase induction generator are connected to the generator side converter via slip rings. The power electronic converter is capable of handling the power flow in both directions allowing the DFIG to vary the output power

by operating in super synchronous and sub synchronous speeds. The total output power from the wind power plant (WPP) is a combined total of power supplied by the stator and the rotor. The rotor speed depends on the frequency of the voltage applied to the rotor and the angular velocity of the rotor which is dependent on the prevailing wind speed.

The rotor side converter, rated at 25-30% of the induction machine rating, acts as the only restriction in the steady state operation of the DFIG. This gives the DFIG an operating range of 75% to 125% of the rated wind speed.

2.2.1. DFIG Control. DFIG can be represented by equivalent circuit shown in Figure 2.3.

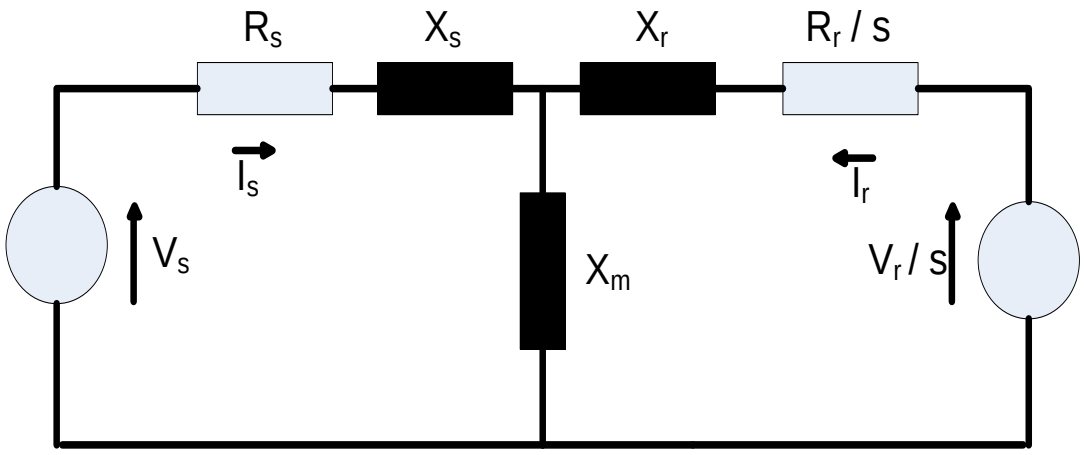

Figure 2.3.Steady state T-equivalent circuit of DFIG.

Mathematically, the following equations govern the equivalent diagram.

$$Is\,R_s + V_s = -\frac{d}{dt}\Psi_s - j\omega\Psi_s \tag{2.4}$$

$$I_r R_r + V_r = -\frac{d}{dt}\Psi_r - j(\omega - \omega_r)\Psi_r \tag{2.5}$$

2.2.2. Generator Side Converter Control. The variations in stator flux are negligible hence are assumed to be constant. Also it is assumed that there would not be any occurrence of saturation. Because of its small presence the stator resistance is considered as zero. To make the calculation simpler it is assumed that the stator flux Ψ_s is along the d axis in the d-q frame. Therefore,

$$\Psi_q = 0 \tag{2.6}$$

$$\frac{d}{dt}\Psi_d = 0 \quad \text{(Assuming constant } \Psi_d\text{)} \tag{2.7}$$

From Equation 2.4 it can be deduced that

$$V_d = 0 \tag{2.8}$$

$$V_q = -\omega \Psi_d \tag{2.9}$$

By applying the current divider rule on the equivalent circuit to obtain the value of stator current in terms of rotor current we get:

$$I_s = \Psi_s - \frac{L_m}{L_s} I_r \tag{2.10}$$

Where $L_s = L_{sl} + L_m$ (2.11)

The power output from the stator can be written as:

$$S_s = V_s * I_s \tag{2.11}$$

Hence,

$$P_s = \frac{3}{2}\left(V_d * I_d + V_q * I_q\right) = \frac{3}{2}\left(V_q * I_q\right) \quad (2.12)$$

And,

$$Q_s = \frac{3}{2}\left(V_d * I_q - V_q * I_d\right) = -\frac{3}{2}\left(V_q * I_d\right) \quad (2.13)$$

From these equations it is evident that the active power delivered at the stator terminals can be controlled by the I_{qr} component and the reactive power can be controlled by the I_{dr} component assuming constant stator flux. Therefore, to control the DFIG output, a control scheme may be applied to vary the I_{dr} and I_{qr} values to achieve the required power output set point.

2.2.3. Grid Side Converter Control. The main purpose of the grid side converter is to maintain a constant dc link voltage. To maintain this dc link voltage, the converter takes power from the grid and generates a dc current which keeps the capacitor in the dc link charged. This charged capacitor maintains a constant voltage at the terminals of the generator side converter. The control signal for the grid side converter is the pre-determined voltage set point.

2.2.4. Capability of Doubly Fed Induction Generator. Active and reactive power capability information of a machine is essential in analyzing the stability of the machine. The capability of any machine depends on its physical construction and materials used. For a DFIG machine, the active power output is limited by the prime mover capability. Similarly, reactive power output is limited by the maximum current and heating limits of the armature and the field coil. These physical limitations guide the capability of the machine.

The capability of a DFIG presents similarities to the conventional synchronous generator capability. The active power varies with the wind speed and the slip is assumed to be constant here. The other three limitations can be formulated as discussed below.

2.2.4.1 DFIG two port model. To find out the influence of the these limitations a two port model of DFIG is used [8]. This two port circuit, shown in Figure 2.4, is a simple representation of the T-equivalent circuit of the DFIG model.

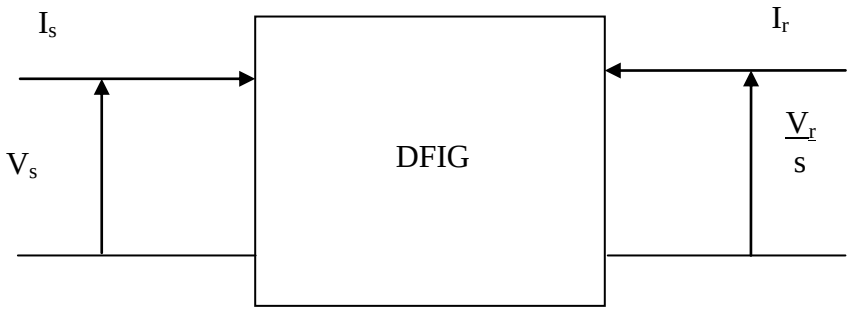

Figure 2.4. Two port equivalent circuit of DFIG.

The following equations can be used to plot the different limitations of the DFIG model on PQ axis. Equations 2.14 - 2.16 are used to estimate the values of any two variables by varying the value of the third variable. The three variable being the rotor current I_r, stator current I_s and V_r/s. The value of one of these variables is varied with the stator voltage V_s which is already known. The derivation of Equations 2.14-2.16 is described in Appendix A.

$$\begin{bmatrix} I_s \\ I_r \end{bmatrix} = Y * \begin{bmatrix} V_s \\ V_r/s \end{bmatrix} \tag{2.14}$$

$$\begin{bmatrix} I_s \\ V_r/s \end{bmatrix} = G * \begin{bmatrix} V_s \\ I_r \end{bmatrix} \tag{2.15}$$

$$\begin{bmatrix} V_r/s \\ -I_r \end{bmatrix} = B * \begin{bmatrix} V_s \\ I_s \end{bmatrix} \tag{2.16}$$

2.2.4.2 Rotor current limitation. This limit takes into account the rotor heating due to the rotor winding's Joule losses. The rotor current limitation in PQ diagram of a DFIG is derived by assuming a fixed rotor current with the rated magnitude and a variable angle relative to the stator voltage. By using Equation 2.15, the stator current can be represented in terms of rotor current as:

$$I_s = G_{11} V_s + G_{12} I_r \tag{2.17}$$

$$I_s = \left(\frac{V_s - Z_m I_r}{Z_s + Z_m} \right) \tag{2.18}$$

The apparent power (S_{s_Ir}) can also be written in terms of the rotor current by the following equation.

$$S_{s\_Ir} = -V_s I_s^* \tag{2.19}$$

$$S_{s\_Ir} = -V_s \left(\frac{V_s - Z_m I_r}{Z_s + Z_m} \right)^* \tag{2.20}$$

$$S_{s\_Ir} = -V_s V_s^* \left(\frac{1}{Z_s + Z_m} \right)^* + V_s I_r^* \left(\frac{Z_m}{Z_s + Z_m} \right)^* \tag{2.21}$$

Since the stator voltage is assumed constant, the first part of Equation 2.21 corresponds to a constant value. The second term makes the apparent power proportional to the rotor current. By setting the rotor current to the rated value and varying the angle, the reactive power limits can be determined. On a PQ capability curve, these equations can be represented as a circle with center c_{s_lr} and radius r_{s_lr}.

$$c_{s\_Ir} = -|V_s|^2 \left| \frac{1}{Z_s + Z_m} \right| \quad (2.22)$$

$$r_{s\_Ir} = |V_s|\,|I_r| \left| \frac{Z_m}{Z_s + Z_m} \right| \quad (2.23)$$

The total power delivered to the grid consists of power generated by the stator and the rotor. The rotor apparent power can be found as :

$$S_{r\_Ir} = -V_r I_r^* \quad (2.24)$$

$$S_{r\_Ir} = -(G_{21} V_s + G_{22} I_r) * s * I_r^* \quad (2.25)$$

$$S_{r\_Ir} = -\left(\frac{Z_m V_s + I_r((Z_r + Z_s)Z_m + Z_s Z_r)}{Z_s + Z_m} \right) * s * I_r^* \quad (2.26)$$

$$S_{r\_Ir} = -\left(\frac{(Z_r + Z_s)Z_m + Z_s Z_r}{Z_s + Z_m} \right) * s * I_r * I_r^* - \left(\frac{Z_m}{Z_s + Z_m} \right) * s * V_s * I_r^* \quad (2.27)$$

Since Z_m dominates the first term, this term can be considered as the reactive power component and the second term as the active power component. Also by comparing Equation 2.26 with 2.21 it can be deduced that,

$$P_r = -s * P_s \quad (2.28)$$

The total active and reactive power output of the DFIG is given by:

$$P_{tot} = (1 - s) * P_s \quad (2.29)$$

$$Q_{tot} = Q_s \quad (2.30)$$

By comparing Equations 2.28, 2.29, 2.22, and 2.23, the following circle equation can be deduced:

$$\left(P_s - Re\left(c_{s\_Ir}\right)\right)^2 + \left(Q_s - Im\left(c_{s\_Ir}\right)\right)^2 = r_{s\_Ir}^2 \tag{2.31}$$

$$\left(\frac{P_{tot}}{(1-s)} - Re\left(c_{s\_Ir}\right)\right)^2 + \left(Q_{tot} - Im\left(c_{s\_Ir}\right)\right)^2 = r_{s\_Ir}^2 \tag{2.32}$$

2.2.4.3 Rotor voltage limitation. The rotor voltage limitation is essential for the rotor speed interval, because the required rotor voltage to provide a certain field is directly proportional to the slip. Thus, the possible rotor speed is limited by the possible rotor voltage. To represent this limitation on the PQ capability graph, we can derive the equation as follows:

From Equation 2.14

$$I_s = Y_{11}V_s + Y_{12}\frac{V_r}{s} \tag{2.33}$$

$$I_s = \left(\frac{V_s(Z_r+Z_m) - Z_m\frac{V_r}{s}}{Z_s Z_r + Z_m(Z_r+Z_s)}\right) \tag{2.34}$$

The apparent power (S_{s_Vr}) can also be written in terms of the rotor voltage by the following equation.

$$S_{s\_Vr} = -V_s I_s^* \tag{2.35}$$

$$S_{s\_Vr} = -V_s\left(\frac{V_s(Z_r+Z_m) - Z_m\frac{V_r}{s}}{Z_s Z_r + Z_m(Z_r+Z_s)}\right)^* \tag{2.36}$$

$$S_{s\_Vr} = -V_s V_s^* \left(\frac{(Z_r+Z_m)}{Z_s Z_r + Z_m(Z_r+Z_s)}\right)^* + V_s * \frac{V_r}{s}\left(\frac{-Z_m}{Z_s Z_r + Z_m(Z_r+Z_s)}\right)^* \quad (2.37)$$

The first term in Equation 2.37 is a constant, and hence the apparent power limitation due to rotor voltage is represented by a circle with center and radius as shown below.

$$c_{s\_Vr} = -|V_s|^2 \left(\frac{(Z_r+Z_m)}{Z_s Z_r + Z_m(Z_r+Z_s)}\right)^* \quad (2.38)$$

$$r_{s\_Vr} = |V_s||\frac{V_r}{s}| \left|\frac{Z_m}{Z_s Z_r + Z_m(Z_r+Z_s)}\right| \quad (2.39)$$

By substituting the value of c_{s_Vr} and r_{s_Vr} in lieu of c_{s_Ir} and r_{s_Ir} in Equations 2.30 and 2.31, we can deduce the circle equation as:

$$\left(P_s - Re(c_{s\_Vr})\right)^2 + \left(Q_s - Im(c_{s\_Vr})\right)^2 = r_{s\_Vr}^2 \quad (2.40)$$

$$\left(\frac{P_{tot}}{(1-s)} - Re(c_{s\_Vr})\right)^2 + \left(Q_{tot} - Im(c_{s\_Vr})\right)^2 = r_{s\_Vr}^2 \quad (2.41)$$

2.2.4.4 Stator current limitation. This limit takes into account the stator heating due to the stator winding's Joule losses. The PQ curve depicting stator current limitation is straight forward and can be derived as:

$$S_{s\_Is} = -V_s I_s^* \quad (2.42)$$

$$c_{s\_Is} = 0 \quad (2.43)$$

$$r_{s\_Is} = |V_s|\,|I_s| \tag{2.44}$$

Equations 2.43 and 2.44 are substituted in Equations 2.30 and 2.31 to get the circle equations as follows:

$$\left(P_s - Re\left(c_{s\_Is}\right)\right)^2 + \left(Q_s - Im\left(c_{s\_Is}\right)\right)^2 = r_{s\_Is}^2 \tag{2.45}$$

$$\left(\frac{P_{tot}}{(1-s)} - Re\left(c_{s\_Is}\right)\right)^2 + \left(Q_{tot} - Im\left(c_{s\_Is}\right)\right)^2 = r_{s\_Is}^2 \tag{2.46}$$

With these three limitations applied to the DFIG in the PQ capability curve, we can use the area of intersection which does not violate any of the limitations as the reactive power varying capacity of the generator. In addition to these three limitations, the prime mover capacity is another limitation applied in the capability curve. To show the capability curve for DFIG with limitations, parameters from Table 2.1 were utilized.

Figure 2.5 displays the combined effect of the three limitations discussed on the PQ capability curve. This figure gives a clear idea of safe operating region for the DFIG machine. The blue line in the figure constitutes the stator current limitations on the DFIG. The red line displays the rotor current limitations and the green lines represent the limitations due to rotor voltage. Because of these limitations, the DFIG can operate only in the overlapping region of all the three limitations. This region lies between the red upper curve and the blue lower curve.

Table 2.1 DFIG machine parameters

Machine Parameter	Value
Rated Mechanical Power	1.5 MW
Rated generator power	1.3 MW
Rated stator voltage	575 V
Rotor to stator turns ratio	3
Machine inertia	30 kg-m^2
Rotor inertia	610000 Kg-m^2
Inductance: Mutual, Stator, Rotor	4.7351, 0.1107, 0.1193p.u.
Resistance: Stator, Rotor	0.0059, 0.0066 ohms
Number of poles	3
Grid frequency	60 Hz
Gearbox ratio	1 : 72
Nominal turbine : rotor speed	16.67 : 1200 rpm
Turbine radius	42 m
Maximum slip range	±30%

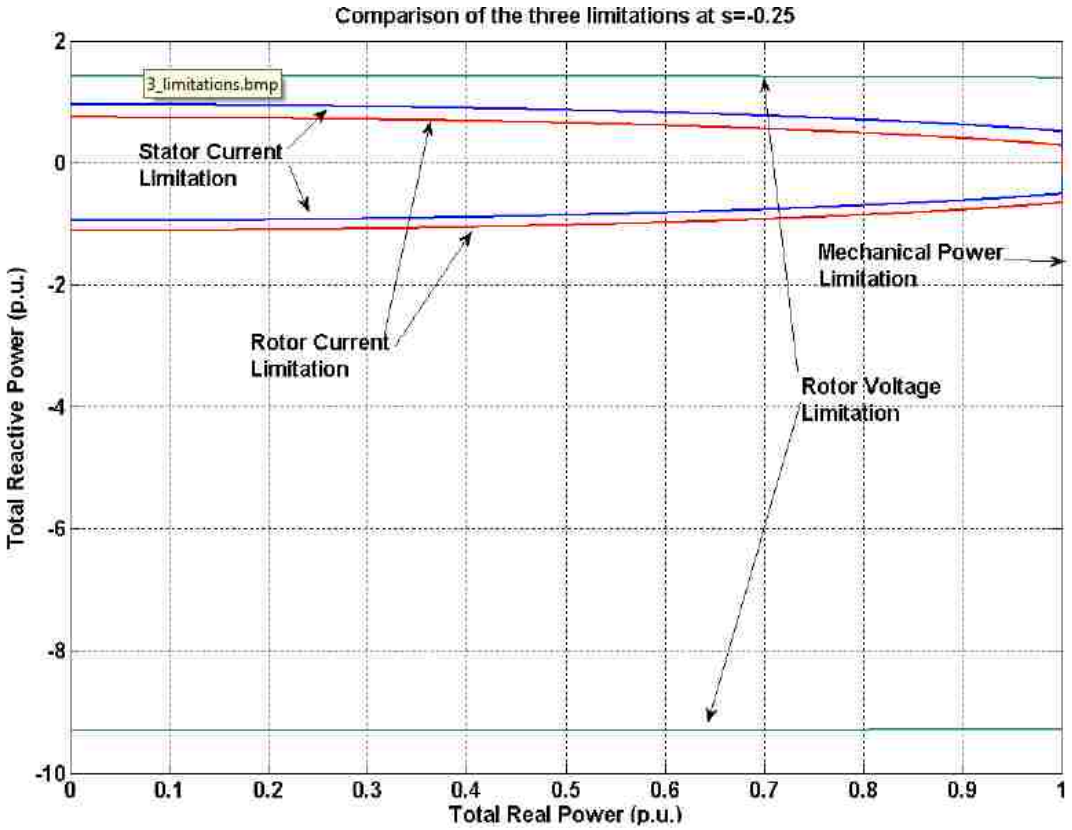

Figure 2.5. Three limitations of a DFIG model.

3. MICROGRID

3.1. INTRODUCTION

Microgrids are autonomous small-scale power grids at the lower distribution voltage levels consisting of interconnected loads and distributed energy resources (DER). In other words, a small group of loads and micro-sources operating as a controllable system, satisfying electric power needs of a nearby area with sufficient reliability. Microgrid posses capability of operating in parallel with the grid and also operate in islanded mode when needed. This type of operation increases the flexibility and reliability of the system while making it more robust in nature. The concept of microgrid may not be fully functional or adopted as of now but with large scale development and deployment of distributed energy resources, microgrid concept seems to be very promising. The constantly evolving IEEE 1547 standards [35] are utilized to govern the interconnection and operation of distributed generation including wind power plants.

The need for microgrids is felt due to the huge challenges faced by the traditional grid. Large amount of power generated is wasted in long transmission lines due to the centralized nature of the grid. The centralized nature of the grid also makes it an easy target to bring down with a cyber-security breach. The renewable energy sources are currently treated like negative loads and are not allowed to help out in times of need. Lastly, the structure is unreliable and adverse effects in a small location may lead to an impact felt by large populations in adjacent large geographical area. The recent example of the massive blackouts across Arizona, California and parts of Mexico shows the unreliable nature of the grid [36]. These blackouts occurred when a 500 KV line was taken offline for planned maintenance.

A network of small autonomous grids, or microgrids, can help the legacy grid to get rid of some of these issues. The microgrid is connected to the conventional grid, but in the event of grid failure, the microgrid can be isolated and allowed to serve the local loads. This feature also allows it to defend itself from the impact of cyber security breaches in interconnected systems. It can quickly isolate itself before the interconnected system goes down. This feature is highly favorable for vital military and commercial establishments in any nation. Local control of microgrids allows expansion of the system

according to the need of the local communities. This also facilitates the local communities to implement green initiatives for power generation more effectively.

One interesting property of a microgrid is islanding, or disconnection from the main grid . Islanding can be originated in a planned way or unintentionally and, in both cases, the isolated part can continue providing energy to its connected loads.

Although a microgrid can provide immunity from system-wide disturbances, there has been a general reluctance to using renewable energy-based generation in the energy-limited grid. This is due to the presence of limited short circuit capacity of inverter fed renewable energy sources like wind, photovoltaic and fuel cell power plants. These devices are forced to trip at the first sign of a system problem, unless low- or high-voltage ride through capabilities are provided for these inverter.

Microgrid has clear advantages but at the same time, new challenges should be resolved. Some of the more complex technical challenges facing the operation of a microgrid in the presence of renewable resources may be summarized as follows:

- Surviving fault-induced transients.
- Providing adequate dynamic damping to ensure oscillatory stability.
- Providing adequate voltage and frequency regulation.
- Ensuring transient/voltage stability of the microgrid.
- Providing communication among entities within the microgrid.
- Assessing the dynamic state of the microgrid in real time.

In the following section, various components required to build the microgrid are discussed and modeled in SIMULINK.

3.1.1. Synchronous Generator Modelling. The synchronous generator model consists of three parts, the synchronous machine model, the governor model with hydraulic turbine, and the excitation system. A governor model takes the frequency change as an input and changes the servomotor output to provide adequate mechanical power to offset the frequency change from the reference. This model produces available mechanical power as an output which is then fed to the synchronous machine. The excitation system produces the required field voltage for the synchronous machine to maintain the commanded generator terminal voltage. The synchronous machine model takes available mechanical power and required field voltage as an input from the governor and excitation system models, and produces the required current and line-to-line voltage. The models used for the excitation system and the governor are displayed in Appendix B. The parameters utilized for these models are shown in TABLE C.1, C.2 and C.3.

3.1.2. Wind Power Plant Modelling. Wind power plants are designed to extract power as demanded from the command signal. To be aware of the wind capacity at all time, it's tracking characteristics should be known as shown in Figure 3.1 .

The power is tracked with a pre-defined power-speed characteristic, namely tracking characteristics. This characteristic is illustrated by the ABCD curve in Figure 3.1 over the turbine power characteristics at different wind speeds. The tracking characteristic is defined by four points: A, B, C and D. In this thesis, the wind turbines are assumed to have coinciding C and D points. Until the speed of point A, the wind power is zero. Between points A and B, the tracking characteristic is a straight line. Between points B and C/D, the tracking characteristic is the locus of the maximum power of the turbine (maxima of the turbine power vs turbine speed curves). Beyond point D, the reference power is a constant equal to one per unit (1 pu).

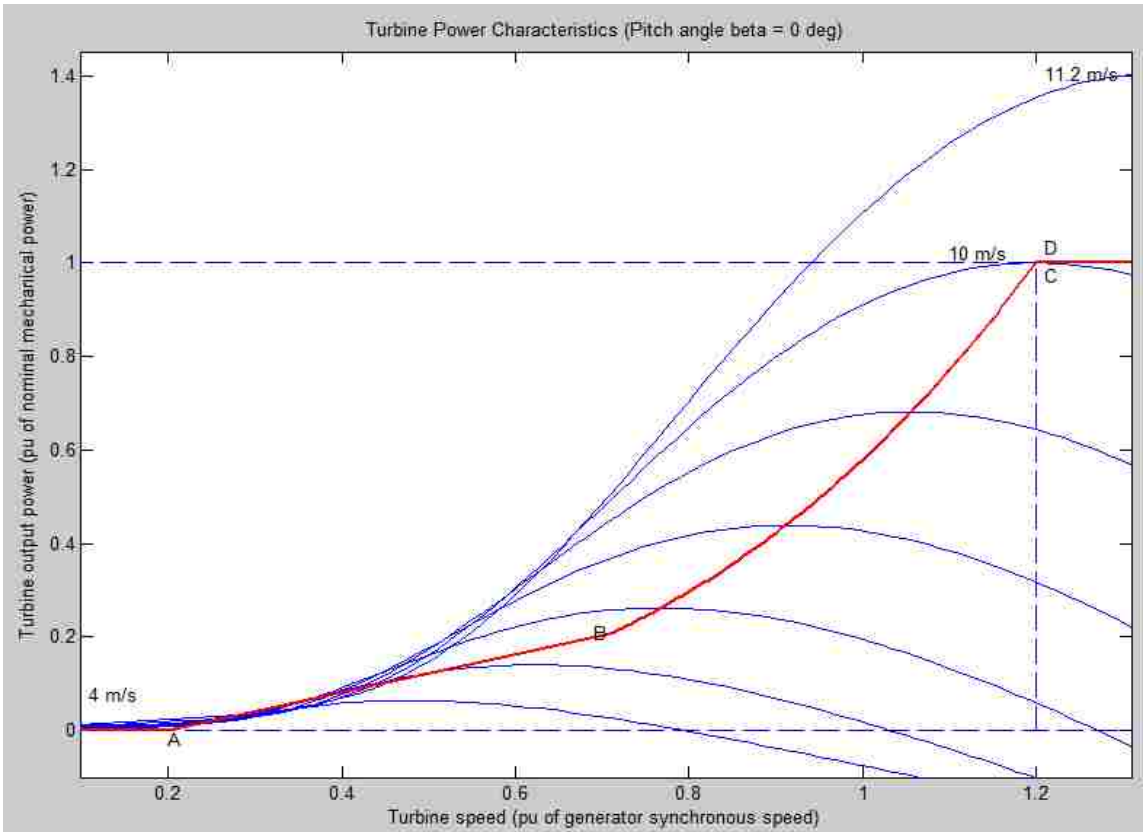

Figure 3.1 Wind turbine power characteristics.

3.1.2.1 Wind turbine modeling. Wind turbines are governed by Equations 2.1, 2.2 and 2.3. A SIMULINK model following these equations is developed as shown in Figure 3.2.

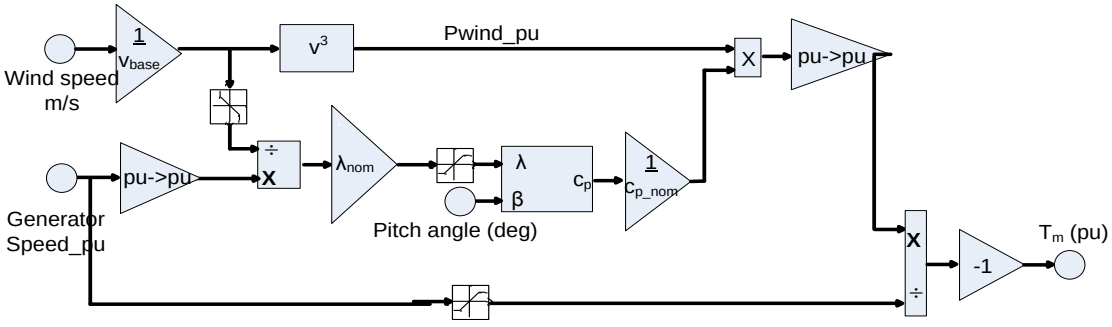

Figure 3.2 SIMULINK Wind Turbine model.

3.1.2.2 DFIG modelling. The Doubly Fed Induction Generator is modeled as an asynchronous machine with the commanded d-q axis voltage as one of the input with the a-b-c phase terminal voltage and the torque produced by the wind turbine as the other two inputs. The model outputs all the a-b-c and d-q axis voltage and current quantities of stator and rotor as an output. The model and the equations used are described in [37].

3.1.2.3 Grid side converter modelling. The grid side converter is used to regulate the voltage of the DC bus capacitor. The control system for the grid side converter is displayed below in Figure 3.3. The d-axis (for d-q transformation) of the rotating reference frame is aligned with the positive sequence of the terminal voltage.

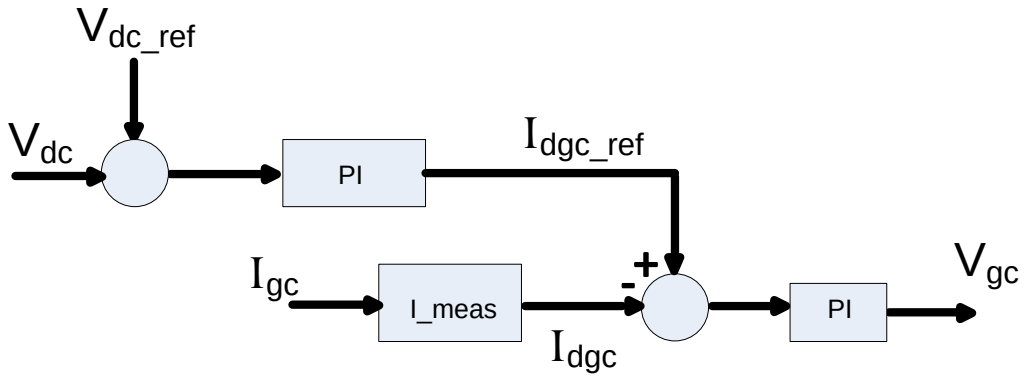

Figure 3.3. Grid side controller [38].

This controller consists of a measurement system to measure the d-axis and q-axis components of AC currents to be controlled, and the DC link capacitor voltage. This controller also includes an outer and inner regulation loop to regulate the DC voltage and the current.

The outer loop generates d-axis reference current I_{dgc_ref} through a DC voltage regulator, in phase with terminal voltage to control the active power flow. This outer loop

output is given to the inner loop as an input. The inner loop controls the converter voltage V_{gc} by comparing the reference current from the outer loop with the measured d-axis current I_{dgc} from the grid side through a current regulator for a specified q-axis reference current.

The logic and the implementation in SIMULINK is displayed in Figure 3.4.

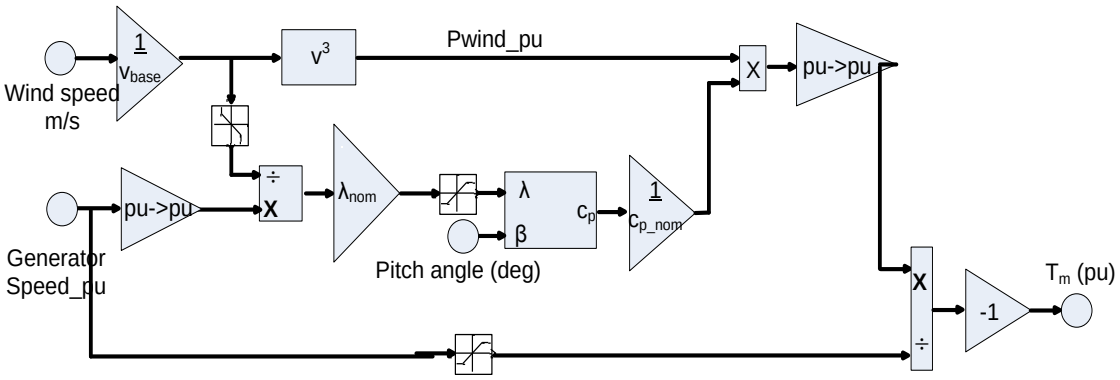

(a) Logic for grid side converter.

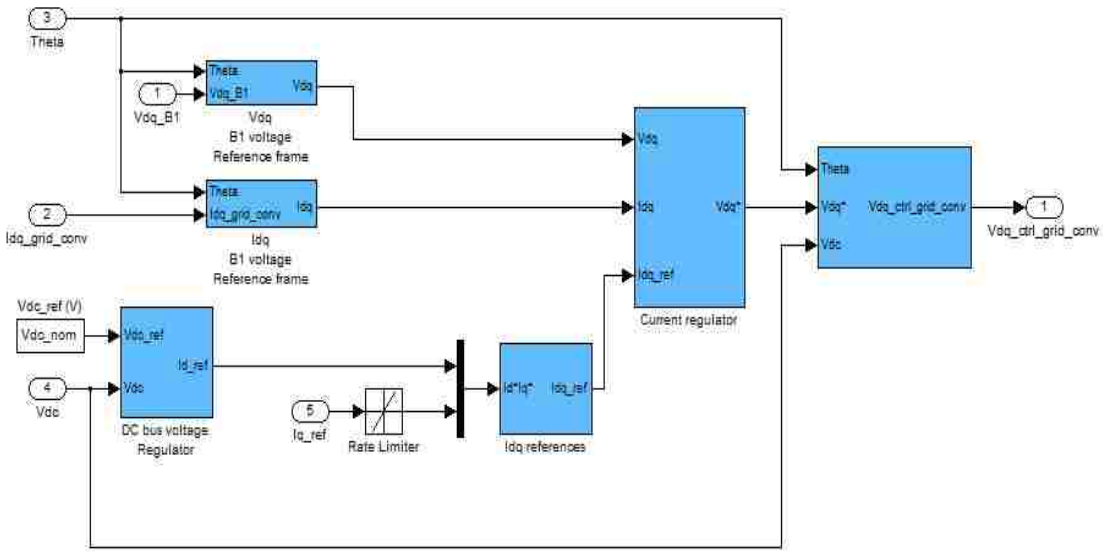

(b) SIMULINK model for grid side converter.

Figure 3.4.Grid side converter.

3.1.2.4 Rotor side converter modelling. The wind turbine output power and the voltage measured at the grid terminals are controlled by the rotor side controller. In this thesis, a power reference from the microgrid controller is used to control the amount of active power supplied by the wind power plant. In a conventional converter, active power reference is generated according to the wind speed to maximize the output. It cannot be controlled by an operator by just changing a power reference.

The control loop used for rotor side controller is shown in Figure 3.5. The d-axis of the rotating reference frame of the rotor is aligned with the air gap flux. As shown in the figure, the measured electrical output at the generator terminals is summed up with the losses incurred and then compared to the reference power from the microgrid controller. The output is then passed through a Proportional-Integral (PI) regulator to minimize the power error. The output of the regulator is used as the reference for the q-axis component of the rotor current I_{qr_ref} and is then compared with the measured I_{qr} and the error is minimized by passing the output through a current regulator. This regulator produces the q-axis component of the rotor voltage V_{qr} required to control the active power out of the wind power plant. The I_{qr} current component is responsible for producing the required electromagnetic torque for the rotor.

The terminal voltage of the wind power plant is controlled by changing the reactive power output of the wind power plant through the rotor side converter. Either commanded reactive power or the required terminal voltage can be used to change the d-axis component of the rotor current reference I_{dr_ref} of the rotor. In this thesis, I_{dr_ref} value is varied to keep the terminal voltage in check. This reference current is then compared with the measured value and reference d-axis rotor voltage V_{dr} is produced through the current controller to control the reactive power output. In a conventional converter the value of I_{dr_ref} is kept to a minimum to so as to maximize the active power generation by improving the I_{qr_ref}.

The reactive power is exchanged between rotor side converter and the grid, through the generator. In the exchange process, the generator absorbs reactive power to supply its mutual and leakage inductances. The excess of reactive power is sent to the grid or to rotor side converter. The rotor side controller can keep the terminal voltage in check until the I_{qr} and I_{dr} follows the current limitations.

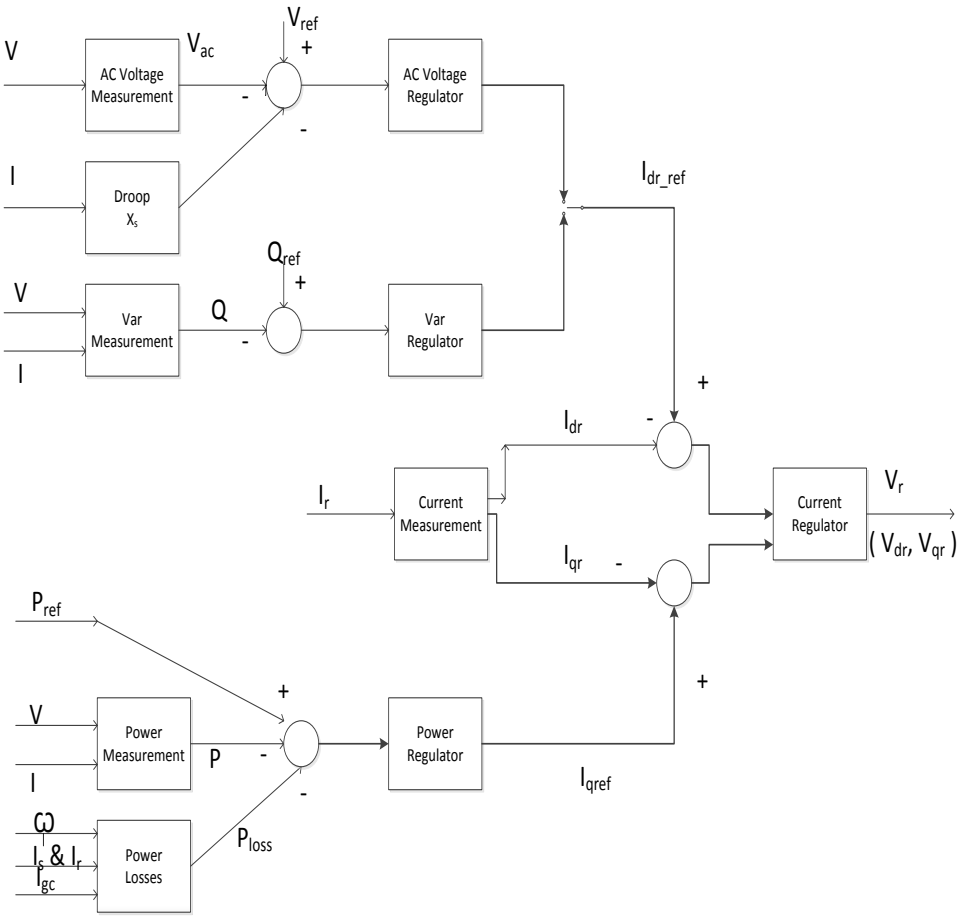

Figure 3.5 Rotor side controller.

The control is implemented in SIMULINK as shown in Figure 3.6.

3.1.2.5 Pitch angle control. The pitch angle control is utilized when wind speeds reach beyond the rated output. This type of control is slow due to the involvement of mechanical motion of rotating the wind turbine blades, and hence is only used to hedge the power output from sudden outbursts of wind speed greater than the rated value. The pitch angle is kept constant at zero degree until the speed reaches the rated value, or the speed point C/D in the tracking characteristic of Figure 3.1. Beyond this point, the pitch angle is proportional to the speed deviations.

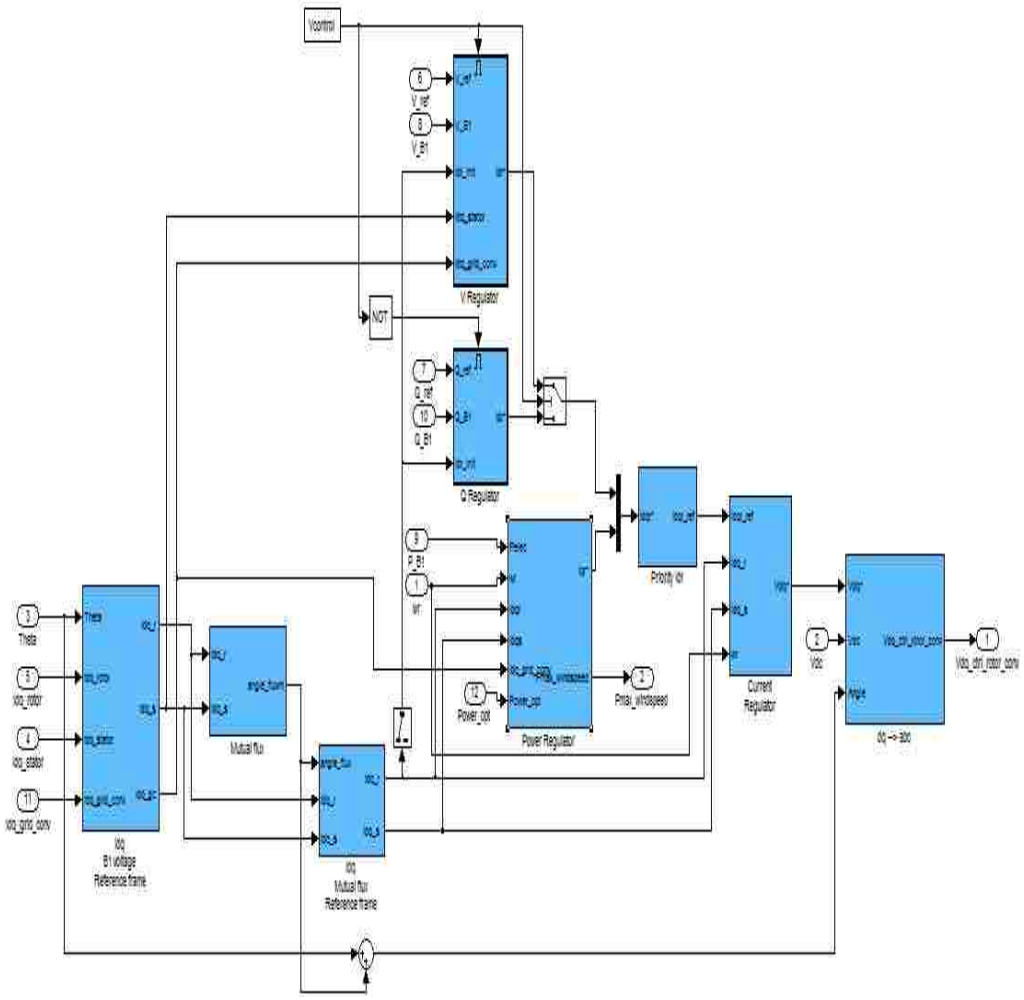

Figure 3.6. SIMULINK model of the rotor side controller.

4. FREQUENCY AND VOLTAGE CONTROL IN MICROGRID

4.1. OBJECTIVES IN MICROGRID CONTROL

This thesis attempts to meet the following critical objectives for reliable operation of a microgrid:

- Derive an adequate generation mix that consists of wind power plants and conventional generating units:
- When adequate wind is available, the wind power plants should operate at 75% of maximum rated active power at the start to provide ±25% power as an additional support for regulation.
- The wind power plants must be able to substantively participate in system frequency control.
- The wind power plants must be able to substantively participate in system voltage control.

4.2. FREQUENCY CONTROL

4.2.1. Introduction. Frequency control in a power system is done to maintain an adequate balance between the consumed and generated active powers, so that the frequency remains within acceptable limits around the nominal frequency. With constantly changing power demand, frequency control becomes an important task for a power system. Generally, the changing system load is predictable and units are committed and dispatched based on the forecasted load levels. Therefore, under normal operating conditions, the balancing of energy is achieved by adjusting the generator active power set-points. Signals to generators for such adjustments are either issued by the system operator or automatically generated and issued by automatic generation control (AGC).

In the event of a load change or any unexpected event like loss of generation, an imbalance of load occurs in the system which causes frequency excursions. Every power system tries to fight the frequency excursion by releasing the stored kinetic energy in the form of system inertia. In every system, with increase in the load, the kinetic energy is

released and reduction of the load results in absorption of the kinetic energy which tries to maintain the nominal frequency of the system.

This inherent system inertial response due to the masses of the connected generators and the load is not sufficient to return the system frequency to its nominal value. Hence frequency control is required to support the stable and secure operation of the power system.

In large interconnected power systems, the power imbalances created due to the loss of single component are small when compared to the total system size. In addition, the inertia of the system also contributes towards limiting the rate of frequency change . Hence the frequency deviations are small in large systems. The frequency relaxation limits for normal operation of the grid as suggested by CERTS [39] is shown in Figure 4.1. In an islanded system, these frequency guidelines are a bit relaxed giving normal frequency operation of ± 1.2 Hz.

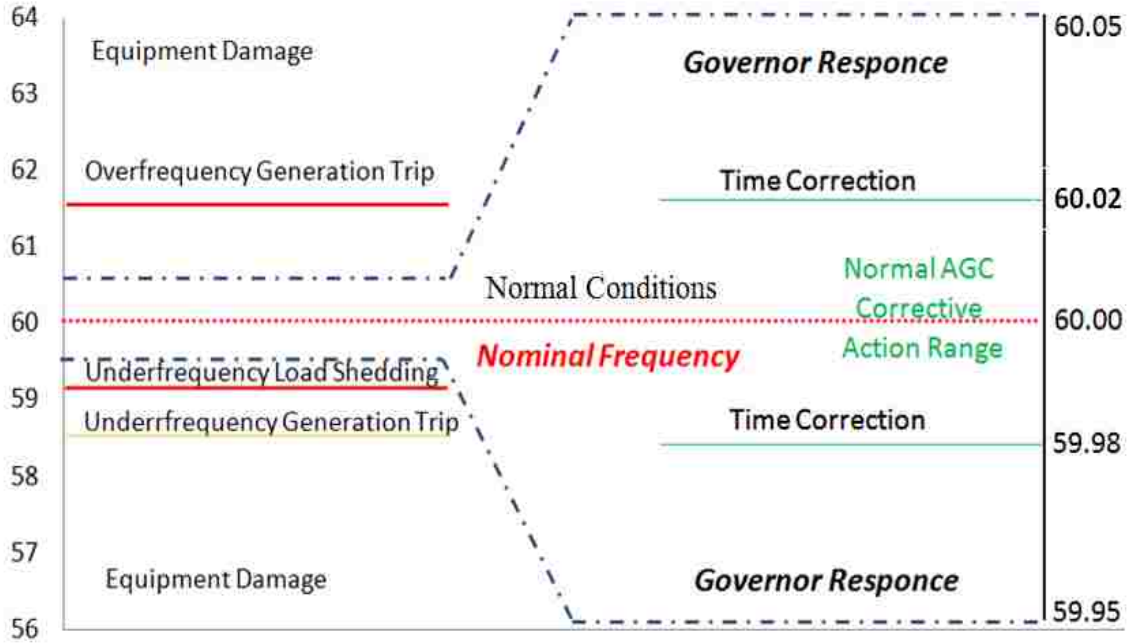

Figure 4.1.: Frequency relaxation limits[39].

4.2.2. Droop Control. Governors in a synchronous generator are designed to respond to any changes in the speed of the rotor. In response to the speed change, the governors open or close the controlling elements like gates or nozzles for controlling the water gushing in the hydro generator or the amount of steam entering the steam turbine. When two or more generators are connected in parallel, usually the output from one generator is not enough to restore the system frequency. Hence another mechanism is required to share the amount of power imbalance in the system between all the generators connected to the system. The amount of sharing for a particular generator is decided by the factor of speed droop. The droop can be described as the decrease in speed set-point with increasing gate/nozzle position. It is also referred as "regulation" for the units taking output power as the feedback signal instead of gate position.

$$Droop = \frac{\%\ Speed\ reference\ change}{\%\ Gate\ Position\ Change} * 100 \quad (4.1)$$

A droop of 5% for a synchronous generator operating at a nominal frequency of 60 Hz would imply that the governor would fully operational for a change of 3 Hz. Generally most of the generators follow a 5% droop when connected to the grid. Figure 4.2 shows an example for droop control between 2 units. The two units are operating at 2% and 5% droop and serving a load at the point of intersection.

When the generators are connected to a small, isolated system, it is normal practice to operate the generators in "Isochronous Mode". The isochronous mode is generally described as mode in which the generators are tuned to zero droop. With a zero droop, the governor will keep on opening the gate/nozzle until the frequency is restored to its original value. The limitations of droop control for wind resources are discussed next, and a new control technique is proposed to overcome the droop control limitations.

4.2.3. Hysteresis Control for Wind Generation. Droop control is a powerful tool to control the generation according to the frequency deviations, but it is not sufficient for the renewable energy sources. Fuel sources for renewable energy are abundant but intermittent in nature. The variability of wind in a particular location can be determined by a Weibull distribution [40]. This statistical tool tells us about how often winds of different speeds can be seen at a location. For a location with an exceptional average wind speed, there is always a time when the wind speed dips for certain period of time reducing the power that can be extracted from the wind turbine. In a microgrid environment, conventional generators operating at a droop of around 1% would quickly pickup this power imbalance created by wind variability, and by the time the wind output reaches the capability of producing rated power, the frequency deviations becomes small denying wind power output to return to a substantial value. After setting up at a low operating point, the droop control will force the wind output to follow the load from a low initial set point. This will result in an unnecessary loss of wind power which could have been utilized instead of the fossil fuel used in conventional generators. To overcome this problem, a new hysteresis control is added to the droop control which enables the restoration of wind power to a fixed high point. This control is activated only when the wind power is reduced below a fixed low point and keeps the control until the output reaches the fixed high point. The control is then returned back to droop control for normal load following. A flowchart for the control is depicted in Figure 4.3.

In this thesis the fixed hysteresis high point is set at 75% of rated capacity and the hysteresis low point is set at 50% of rated capacity.

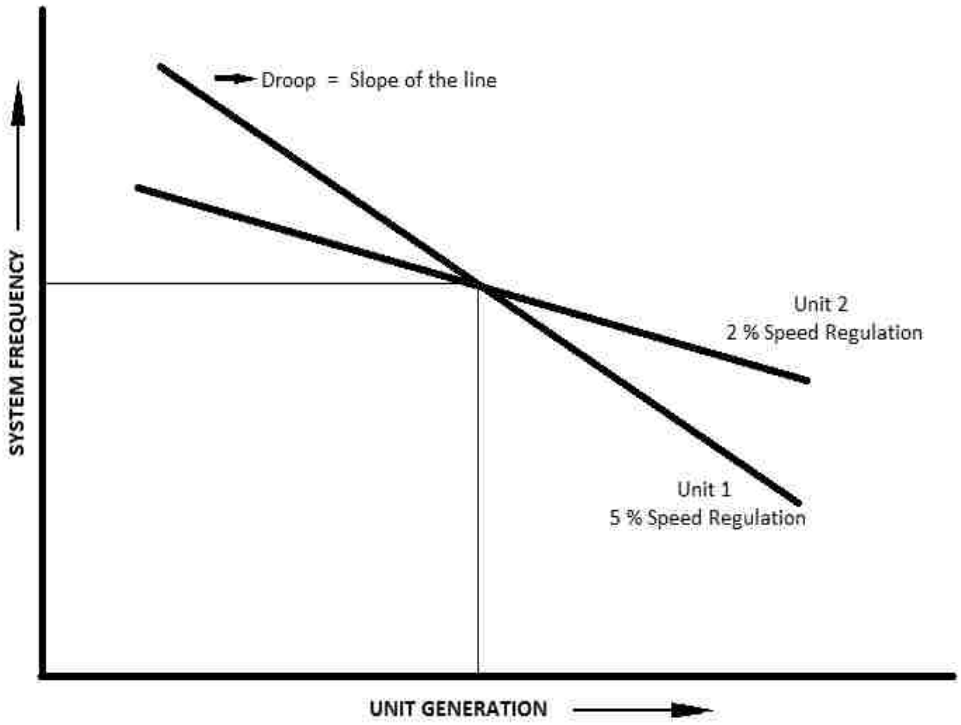

Figure 4.2: Droop characteristics for Unit, 1 & 2.

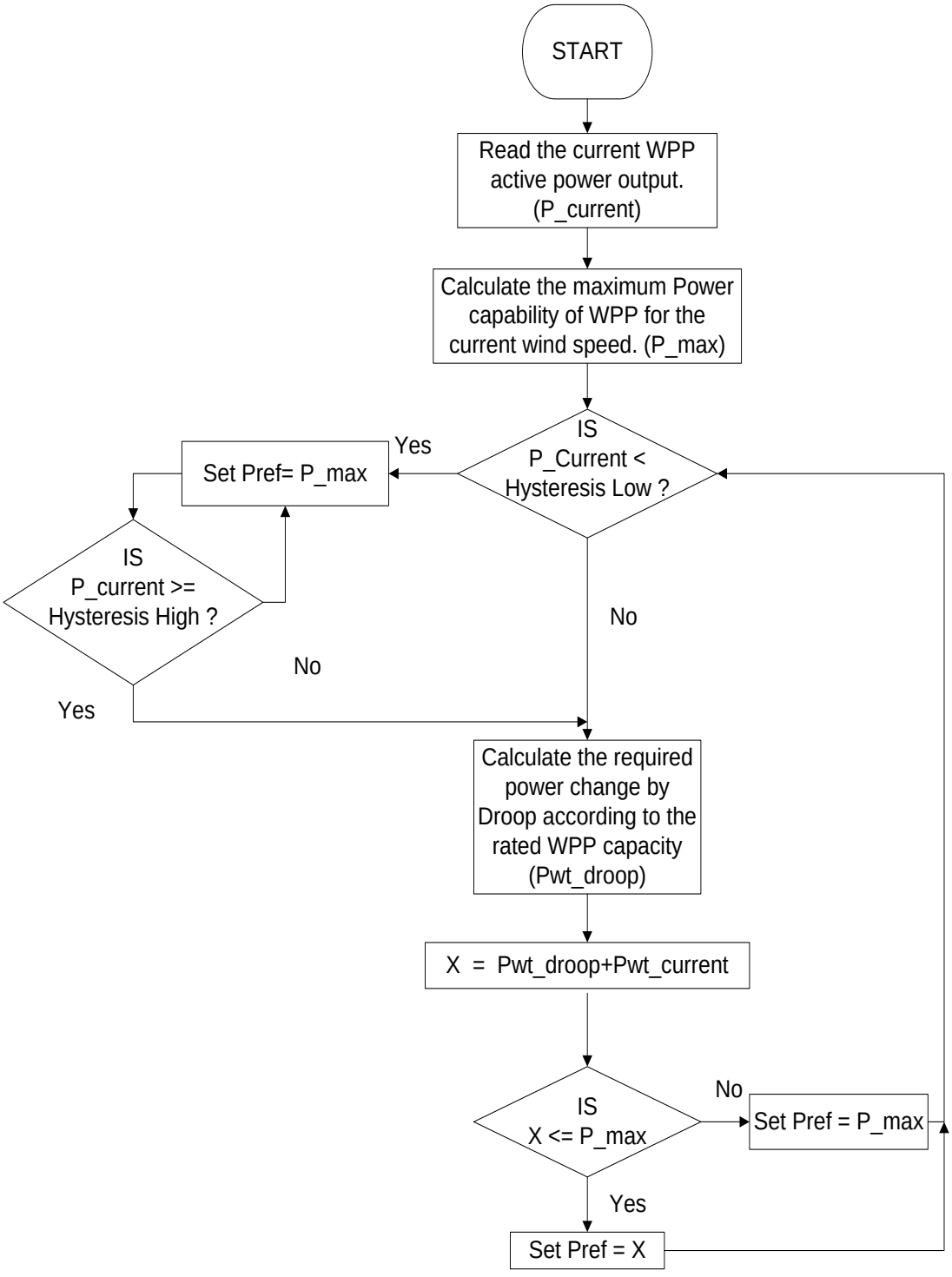

Figure 4.3. Flowchart for hysteresis control for WPP.

4.3. VOLTAGE CONTROL

4.3.1. Introduction. Maintaining the voltage profile in any power system plays a key role in the improvement of power system stability and reliability. Automatic voltage regulators (AVR) equipment installed at power plants helps to keep the voltage levels in check at the generator terminals. An AVR comprises of an excitation system which controls the dc current flowing into the field winding of a synchronous generator. By adjusting the generator field current, the reactive power output of the generator is controlled which helps in regulating the generator terminal voltage. The microgrid model used in this thesis uses individual voltage control at each generating unit. The generating units regulate the amount of reactive power supplied to the system in order to maintain their respective terminal voltages.

4.3.2. Excitation System. Conventional generating units i.e. synchronous generators, used in the microgrid implements a type DC1A –DC Commutator excitation system model to control the generator field current as shown in Appendix B.

4.3.3. Voltage Control in Wind Power Plant. The wind power plant model used in the microgrid system in this thesis can be used in either a VAR control mode or voltage control mode. The VAR control would be activated in the event when the microgrid is connected to the main grid. In this type of control, the reactive power supplied by the wind power plant would be controlled by a reference command generated by the operator. The difference between the reactive power generated by the plant and the reference command decides the amount of change needed by the I_{dr} - the d axis component of the rotor current, in the inverter controlled wind power plant.

In the islanded mode, the voltage control mode of the wind power plant is activated which tries to maintain the voltage of the generator terminals by adjusting the reactive power output of the plant. The change in the reactive power is determined by the voltage droop characteristics as displayed in Figure 4.5. If the current becomes negative, the rotor starts absorbing reactive power and brings the voltage down. If the current is positive that implies, rotor is supplying reactive to bring the voltage up. The voltage can be compensated with a rate of X_s .This V-I characteristics displays the amount of voltage regulation available according to the rotor current limits.

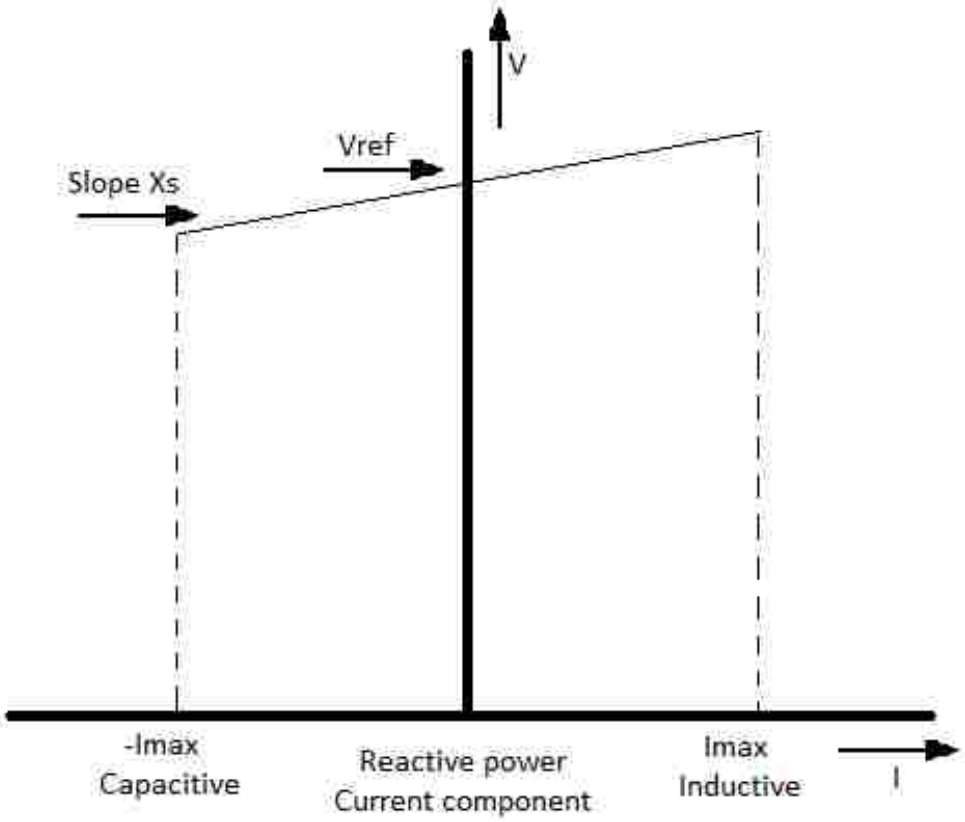

Figure 4.5. Voltage droop for WPP.

5. MICROGRID TEST SYSTEM

5.1. INTRODUCTION

The increasing interest in wind power combined with the concept of microgrid, has given rise to a scenario with high penetration of wind power in a small system with limited inertia. This scenario has the potential for frequency and voltage fluctuations. One way to reduce these fluctuations is by utilizing the wind power potential to provide ancillary services like reactive and active powers to provide voltage and frequency stabilization.

As mentioned earlier, a study is carried out in this thesis in order to get a sense of an acceptable configuration of generation mix when WPPs are allowed to participate in voltage and frequency regulation.

In this thesis, the microgrid test system is small and isolated but has three synchronous generators and two wind power plants. All the generators are assigned 1% droop which makes sure the full operation of governors for a frequency deviation of ±0.6 Hz and equal participation from all of the generators.

5.2. TEST SYSTEM - ONE LINE DIAGRAM

This sub-section displays the one line diagram of the microgrid system used in this thesis in Figure 5.1. Different parameters used for the system are described in Table 5.1 and 5.2.

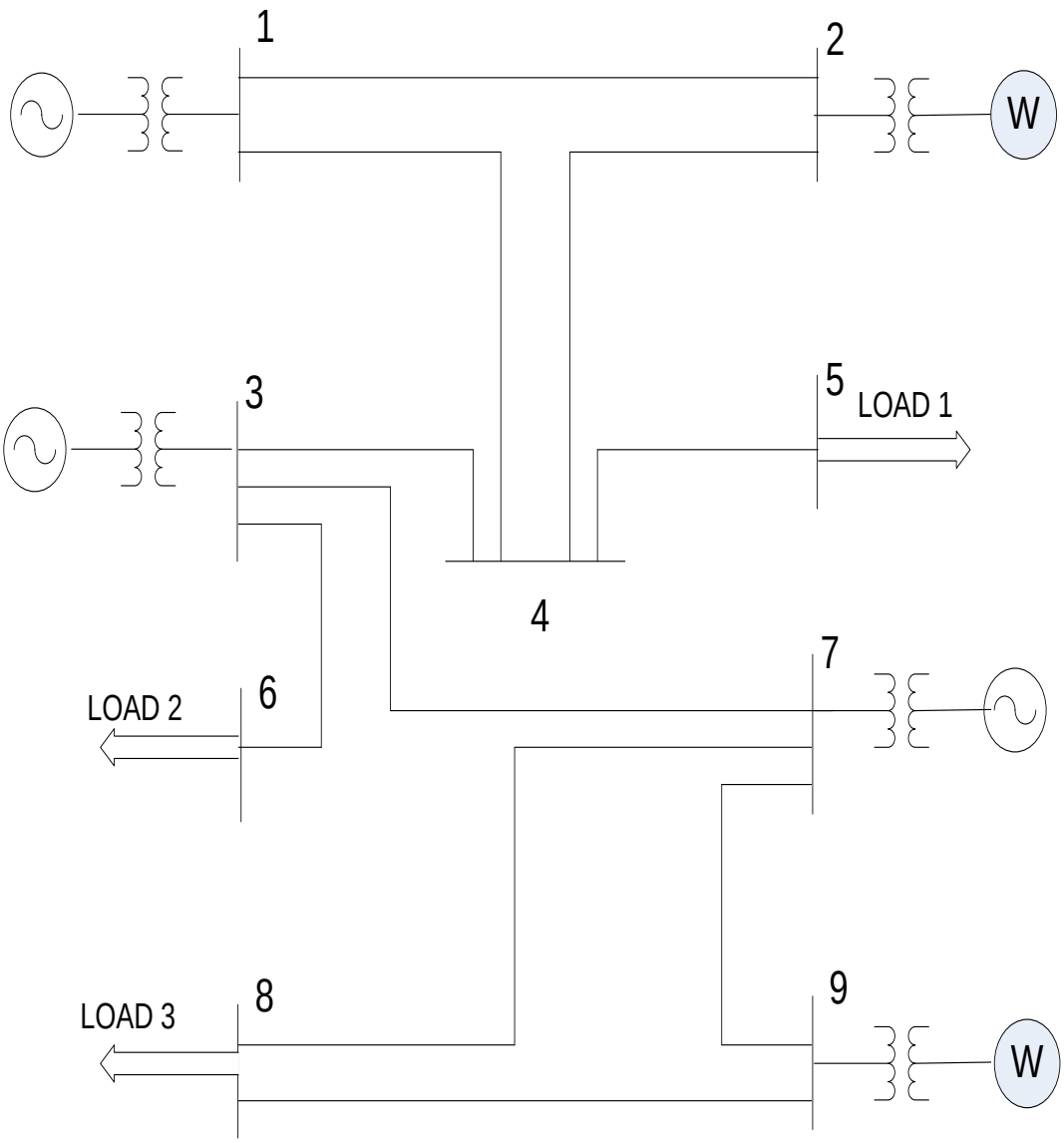

Figure 5.1. One line diagram for the test system.

The line data, transformer data, synchronous machine data and the bus data used for this test system is given in Appendix C under TABLE C.3, C.4, C.5, C.6.

5.2.1. The Test System. A microgrid model is developed in Simulink as shown in Figure 5.2 based on the one line diagram of Figure 5.1. This model is developed as a phasor model to expedite the simulation process. In phasor simulation, changes in magnitude and phases are calculated instead of solving complex differential equations. This type of simulation saves computational time that is required to solve the differential equations.

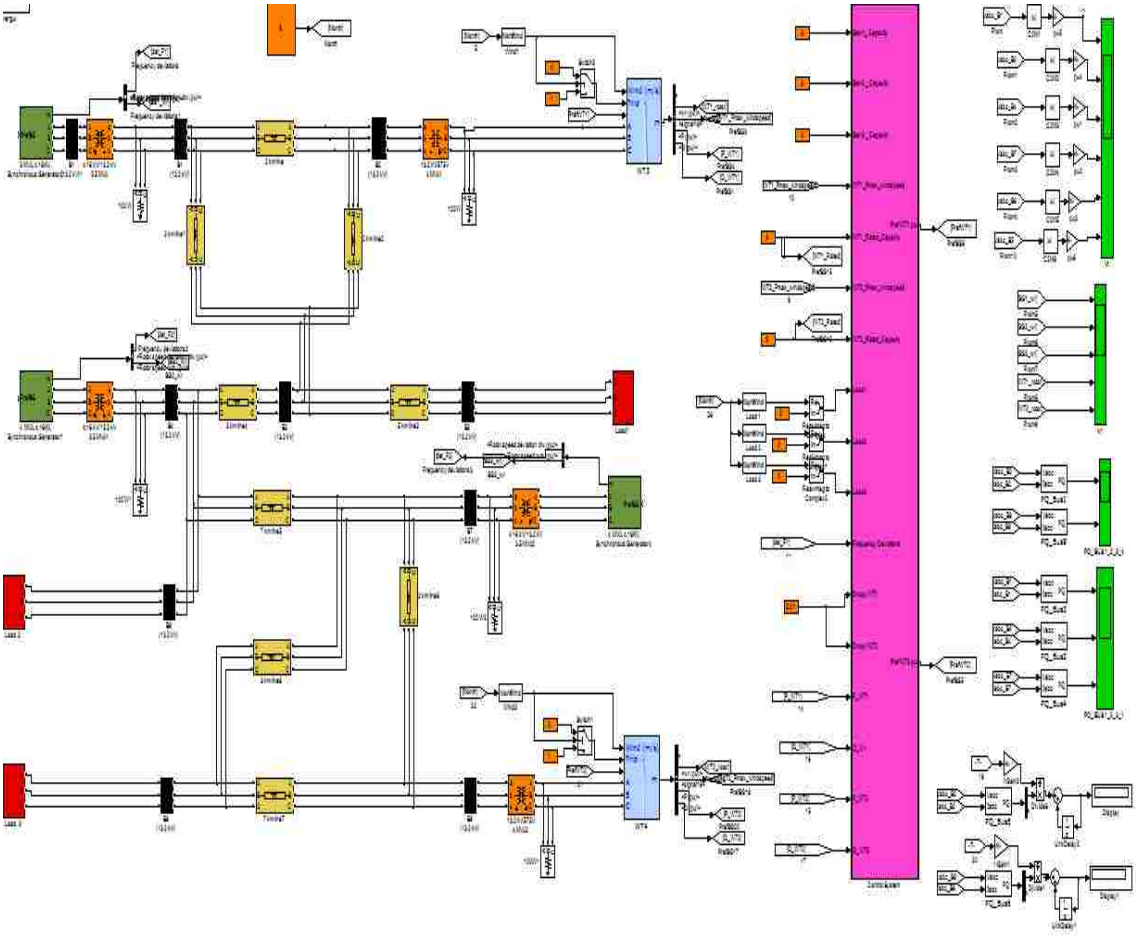

Figure 5.2 Microgrid test system implemented in Simulink.

The dark green colored blocks in the system represents the synchronous generators. The components in light blue represent the wind power plants and the red colored components are the three loads in the system. The black blocks represent bus bars

which actually are used to measure the voltage and current at that particular location. The orange blocks and the light yellow blocks represent transformers and transmission lines respectively. The pink colored blocks are the microgrid control system for wind power plants and the light green blocks are for recording the output.

5.2.2. Controller Testing on Microgrid Model. For testing the controller in the microgrid for the required performance, the system was subjected to 24 hour load profile with full wind support i.e the wind is always kept above the rated wind speed. To verify the performance, the output of the wind turbine connected to bus 2 was mapped together with the output of the synchronous generator connected to bus 1. It is expected that the active power output of wind should closely follow the output pattern of synchronous generator because the governor for the synchronous generator are tuned to compensate for frequency deviations. Figure 5.3 displays the output. In this example, a configuration of 40 % wind penetration is chosen for the test microgrid model. Load data for this configuration is given in Appendix C Table C.6.

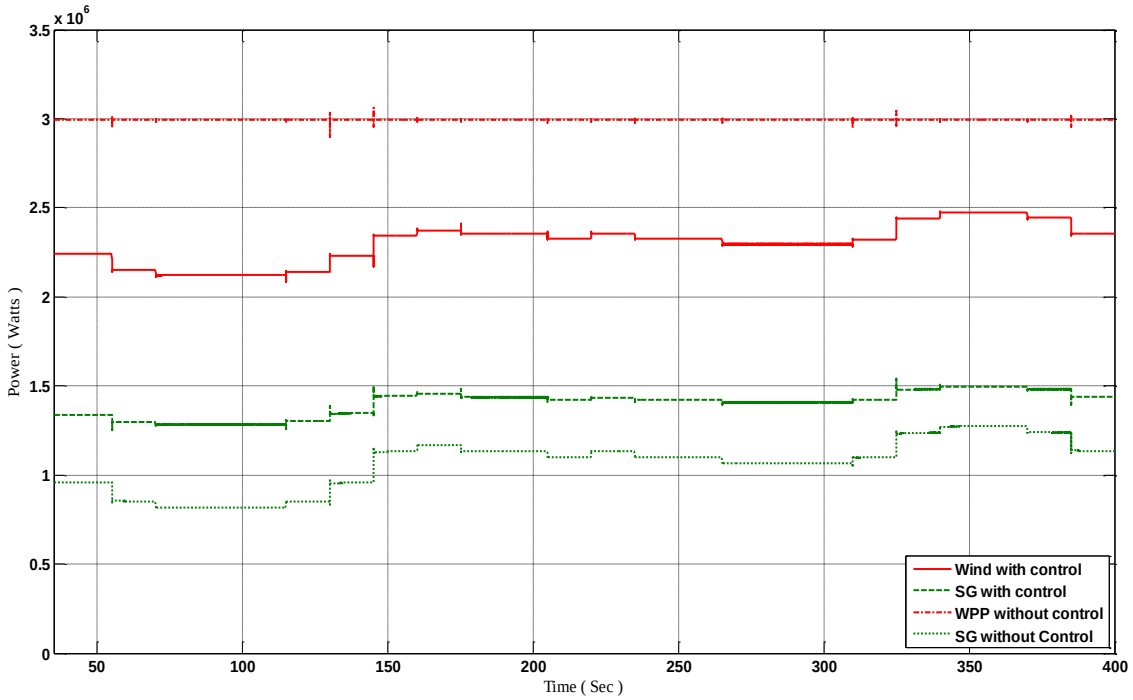

Figure 5.3. Active power output: SG at bus 1 and WPP at bus 2 for 60-40.

Since the wind power plant output changes with frequency deviations which is similar to synchronous generator output pattern, it confirms the required performance of the controller. For example, in Table 5.1, between the 130 sec and 115 sec interval, there is a load change of +0.3 MW which is shared between the 5 generators (WPP1: +0.09, WPP2 : +0.09, SG1: +0.04, SG2: +0.04, SG3: 0.04). Between the 175 sec and 160 sec interval, there is a load change of -0.1 MW which is shared between the 5 generators (WPP1: -0.014, WPP2 : -0.014, SG1: -0.024, SG2: -0.024, SG3: -0.024). Also, between the 190 sec and 205 sec intervals, there is no load change and hence no change in generation. Without control, the wind power plant operates at constant power and does not participate in load sharing and the load is only shared by synchronous generators Table 5.1(b). For example, in Table 5.1(b), between the 175 sec and 160 sec intervals, there is a load change of -0.1 MW which is shared between the 5 generators (WPP1: 0, WPP2 : 0, SG1: -0.033, SG2: -0.033, SG3: -0.033). Also, between the 190 sec and 175 sec intervals, there is no load change and hence no change in generation is observed. Similarly, between the 205 and 190 sec intervals, the load change is -0.1 MW which is shared between the generators as WPP1: 0, WPP2: 0, SG1: -0.033, SG2: -0.033, SG3: -0.033.

Table 5.1 Power flow snapshots for 40% wind penetration.

(a) Power flow snapshots for 40% wind penetration configuration with control for load data in intervals 6 through 12 in Table C.6.

Time	Wind power plant 1		Wind power plant 2		Synchronous Generator 1		Synchronous Generator 2		Synchronous Generator 3	
Sec	P - MW	Q - MVAR	P - MW	Q - MVAR	P – MW	Q - MVAR	P - MW	Q - MVAR	P - MW	Q – MVAR
115	2.14	-1.55	2.14	-1.4	1.31	0.885	1.31	1.152	1.31	1.05
130	2.23	-1.55	2.23	-1.42	1.35	0.88	1.35	1.158	1.35	1.03
145	2.37	-1.542	2.37	-1.4	1.43	0.868	1.42	1.164	1.43	1
160	2.394	-1.54	2.394	-1.4	1.444	0.862	1.444	1.164	1.444	0.99
175	2.38	-1.542	2.38	-1.4	1.42	0.868	1.42	1.164	1.42	1
190	2.38	-1.542	2.38	-1.4	1.42	0.868	1.42	1.164	1.42	1
205	2.36	-1.545	2.36	-1.4	1.4	0.87	1.4	1.163	1.4	1.01

Table 5.1 Power flow snapshots for 40% wind penetration.(contd.)

(a)Power flow snapshots for 40% wind penetration configuration with control for load data in intervals 6 through 12 in Table C.6.

Time	Total Generation		Voltage Bus 4	Total Load	Wind Speed
Sec	P – MW	Q – MVAR	V (pu)	P – MW	(m/s)
115	8.21	0.137	1.0257	7.8	12
130	8.51	0.098	1.0255	8.1	12
145	9.02	0.09	1.025	8.6	12
160	9.12	0.076	1.025	8.7	12
175	8.92	0.098	1.0254	8.6	12
190	9.02	0.09	1.0254	8.6	12
205	8.92	0.098	1.0255	8.5	12

(b)Power flow snapshots for 40% wind penetration configuration without control for load data in Table C.6.

Time	Wind power plant 1		Wind power plant 2		Synchronous Generator 1		Synchronous Generator 2		Synchronous Generator 3	
Sec	P - MW	Q - MVAR	P - MW	Q - MVAR	P – MW	Q - MVAR	P - MW	Q - MVAR	P – MW	Q - MVAR
115	3	0	3	0	0.883	-0.15	0.883	0.21	0.883	0.034
130	3	0	3	0	0.983	-0.1524	0.983	0.22	0.983	0.0375
145	3	0	3	0	1.15	-0.1575	1.15	0.23	1.15	0.043
160	3	0	3	0	1.183	-0.16	1.183	0.235	1.183	0.043
175	3	0	3	0	1.15	-0.16	1.15	0.23	1.15	0.04
190	3	0	3	0	1.15	-0.16	1.15	0.23	1.15	0.04
205	3	0	3	0	1.117	-0.1559	1.117	0.23	1.117	0.04

Table 5.1 Power flow snapshots for 40% wind penetration.(contd.)

(b) Power flow snapshots for 40% wind penetration configuration without control for load data in Table C.6. (contd.)

Time	Total Generation		Voltage Bus 1	Total Load	Wind Speed
(Sec)	P – MW	Q – MVAR	V (pu)	P – MW	(m/s)
115	8.65	0.094	1.049	7.8	12
130	8.95	0.1051	1.048	8.1	12
145	9.45	0.1155	1.047	8.6	12
160	9.549	0.118	1.047	8.7	12
175	9.45	0.11	1.0475	8.6	12
190	9.45	0.11	1.0475	8.6	12
205	9.351	0.1141	1.0478	8.5	12

5.3. MICROGRID STUDY

5.3.1. Wind and Load Variations from Texas. For this study, the test site #27, near Floydada, TX is selected. This site has a density of 12.7 MW/ Km^2 (Lat 34.06 °N, Long 101.08°W) in an area spread for 47.9 sq. km (location on map is shown in Appendix D). The wind speed data is taken from NREL website which was recorded in 2006. In this study, a randomly selected day (10^{th} day) is chosen for the month of January and the wind and load data for this particular date is studied. To get a better analysis of variability of the wind in contrast with the varying load, the load and wind data for 10^{th} day are also selected for the months of February to December. This selection takes care of the wind and load variability for that region for an entire year. Wind variability for this location used here can be seen in Figure 5.4 (a) and (b).

The wind variations used in this study are based on hourly data. A higher resolution data for wind is also available but hourly data is used to match the resolution of load data. The simulation period of the microgrid system for this study is set for 400 seconds and 24 variations in load and wind are simulated after every 15 seconds starting from 40 seconds mark. Fifteen seconds for a fluctuation is considered as sufficient response time for a governor to allow the frequency to stabilize. A droop of 1% is used for every generating plant in the microgrid.

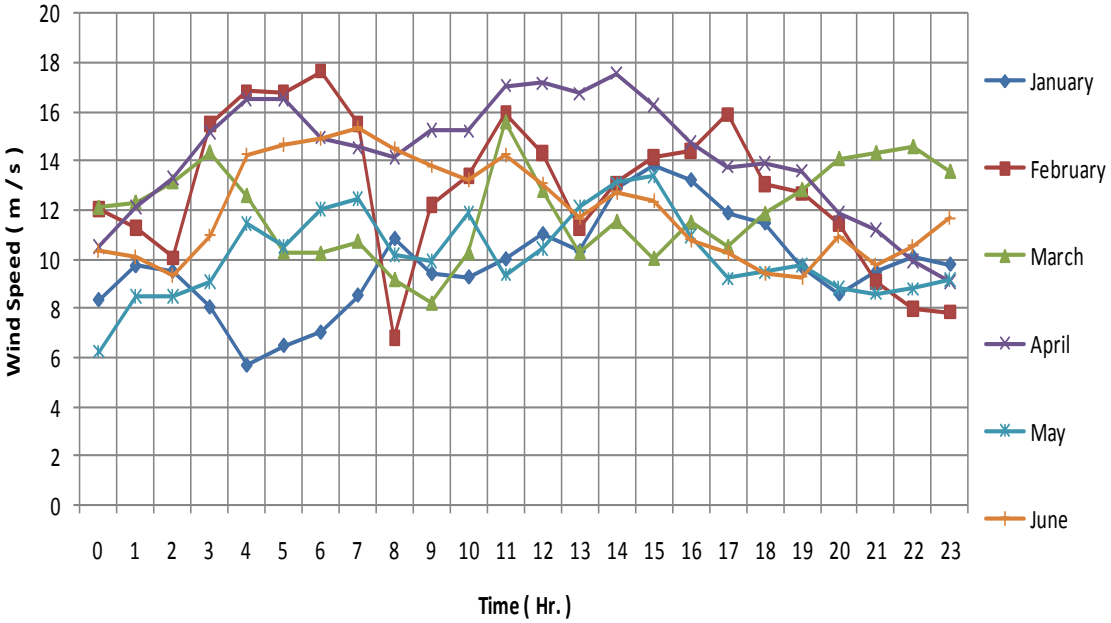

(a) Wind speed - January to June, Location : Floydada, Texas.

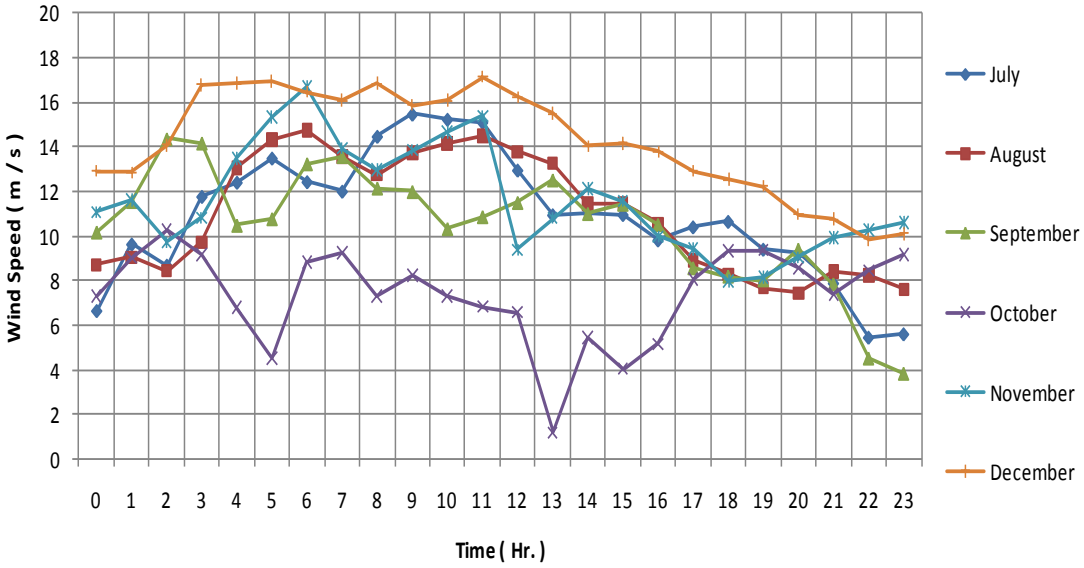

(b) Wind speed - July to December, Location : Floydada, Texas.

Figure 5.4 Wind speed variation- Location: Floydada, Texas.

The total load of the Texas system for 12 days is shown in Table 5.2 and plotted for better visualization in Figure 5.5. The load data is taken from ERCOT website for the North part of Texas [41]. The load data is scaled down to fit a scale of 0-13 MW retaining the load variations. The system has a maximum generation capacity of 15 MW. This system consists of two wind power plants and three synchronous generators as shown in the one line diagram of Figure 5.1.

Table 5.2: Hourly load data for the Floydada, Texas system.

Hr	Jan	Feb	Mar	Apr	May	Jun	July	Aug	Sep	Oct	Nov	Dec
00	9.3	9.4	7.9	8.1	8.6	10.3	9	9.8	9.2	8.6	8.1	9.1
01	9.6	9.2	7.7	7.7	8.1	9.5	8.5	9.5	8.7	8.2	7.8	9.1
02	9.6	9.2	7.6	7.5	8	9.1	8.2	9.2	8.4	7.9	7.7	9.1
03	9.6	9.2	7.7	7.4	7.8	8.9	8	8.9	8.3	7.8	7.7	9.1
04	9.7	9.2	7.8	7.4	7.9	8.8	7.8	8.8	8.3	7.7	7.7	9.1
05	9.7	9.3	7.9	7.4	7.9	8.8	7.8	8.7	8.3	7.7	7.8	9.2
06	9.8	9.8	8.3	7.5	8.1	8.8	7.9	8.7	8.5	7.6	8.1	9.6
07	9.8	10.3	9	7.7	8.7	9.2	8	9.1	9	7.7	8.6	10.1
08	10.1	10.5	9	7.8	8.9	9.3	8	9.4	9.3	7.8	8.7	10.3
09	10.3	10.1	8.8	8	8.9	9.6	8.3	9.6	9.3	8	8.6	9.9
10	10.1	9.9	8.7	8.2	9.2	10	8.6	10	9.5	8.1	8.6	9.6
11	10	9.7	8.6	8.3	9.4	10.4	9	10.6	9.7	8.3	8.5	9.4
12	9.6	9.4	8.4	8.5	9.7	11	9.4	11.1	10	8.5	8.6	9.2
13	9.5	9.1	8.3	8.6	10.1	11.4	9.8	11.5	10.3	8.7	8.5	9
14	9.1	9	8.2	8.7	10.3	11.9	9.9	12	10.7	8.8	8.5	8.9
15	9	8.8	8.1	8.7	10.4	12.3	10	12.3	11	9	8.4	8.7
16	8.8	8.8	8.1	8.8	10.6	12.8	10.2	12.6	11.5	9.3	8.4	8.7
17	8.8	9	8.1	8.9	10.8	13	10.2	12.7	11.7	9.6	8.4	8.7
18	9	9.3	8.1	8.9	10.8	13	10.2	12.7	11.6	9.6	8.5	8.9
19	9.6	9.7	8.3	8.8	10.8	12.5	10.2	12.7	11.5	9.5	8.9	9.3
20	10.2	10.1	8.8	8.8	10.6	12.1	10.1	12.5	11.1	9.4	9	9.4
21	10.2	10.3	9	9.1	10.6	11.8	10.1	12.3	10.9	9.4	9	9.4
22	10.2	10.1	8.8	9	10.5	11.5	10	11.9	10.6	9.2	8.9	9.3
23	9.8	9.7	8.6	8.8	9.7	11	9.6	11.3	10.1	9	8.6	9.1

This study performs simulations for different capacities of the wind power plants and the synchronous generators, based on a specific configuration of the generation mix.

The various configurations participating in this study are 90%-10%, 80%-20%, 70%-30%, 60%-40%, 50%-50% in the fashion of convention generation % - wind generation %. A total of 60 scenarios are simulated in this study with the wind power plants participating in voltage and frequency regulation functions. These 60 scenarios are compared with another set of 60 scenarios in which the wind power plants are operated without any frequency or voltage regulation capability. The wind power plant operating without any control/regulation is operated as a negative load and provides maximum possible active power from the wind without providing any frequency or voltage support.

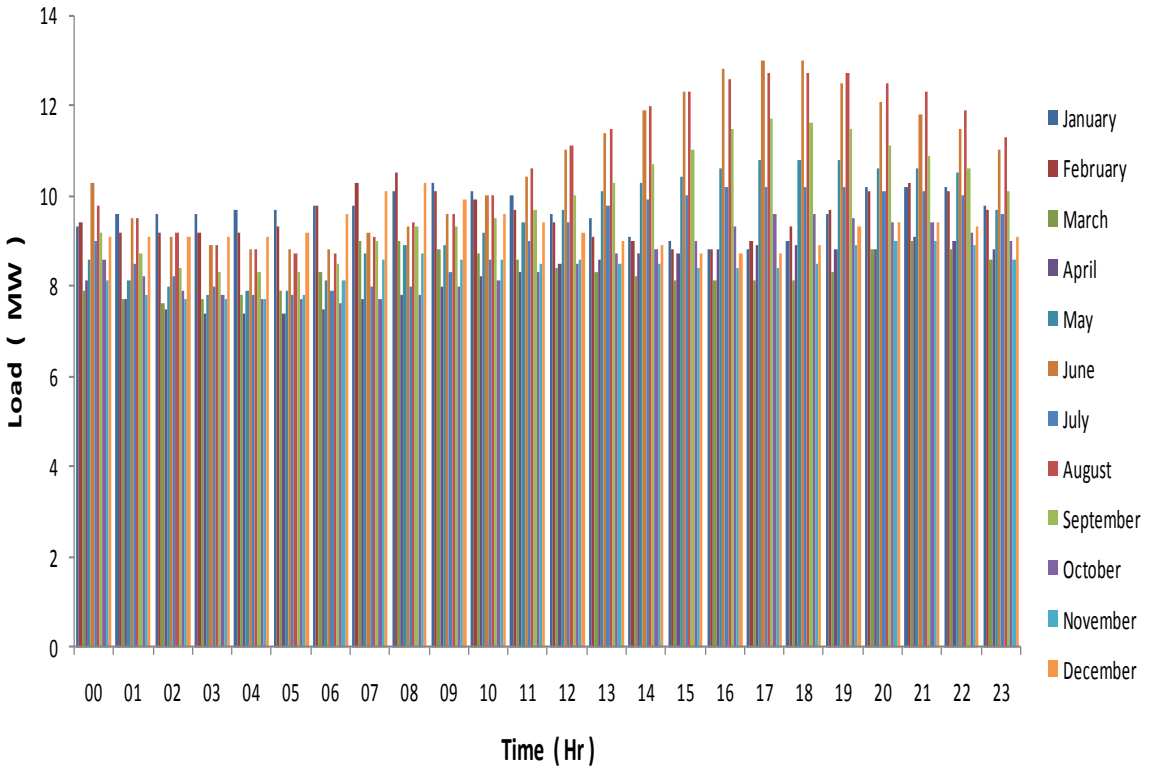

Figure 5.5: Hourly load variations - ERCOT.

To get a better view of the input data used in the simulations, one typical day in the month of June for the Floydada, Texas test location is shown in Figure 5.6 and 5.7. The figures show the load data with the amount wind received for the day.

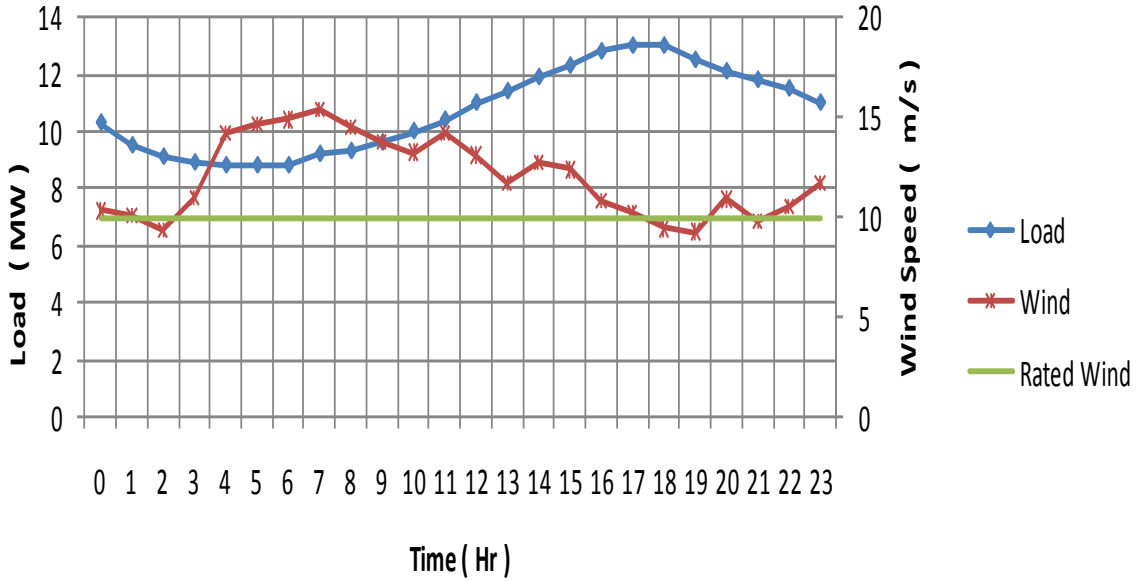

Figure 5.6 Wind vs load, June – Floydada, Texas.

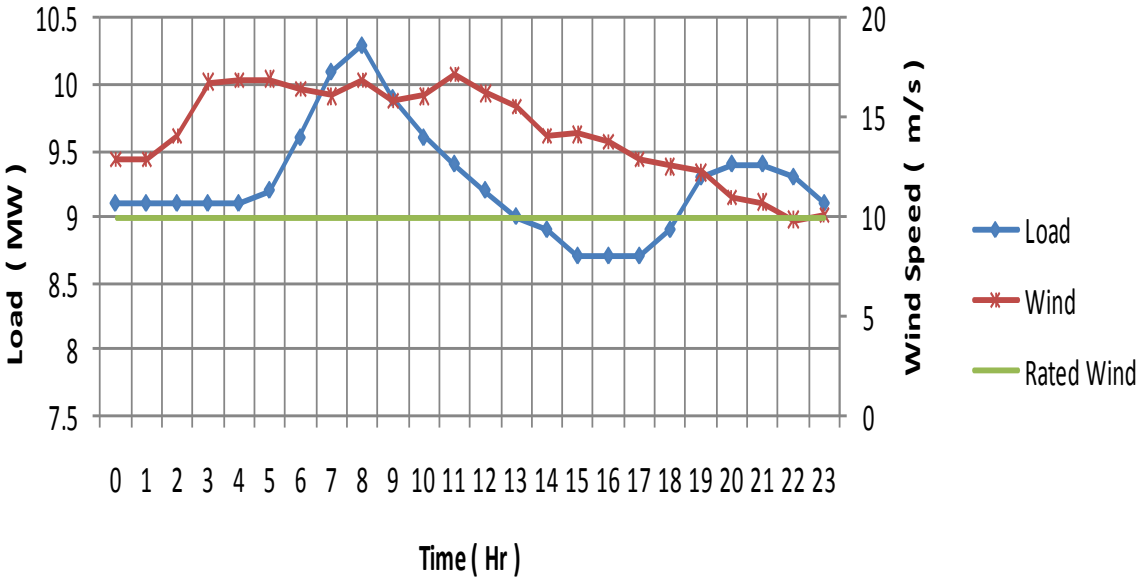

Figure 5.7 Wind vs load, December – Floydada, Texas.

5.3.2. Wind and Load Variations from California. The test site #12622 in the city of Fortuna near Sacramento, California is selected (40.24°N 124.36°W) (location on map is shown in Appendix D). The wind speed data is taken from NREL [42] which was recorded in 2006. For this location, a randomly selected day (15^{th}) is chosen for the month of January and the wind and load data for this particular date is studied. To keep the study similar to the Texas data, the 15^{th} day is also selected for the months of February to December. Wind variability for this location can be seen in Figure 5.8 (a) and (b).

The wind variations are also based on hourly data even though higher resolution data for wind is available but hourly data is used to match the resolution of the load data. All the parameters for the simulation are kept the same as before.

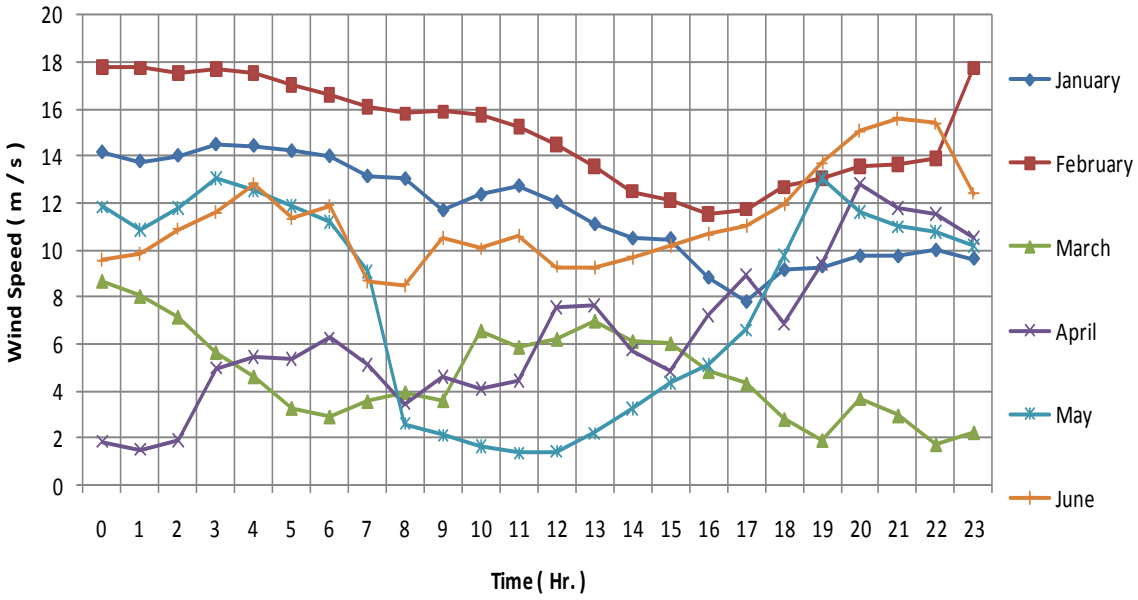

(a) Wind speed - January to June.

Figure 5.8. Wind speed variation- location: Fortuna, California.

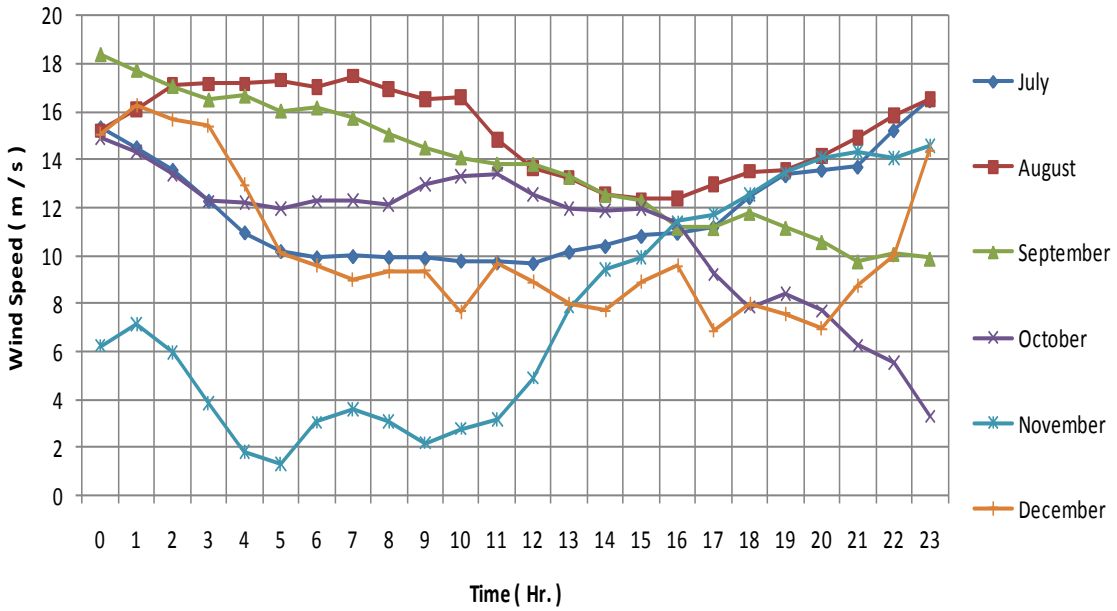

(b)Wind speed - July to December

Figure 5.8. Wind speed variation- location: Fortuna, California. (contd.)

The total load of the California system for 12 days is shown in Table 5.3 and plotted for better visualization in Figure 5.9. The load data is taken from Southern California Edison website [43]. Similar to the data from Texas, the load data is scaled down to fit a scale of 0-13 MW retaining the load variations.

Table 5.3. Hourly load data for the California system.

Hr	Jan	Feb	Mar	Apr	May	Jun	July	Aug	Sep	Oct	Nov	Dec
00	11.0	10.7	11.1	11.6	11.1	11.6	12.0	11.7	11.8	11.1	11.2	10.8
01	11.0	10.6	11.1	11.5	11.2	11.4	11.9	11.8	11.7	11.1	11.1	10.7
02	10.9	10.5	11.0	11.4	11.1	11.4	11.9	11.8	11.7	11.1	11.0	10.7
03	10.9	10.6	11.0	11.5	11.1	11.6	12.0	11.9	11.8	11.1	11.0	10.7
04	10.9	10.7	11.2	11.6	11.1	11.6	12.1	12.1	12.0	11.1	11.1	10.7
05	10.9	11.0	11.3	11.7	11.0	11.7	12.2	12.2	12.2	11.0	11.2	10.8
06	11.0	11.1	11.5	11.9	11.0	11.9	12.4	12.4	12.3	10.9	11.3	11.0
07	11.0	11.2	11.6	12.0	11.0	12.0	12.5	12.5	12.5	11.0	11.6	11.0
08	11.0	11.4	11.6	12.0	11.0	12.1	12.5	12.7	12.6	11.0	11.6	11.2
09	11.1	11.6	11.7	12.1	11.1	12.3	12.6	12.8	12.8	11.2	11.7	11.2
10	11.2	11.7	11.7	12.1	11.2	12.1	12.5	12.8	12.8	11.1	11.8	11.3
11	11.2	11.7	11.8	12.1	11.2	11.8	12.2	12.4	12.3	11.2	11.8	11.3
12	11.2	11.7	11.8	12.1	11.2	11.8	12.2	12.4	12.4	11.2	11.8	11.2
13	11.2	11.7	11.7	11.9	11.2	11.8	12.2	12.3	12.4	11.2	11.8	11.1
14	11.1	11.6	11.7	12.0	11.2	11.8	12.1	12.2	12.3	11.2	11.7	11.0
15	11.0	11.6	11.6	11.9	11.1	11.7	12.0	12.1	12.2	11.1	11.7	11.0
16	11.0	11.5	11.5	11.8	11.0	11.5	11.7	11.9	12.0	11.1	11.6	10.9
17	11.0	11.3	11.4	11.7	10.9	11.5	11.7	11.8	11.9	11.1	11.7	11.0
18	10.9	11.3	11.5	11.7	10.9	11.6	11.7	11.8	12.0	11.0	11.4	10.9
19	10.8	11.2	11.5	11.7	11.0	11.7	11.8	12.2	12.2	10.9	11.3	10.8
20	10.7	11.3	11.4	11.6	10.9	11.7	11.8	12.2	12.2	10.9	11.3	10.7
21	10.7	11.3	11.3	11.5	11.0	11.8	11.8	12.1	12.1	10.8	11.3	10.7
22	10.5	11.2	11.1	11.4	11.0	11.7	11.8	12.1	12.1	10.8	11.2	10.6
23	10.5	11.2	11.2	11.4	10.9	11.7	11.9	11.9	12.1	10.7	11.2	10.5

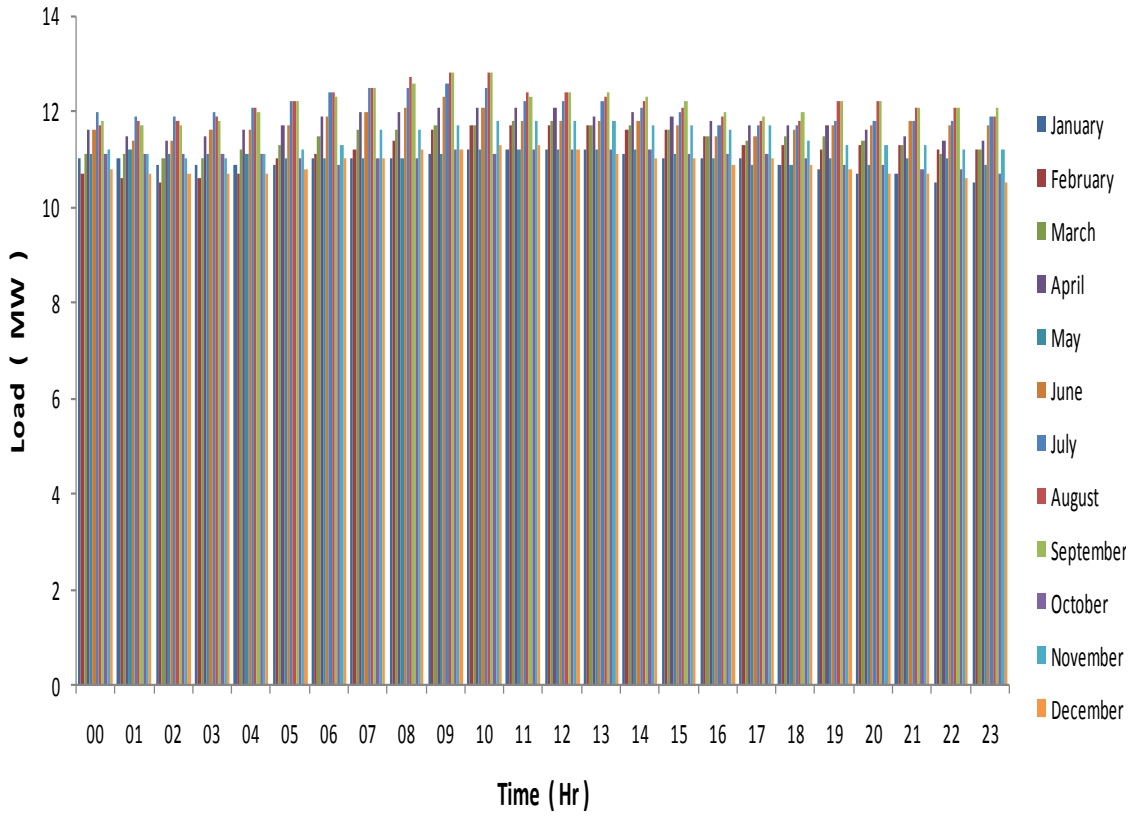

Figure 5.9. : Hourly load variations for location : Fortuna, California.

To get a better view of the input data used in the simulations, one typical day in the month of September for the Fortuna, California test location is shown in Figure 5.10 and 5.11. The figures show the load with the amount of wind received for the day

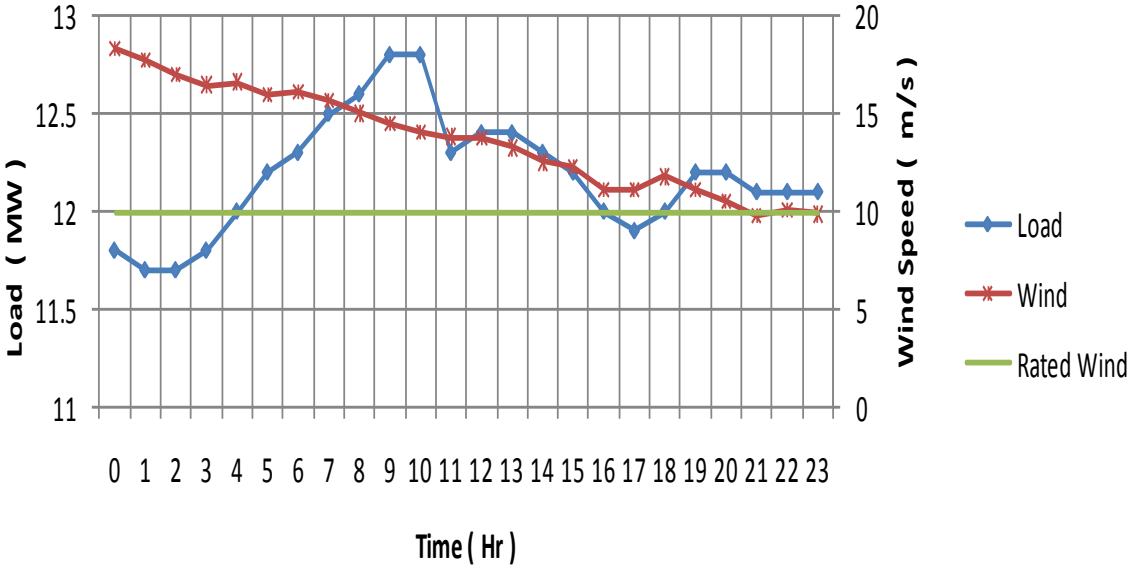

Figure 5.10 Wind vs load, September- Fortuna, California.

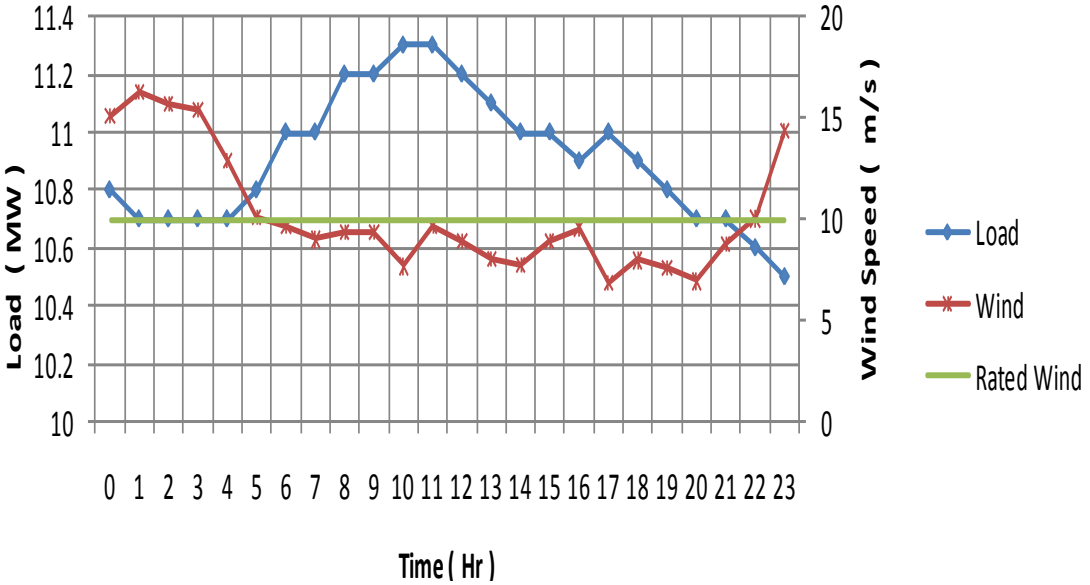

Figure 5.11 Wind vs load, December - Fortuna, California.

Wind speeds for the typical day in the month of December appear to be below the rated speed for most of the day when the load is high.

5.3.3. Study Methodology. The microgrid system is subjected to actual wind and load data from the two locations in Texas and California. The following methodology was followed to capture the results for this study

- Set up the input data for performing a dynamic analysis of the system for each of the twelve typical days in the year for the two locations mentioned above.
- Create five configurations of generation mix. The penetration of wind power is varied from 10% to 50 % while the rest of the generation is from conventional synchronous generators.
- The simulations are carried out first without any control of wind power plant and then repeated with the controls added to the wind power plants.
- Frequency, bus voltages, wind power plant rotor speed, output powers are recorded.
- Analyze the output data for acceptability.

5.3.4. Study Results. To quantify the results of this study, it is necessary to observe variations in voltage and frequency. Variations can be typically quantified by taking RMS or average values over a certain period of time.

For frequency, the results are quantified as per the following criteria [44]:

Criterion A: The frequency should be between ±2% from the nominal value for 95% of the time.

Criterion B: Frequency should not be less than ±15% of the nominal value at all times.

For voltage variations, the results would be quantified as per criterion 3 and 4.

Criterion C: The 1 second RMS value voltage should be in between 90% to 110% of the nominal value.

Criterion D: The 1 cycle RMS value voltage should be between 70% to 115% of the nominal value.

Tables 5.4 and 5.5 display the results of the study done for wind and load variations from the test location in Texas, and Tables 5.6 and 5.7 show the same for the location in California. Each simulation for every month and configuration is checked for the above mentioned 4 criteria. Successful completion of a criterion is displayed by a ✓ symbol and a ✗ symbol for failing a criterion. The third symbol ☑ express that although a

criterion is failed, it's failed by a small margin and can be made successful with some additional support.

Table 5.4. Study results for Floydada, Texas - January to June.

		90-10		80-20		70-30		60-40		50-50	
		WC	NC	WC	NC	WC	NC	WC	NC	WC	NC
January	A	✓	✓	✓	✓	☑	☑	×	×	×	×
	B	✓	✓	✓	✓	✓	✓	×	×	×	×
	C	✓	✓	✓	✓	✓	✓	✓	✓	✓	✓
	D	✓	✓	✓	✓	☑	☑	×	×	×	×
February	A	✓	✓	✓	✓	☑	×	×	×	×	×
	B	✓	✓	✓	✓	✓	✓	✓	✓	✓	×
	C	✓	✓	✓	✓	✓	✓	✓	✓	✓	✓
	D	✓	✓	✓	✓	✓	✓	✓	✓	✓	✓
March	A	✓	✓	✓	✓	✓	✓	✓	☑	✓	×
	B	✓	✓	✓	✓	✓	✓	✓	✓	✓	✓
	C	✓	✓	✓	✓	✓	✓	✓	✓	✓	✓
	D	✓	✓	✓	✓	✓	✓	✓	✓	✓	✓
April	A	✓	✓	✓	✓	✓	✓	✓	✓	✓	×
	B	✓	✓	✓	✓	✓	✓	✓	✓	✓	×
	C	✓	✓	✓	✓	✓	✓	✓	✓	✓	×
	D	✓	✓	✓	✓	✓	✓	✓	✓	✓	×
May	A	✓	✓	✓	✓	✓	✓	✓	☑	☑	×
	B	✓	✓	✓	✓	✓	✓	✓	✓	✓	✓
	C	✓	✓	✓	✓	✓	✓	✓	✓	✓	✓
	D	✓	✓	✓	✓	✓	✓	✓	✓	✓	☑
June	A	✓	✓	✓	✓	✓	✓	✓	✓	☑	×
	B	✓	✓	✓	✓	✓	✓	✓	✓	✓	✓
	C	✓	✓	✓	✓	✓	✓	✓	✓	✓	✓
	D	✓	✓	✓	✓	✓	✓	✓	✓	✓	✓

*WC – With Control NC --- No Control.

Table 5.5. Study results for Floydada, Texas – July to December.

		90-10		80-20		70-30		60-40		50-50	
		WC	NC	WC	NC	WC	NC	WC	NC	WC	NC
July	A	✓	✓	✓	✓	✓	✓	×	×	×	×
	B	✓	✓	✓	✓	✓	✓	☑	☑	×	×
	C	✓	✓	✓	✓	✓	✓	✓	✓	✓	✓
	D	✓	✓	✓	✓	✓	✓	✓	☑	☑	×
August	A	✓	✓	✓	✓	✓	✓	×	×	×	×
	B	✓	✓	✓	✓	✓	✓	✓	✓	×	×
	C	✓	✓	✓	✓	✓	✓	✓	✓	✓	✓
	D	✓	✓	✓	✓	✓	✓	✓	✓	✓	✓
September	A	✓	✓	✓	✓	☑	☑	×	×	×	×
	B	✓	✓	✓	✓	✓	✓	×	×	×	×
	C	✓	✓	✓	✓	✓	✓	✓	✓	✓	✓
	D	✓	✓	✓	✓	✓	✓	✓	✓	✓	✓
October	A	✓	✓	☑	☑	×	×	×	×	×	×
	B	✓	✓	✓	✓	✓	✓	✓	✓	☑	×
	C	✓	✓	✓	✓	✓	✓	✓	✓	✓	✓
	D	✓	✓	✓	✓	✓	✓	✓	✓	✓	✓
November	A	✓	✓	✓	✓	✓	☑	☑	×	☑	×
	B	✓	✓	✓	✓	✓	✓	✓	✓	✓	✓
	C	✓	✓	✓	✓	✓	✓	✓	✓	✓	✓
	D	✓	✓	✓	✓	✓	✓	✓	✓	✓	✓
December	A	✓	✓	✓	✓	✓	✓	✓	✓	✓	✓
	B	✓	✓	✓	✓	✓	✓	✓	✓	✓	✓
	C	✓	✓	✓	✓	✓	✓	✓	✓	✓	✓
	D	✓	✓	✓	✓	✓	✓	✓	✓	✓	✓

* WC – With Control NC --- No Control.

From Tables 5.4 and 5.5, it may be observed that with increased wind penetration of wind power, the overall reliability of the system decreases, but it can be improved by controlling the wind output. According to the test results for Floydada, Texas, wind participation played an instrumental role in improving the frequency and voltage fluctuations observed during islanded situation of the microgrid. The months of February, March, May, June and November clearly display an improved system owing to the wind

control. For the month of February, 30% wind penetration was not feasible with wind power operating on maximum power but with wind control, the frequency fluctuations were improved and the 30% wind penetration became possible with additional support. The same phenomenon may be observed for the months of March, May, June and November. It was observed that Floydada, Texas can comfortably handle a wind penetration of about 30% of the system with wind power controller involved. Without wind power control, the feasibility is reduced to 20% of wind penetration. Two examples of frequency comparison between 70-30 and 60-40 configuration for months of August and September are shown in Figures 5.12 (a) and (b) in support of the claim.

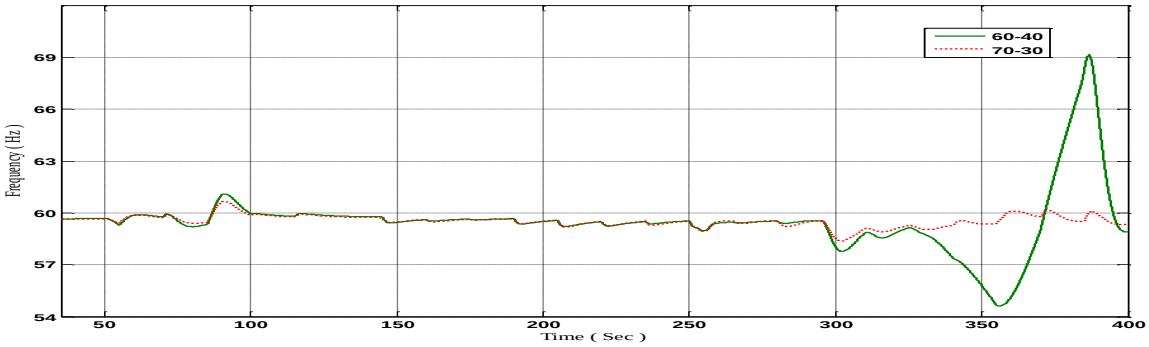

(a) Results of frequency response in August with 70-30 mix and 60-40 mix in Floydada, TX.

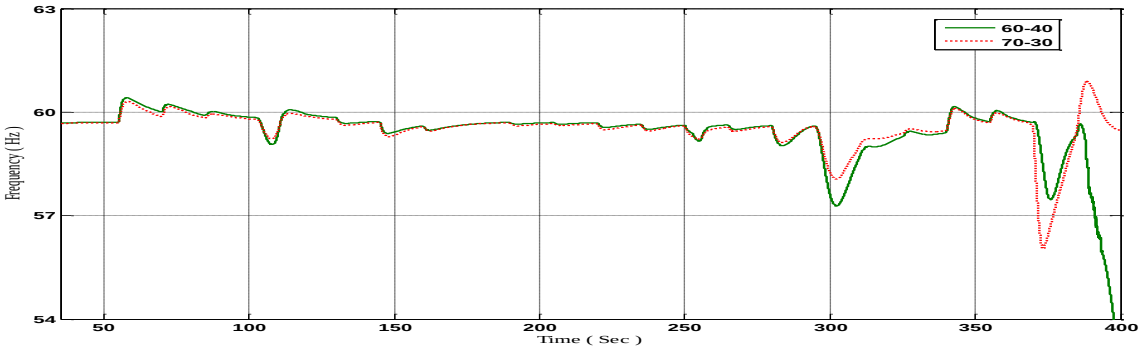

(b) Results of frequency response in September with 70-30 mix and 60-40 mix in Floydada, TX.

Figure 5.12 Frequency response August and Sept 70-30 & 60-40 (Floydada, TX).

Table 5.6. : Study results for Fortuna, California - January to June.

		90-10		80-20		70-30		60-40		50-50	
		WC	NC	WC	NC	WC	NC	WC	NC	WC	NC
January	A	✓	✓	✓	✓	✓	✓	✓	☑	☑	×
	B	✓	✓	✓	✓	✓	✓	✓	✓	✓	✓
	C	✓	✓	✓	✓	✓	✓	✓	✓	✓	✓
	D	✓	✓	✓	✓	✓	✓	✓	✓	✓	✓
February	A	✓	✓	✓	✓	✓	✓	✓	✓	✓	✓
	B	✓	✓	✓	✓	✓	✓	✓	✓	✓	✓
	C	✓	✓	✓	✓	✓	✓	✓	✓	✓	✓
	D	✓	✓	✓	✓	✓	✓	✓	✓	✓	✓
March	A	✓	✓	☑	☑	×	×	×	×	×	×
	B	✓	✓	✓	✓	×	×	×	×	×	×
	C	✓	✓	✓	✓	✓	✓	×	×	×	×
	D	✓	✓	✓	✓	☑	×	×	×	×	×
April	A	✓	✓	✓	✓	×	×	×	×	×	×
	B	✓	✓	✓	✓	×	×	×	×	×	×
	C	✓	✓	✓	✓	✓	✓	×	×	×	×
	D	✓	✓	✓	✓	✓	×	×	×	×	×
May	A	✓	✓	✓	✓	×	×	×	×	×	×
	B	✓	✓	✓	✓	×	×	×	×	×	×
	C	✓	✓	✓	✓	✓	✓	×	×	×	×
	D	✓	✓	✓	✓	✓	✓	×	×	×	×
June	A	✓	✓	✓	✓	✓	✓	✓	✓	✓	✓
	B	✓	✓	✓	✓	✓	✓	✓	✓	✓	✓
	C	✓	✓	✓	✓	✓	✓	✓	✓	✓	✓
	D	✓	✓	✓	✓	✓	✓	✓	✓	✓	✓

*WC – With Control NC --- No Control.

Table 5.7. Study results for Fortuna, California – July to December.

		90-10		80-20		70-30		60-40		50-50	
		WC	NC	WC	NC	WC	NC	WC	NC	WC	NC
July	A	✓	✓	✓	✓	✓	✓	✓	✓	✓	✓
	B	✓	✓	✓	✓	✓	✓	✓	✓	✓	✓
	C	✓	✓	✓	✓	✓	✓	✓	✓	✓	✓
	D	✓	✓	✓	✓	✓	✓	✓	✓	✓	✓
August	A	✓	✓	✓	✓	✓	✓	✓	✓	✓	✓
	B	✓	✓	✓	✓	✓	✓	✓	✓	✓	✓
	C	✓	✓	✓	✓	✓	✓	✓	✓	✓	✓
	D	✓	✓	✓	✓	✓	✓	✓	✓	✓	✓
September	A	✓	✓	✓	✓	✓	✓	✓	✓	✓	✓
	B	✓	✓	✓	✓	✓	✓	✓	✓	✓	✓
	C	✓	✓	✓	✓	✓	✓	✓	✓	✓	✓
	D	✓	✓	✓	✓	✓	✓	✓	✓	✓	✓
October	A	✓	✓	✓	✓	×	×	×	×	×	×
	B	✓	✓	✓	✓	✓	✓	☑	×	×	×
	C	✓	✓	✓	✓	✓	✓	✓	✓	✓	✓
	D	✓	✓	✓	✓	✓	✓	✓	✓	✓	✓
November	A	✓	✓	✓	☑	×	×	×	×	×	×
	B	✓	✓	✓	✓	×	×	×	×	×	×
	C	✓	✓	✓	✓	×	×	×	×	×	×
	D	✓	✓	✓	✓	×	×	×	×	×	×
December	A	✓	✓	✓	✓	☑	×	×	×	×	×
	B	✓	✓	✓	✓	✓	✓	✓	✓	✓	✓
	C	✓	✓	✓	✓	✓	✓	✓	✓	✓	✓
	D	✓	✓	✓	✓	✓	✓	✓	✓	✓	✓

*WC – With Control NC --- No Control.

For the test location in California, it can be seen that this location cannot commit to wind penetration of 30% with adequate system reliability. The wind is highly intermittent in this location and this location can handle only up to 20% of wind penetration. Although wind is highly intermittent in this location, the simulation results replicate the advantages of having wind power control from the smoothening of frequency and voltage fluctuations.

5.3.5. Observations. The various observations noticed in the study are listed in this section. These observations display the effects of voltage and frequency regulation by wind power.

5.3.5.1 Effect of wind participation on frequency. Figure 5.13 displays the frequency response of the simulation done with 60% conventional -40% wind (referred to as 60-40) as the configuration for the month of November for the Texas test location. This frequency response shows a comparison of frequencies between the scenarios when the wind power control is utilized and the one without it. Another similar example, taken from the simulation studies of Fortuna, CA is displayed in Figure 5.14.

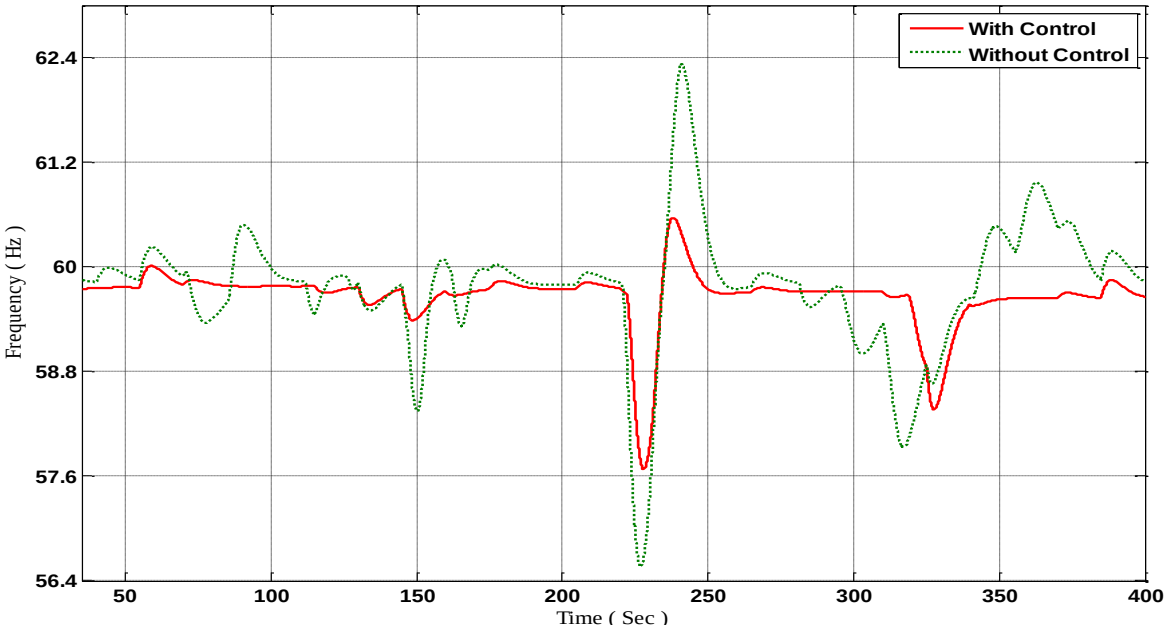

Figure 5.13. Frequency response - November 60-40, Location: Floydada, Texas.

It is observed that the frequency response with wind power control present complies with *Criteria A and B,* but the system without the controller violates the first criterion. Although, in the process, around 12% of wind power is lost. The variation of wind power for the scenarios mentioned above is displayed in Figure 5.14. In this figure, the power response with wind power control starts producing power as per the predefined

value of hysteresis high as discussed in Section 4 which is 75% of the rated power. i.e. 2.25 MW (75% of 3 MW). The output of wind power changes according to the load variations to reduce the frequency fluctuations as shown in Figure 5.13. At around 1 PM (220 sec mark in Figure 5.14) the wind speed drops and hence the wind power output is also reduced. The controller allows the wind power plant to follow the maximum power point until adequate amount of wind speed is available. At 2 PM (235 time mark in Figure 5.14), adequate amount of wind speed is available; hence the controller starts driving the power output according to the requirements. The wind power plant without the controller always operates at the maximum power point. Due to this type of operation, spikes in frequency may be observed in Figure 5.13.

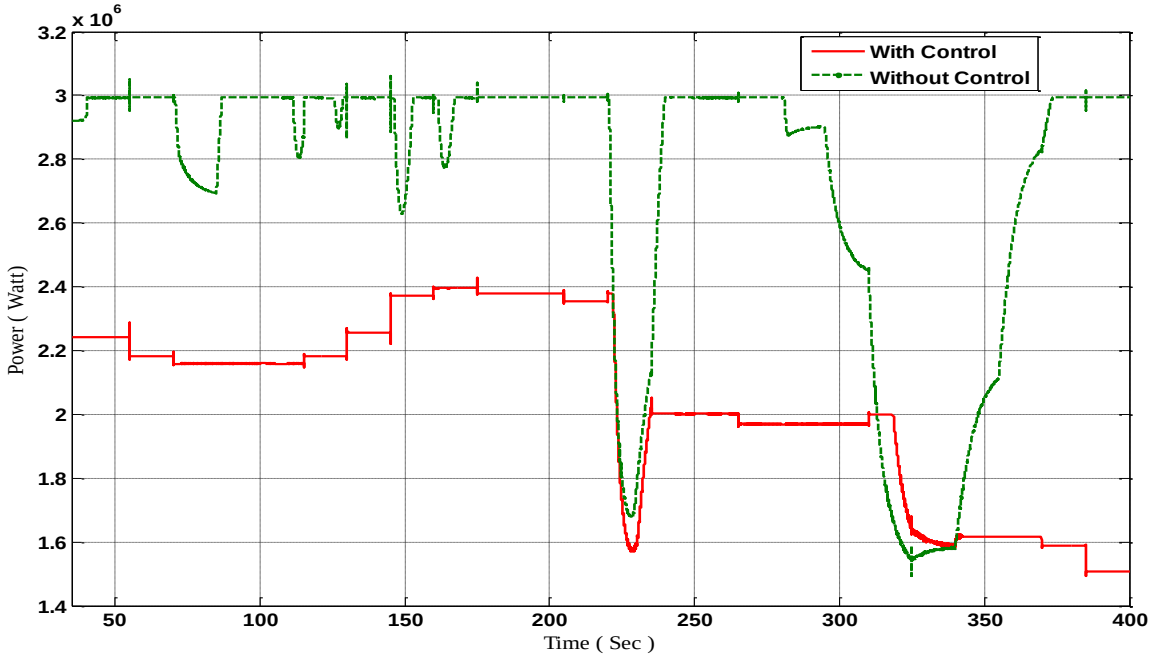

Figure 5.14: Wind power response – November 60-40, Location: Floydada, Texas.

Power flow snapshots for November 60-40 (Floydada, TX) at five points in the simulation time is tabulated in Tables 5.8 and 5.9.These simulation points corresponds to the hourly change of wind and load data. For example, the 175 sec interval corresponds to the wind and load data at 9AM. Similarly, the 190 sec interval represents 10 AM, and

so on. The table consists of the power generations at the generator buses 1, 2, 3, 7 and 9. It is observed that the power balance equation of the system is satisfied. For example, in the second part of Tables 5.9 and 5.10, one can see that the total generation of active power has the same difference between consecutive intervals as compared to the load change during the same interval. Individually, the participation is quantified as follows: From Table 5.8, the load change between the intervals 145 sec and 160 sec is +0.1 MW which is shared between the 5 generators (WPP1: +0.02, WPP2: +0.02, SG1: +0.02, SG2: +0.02, SG3: +0.02). Also, between the 175 sec and 190 sec intervals, there is no load change and hence no change in generation. Similarly between the 205 sec and 190 sec intervals, the load change is -0.1 MW which is shared between the generators as WPP1: -0.026, WPP2: -0.026, SG1: -0.016, SG2: -0.016, SG3: -0.016. When there is no control of wind power plants in the system, it is operated at the maximum possible operating point allowed by the prevailing wind speed, WPP1 and WPP2 do not show any load participation and are therefore constant throughout all load changes as shown in Table 5.9. All the load changes are shared between the three synchronous generators.

The voltage is maintained at 1.0255 pu and 1.026 pu at bus 4 in the system with control and without control respectively as shown in Tables 5.8 and 5.9. Comparing the total reactive power generation for maintaining the voltage at Bus 4, it can be observed in Tables 5.8 that between the 160 sec and 175 sec interval, decrease in reactive power by0.5 KVAR was shared by the generators as WPP1: -2, WPP2: -5, SG1: +6, SG2: -0.5, SG3: 0. Also, between 190 and 205 sec interval, one can see that a reactive power increase of 3 KVAR was shared by the generators as WPP1: -3, WPP2: -5, SG1: +2, SG2: -1, SG3: +10. Reactive power is shared between the 5 generators to maintain their terminal voltages respectively. Comparing with the case without control, it can be seen that the synchronous generators had to produce large amounts of reactive power to support the microgrid voltage without the support from the wind power plants.

Table 5.8 Power flow snapshots- November 60-40 (WC), Floydada, TX.

Time	Wind power plant 1		Wind power plant 2		Synchronous Generator 1		Synchronous Generator 2		Synchronous Generator 3	
(Sec)	P	Q	P	Q	P	Q	P	Q	P	Q
145	2.375	-1.542	2.375	-1.4	1.425	0.868	1.425	1.1645	1.425	1
160	2.395	-1.54	2.395	-1.395	1.445	0.862	1.445	1.1645	1.445	1
175	2.381	-1.542	2.381	-1.4	1.421	0.868	1.421	1.164	1.421	1
190	2.381	-1.542	2.381	-1.4	1.421	0.868	1.421	1.164	1.421	1
205	2.355	-1.545	2.355	-1.405	1.405	0.87	1.405	1.163	1.405	1.01

Time	Total Generation		Voltage Bus 4	Total Load	Wind Speed
(Sec)	P	Q	V (pu)	P	(m/s)
145	9.025	0.0905	1.025	8.6	12.947
160	9.125	0.0905	1.025	8.7	13.853
175	9.025	0.09	1.0254	8.6	14.644
190	9.025	0.09	1.0254	8.6	15.381
205	8.925	0.093	1.0255	8.5	9.376

Table 5.9 Power flow snapshots- November 60-40 (NC), Floydada, TX.

Time	Wind power plant 1		Wind power plant 2		Synchronous Generator 1		Synchronous Generator 2		Synchronous Generator 3	
Sec	P – MW	Q - MVAR	P - MW	Q - MVAR	P - MW	Q - MVAR	P - MW	Q – MVAR	P – MW	Q - MVAR
145	3	0	3	0	1.015	0.94	1.055	1.24	1.015	1.052
160	3	0	3	0	1.055	0.92	1.055	1.225	1.055	1.051
175	3	0	3	0	1.02	0.925	1.02	1.22	1.02	1.051
190	3	0	3	0	1.02	0.925	1.02	1.22	1.02	1.051
205	3	0	3	0	0.977	0.935	0.977	1.225	0.977	1.052

Table 5.9 Power flow snapshots- November 60-40 (NC), Floydada, TX (contd.).

Time	Total Generation		Voltage Bus 4	Total Load	Wind Speed
(Sec)	P - MW	Q - MVAR	V (pu)	P - MW	(m/s)
145	9.085	3.232	1.026	8.6	12.947
160	9.165	3.196	1.0258	8.7	13.853
175	9.06	3.196	1.0259	8.6	14.644
190	9.06	3.196	1.0259	8.6	15.381
205	8.931	3.212	1.026	8.5	9.376

Another example for this observation is shown in Figures 5.15 and 5.16. These two figures are taken from simulation studies done for Fortuna, California.

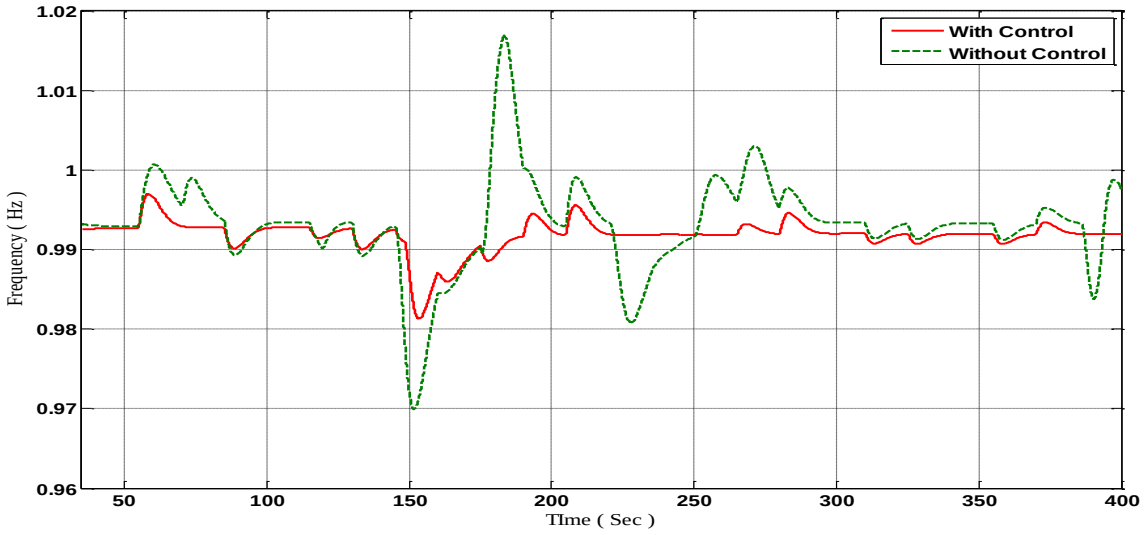

Figure 5.15. Frequency response - June 70-30, Location: Fortuna, California.

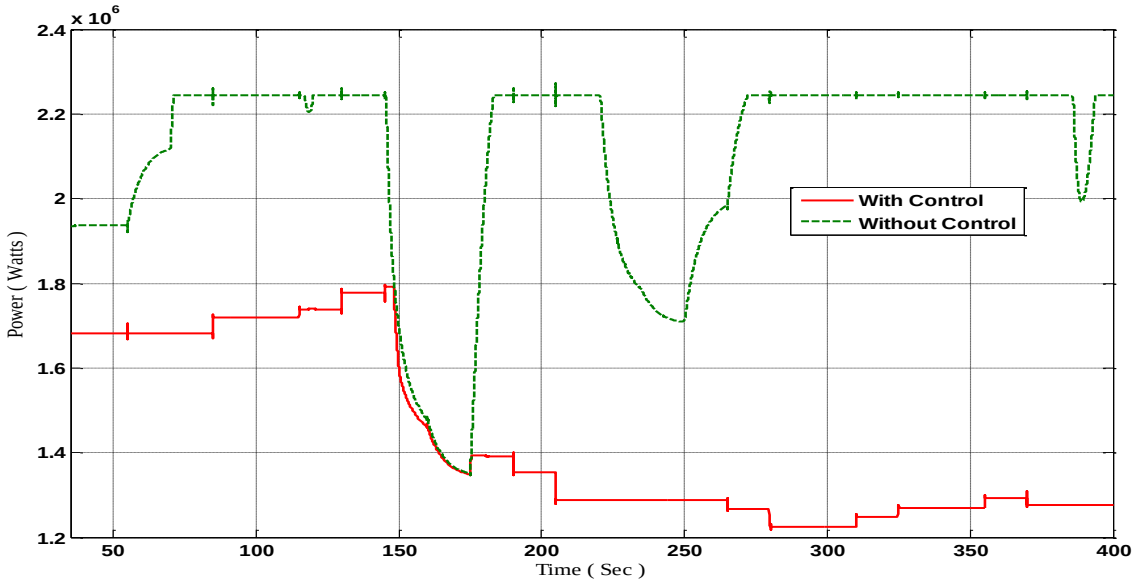

Figure 5.16. Wind power response – June 70-30, Location: Fortuna, California.

Power flow snapshots for the 70-30 configuration in June for Fortuna, CA for 5 points in the simulation time are shown in Tables 5.10 and 5.11. The table consists of the power generations at the generator buses 1, 2, 3, 7 and 9 (synchronous generator and wind power plant). This table confirms the balance between the generation and the load. This table provides information on the sharing of loads between the 5 generators. For example, in Table 5.10, between the 175 sec and 160 sec intervals, there is a load change of +0.2 MW which is shared between the 5 generators as: WPP1: +0.04, WPP2: +0.04, SG1: +0.04, SG2: +0.04, SG3:+0.04. Also, between the 190 sec and 175 sec intervals, there is a load change of -0.2 MW which is shared between the 5 generators as: WPP1: -0.04, WPP2: -0.04, SG1: -0.04, SG2: -0.04, SG3: -0.04. Similarly between the 205 and 190 sec intervals, the load change is -0.3MW which is shared between the generators as WPP1: -0.06, WPP2: -0.06, SG1: -0.06, SG2: -0.06, SG3: -0.06. When there is no control of wind power plants in the system, it is operated at the maximum possible power point as dictated by the wind speeds and WPP1 and WPP2 do not show load participation and therefore remain constant throughout all the load changes as shown in Table 5.11. In that case, all load changes are shared between the three synchronous generators.

Table 5.10 Power flow snapshots- 70-30 (WC) in June, (Fortuna, CA).

Time	Wind power plant 1		Wind power plant 2		Synchronous Generator 1		Synchronous Generator 2		Synchronous Generator 3	
Sec	P – MW	Q – MVAR	P – MW	Q - MVAR	P – MW	Q - MVAR	P – MW	Q - MVAR	P – MW	Q - MVAR
145	1.46	-1.05	1.46	-0.9	3.19	0.448	3.19	0.96	3.19	0.675
160	1.36	-1.02	1.36	-0.87	3.29	0.42	3.29	0.94	3.29	0.651
175	1.4	-1	1.4	-0.86	3.33	0.405	3.33	0.94	3.33	0.644
190	1.36	-1.02	1.36	-0.87	3.29	0.42	3.29	0.94	3.29	0.655
205	1.3	-1.025	1.3	-0.885	3.23	0.43	3.23	0.94	3.23	0.66

Time	Total Generation		Voltage Bus 4	Total Load	Wind Speed
Sec	P – MW	Q – MVAR	V (pu)	P – MW	(m/s)
145	12.49	0.133	1.0218	12	8.66
160	12.59	0.121	1.0212	12.1	8.5
175	12.79	0.129	1.0209	12.3	10.5
190	12.59	0.125	1.0212	12.1	10.06
205	12.29	0.12	1.0216	11.8	10.6

Table 5.11 Power flow snapshots- 70-30 (NC) in June, (Fortuna, CA).

Time	Wind power plant 1		Wind power plant 2		Synchronous Generator 1		Synchronous Generator 2		Synchronous Generator 3	
Sec	P – MW	Q - MVAR	P – MW	Q - MVAR	P - MW	Q - MVAR	P – MW	Q - MVAR	P – MW	Q – MVAR
160	1.478	0	1.478	0	3.25	-0.255	3.25	0.35	3.25	0.04
175	1.36	0	1.36	0	3.37	-0.26	3.37	0.355	3.37	0.04
190	2.24	0	2.24	0	2.87	-0.26	2.87	0.372	2.87	0.051
205	2.244	0	2.244	0	2.8	-0.256	2.8	0.365	2.8	0.05
220	2.243	0	2.243	0	2.71	-0.248	2.71	0.354	2.71	0.05

Table 5.11 Power flow snapshots- 70-30 (NC) in June, (Fortuna, CA) (contd.)

Time	Total Generation		Voltage Bus 4	Total Load	Wind Speed
Sec	P – MW	Q – MVAR	V (pu)	P – MW	(m/s)
160	12.706	0.135	1.0321	12	8.66
175	12.83	0.135	1.031	12.1	8.5
190	13.09	0.163	1.036	12.3	10.5
205	12.888	0.159	1.037	12.1	10.06
220	12.616	0.156	1.078	11.8	10.6

Comparing the total generation of reactive power to maintain the voltage at Bus 4as seen in Tables 5.10, it can be observed that between the 190 sec and 175 sec interval, a change in reactive power by -4 KVAR is shared by the generators as WPP1: -20, WPP2: -10, SG1: +15, SG2: 0, SG3: +11 . Also, between 160 and 175 sec interval, one can see that a reactive power change of +8 KVAR was shared by the generators as WPP1: +20, WPP2: +10, SG1: -15, SG2: 0, SG3: -7. The reactive power is shared between the 5 generators to maintain their terminal voltages respectively. In the case of no control all the reactive power required is generated by the synchronous generators.

5.3.5.2 Variation of frequency with configurations. This subsection is instrumental in highlighting the frequency variations for different configurations having different levels of wind power penetration. The configurations used in this subsection are 80-20 (meaning 80% conventional and 20% wind power generation), 70-30, 60-40, 50-50 as shown in Figure 5.17.

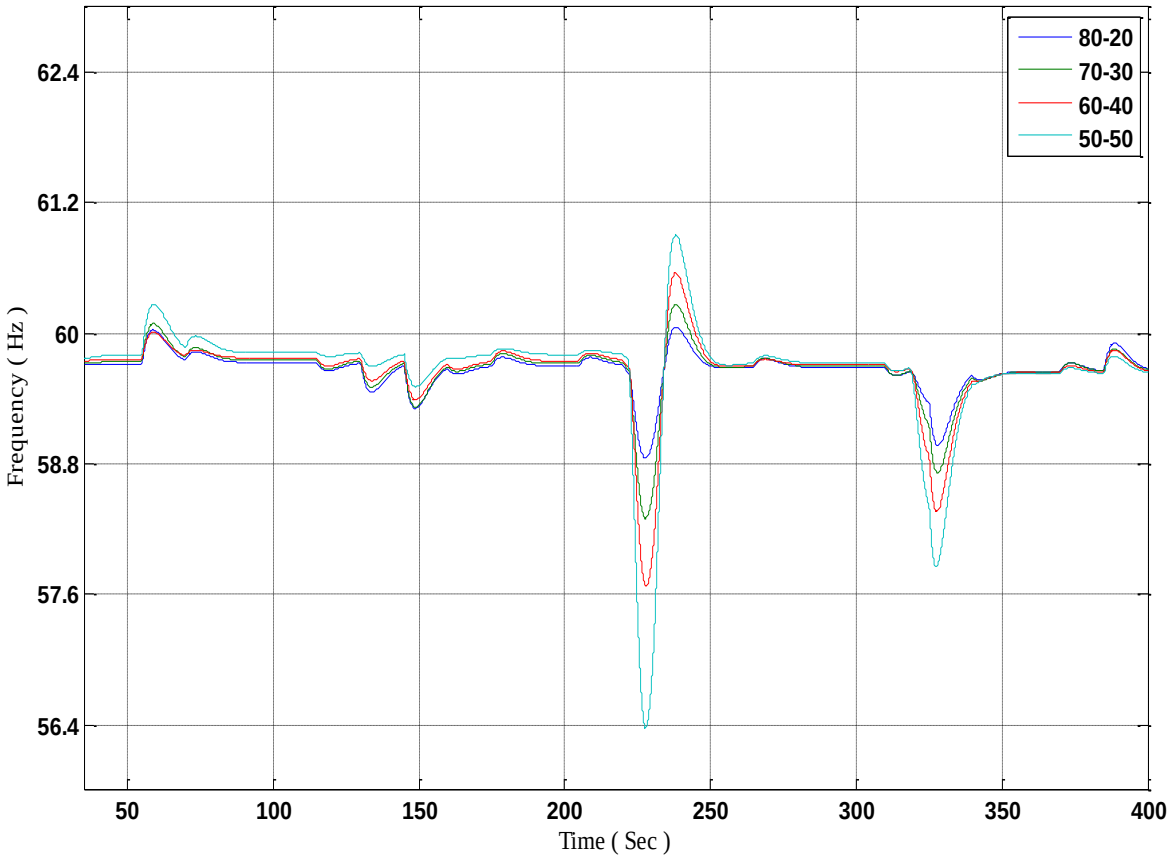

Figure 5.17: Frequency variation - WC November, Location: Floydada, Texas.

It can be observed from Figure 5.17 that increasing wind penetration results in increased fluctuations. This is due to the increased dependence on wind which creates a power balance deficiency because of the intermittency of wind. Although increased wind penetration creates frequency fluctuations, the wind plant control tries to smooth out the frequency fluctuations whenever there is an adequate supply of wind. The comparison can be done by comparing Figures 5.17 and 5.18. In Figure 5.18, the system is operating without any wind power control. The frequency fluctuations tend to spike in both positive and negative directions, which in turn results in violation of both the frequency limits.

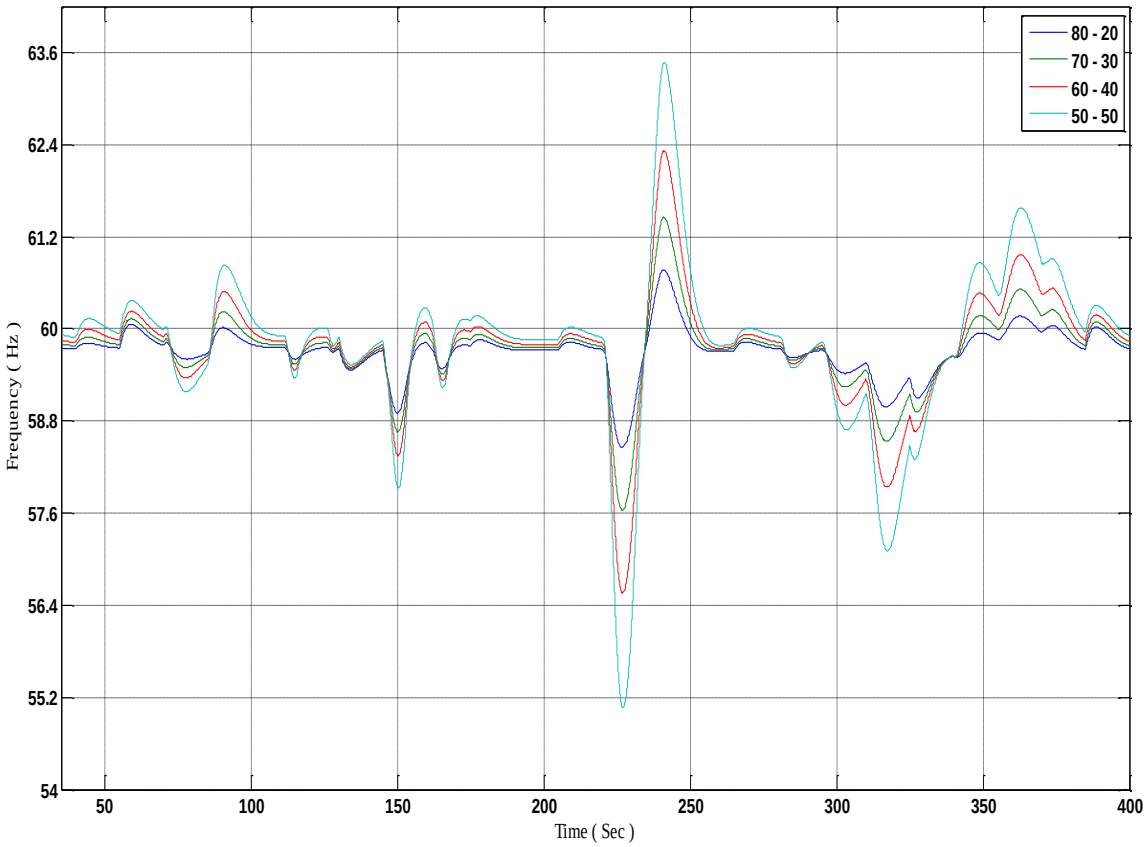

Figure 5.18: Frequency variation- NC November, Location: Floydada, Texas.

A similar example for the test location in Fortuna, California is recorded in Figures 5.19 and 5.20.

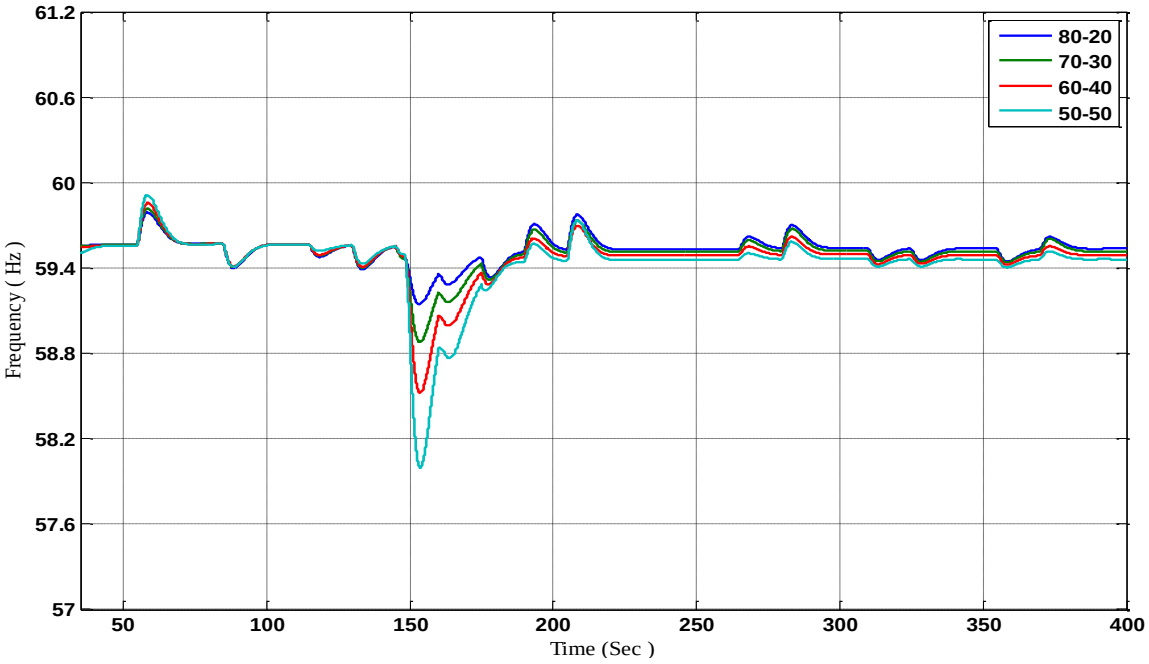

Figure 5.19: Frequency variation- WC June, Location: Fortuna, California.

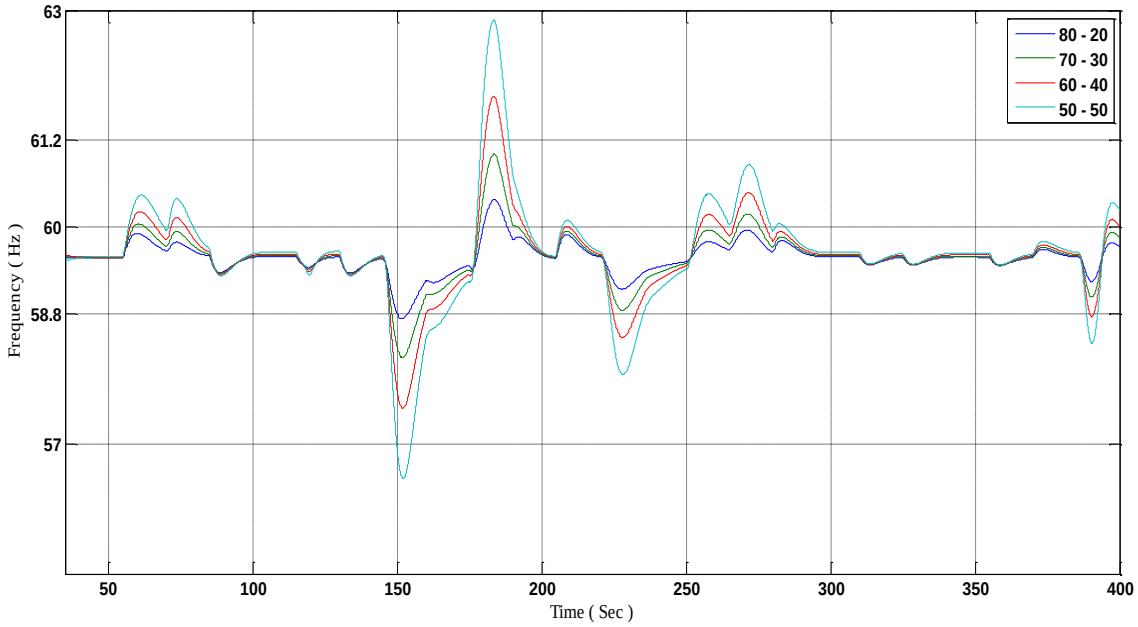

Figure 5.20: Frequency variation- NC June, Location: Fortuna, California.

5.3.5.3 Voltage profile variations with reactive power contribution. This subsection highlights the effects of voltage regulation in the microgrid by wind power plants. In the grid connected mode, the wind turbine provides voltage regulation by providing the commanded reactive power. But in islanded mode, the wind power plant supports the microgrid by maintaining its terminal voltage to a set point. In this part, the effect on voltage profile in islanded mode is displayed in comparison with a system not participating in voltage control. Figure 5.21 shows the effect of wind power support on the voltage profile.

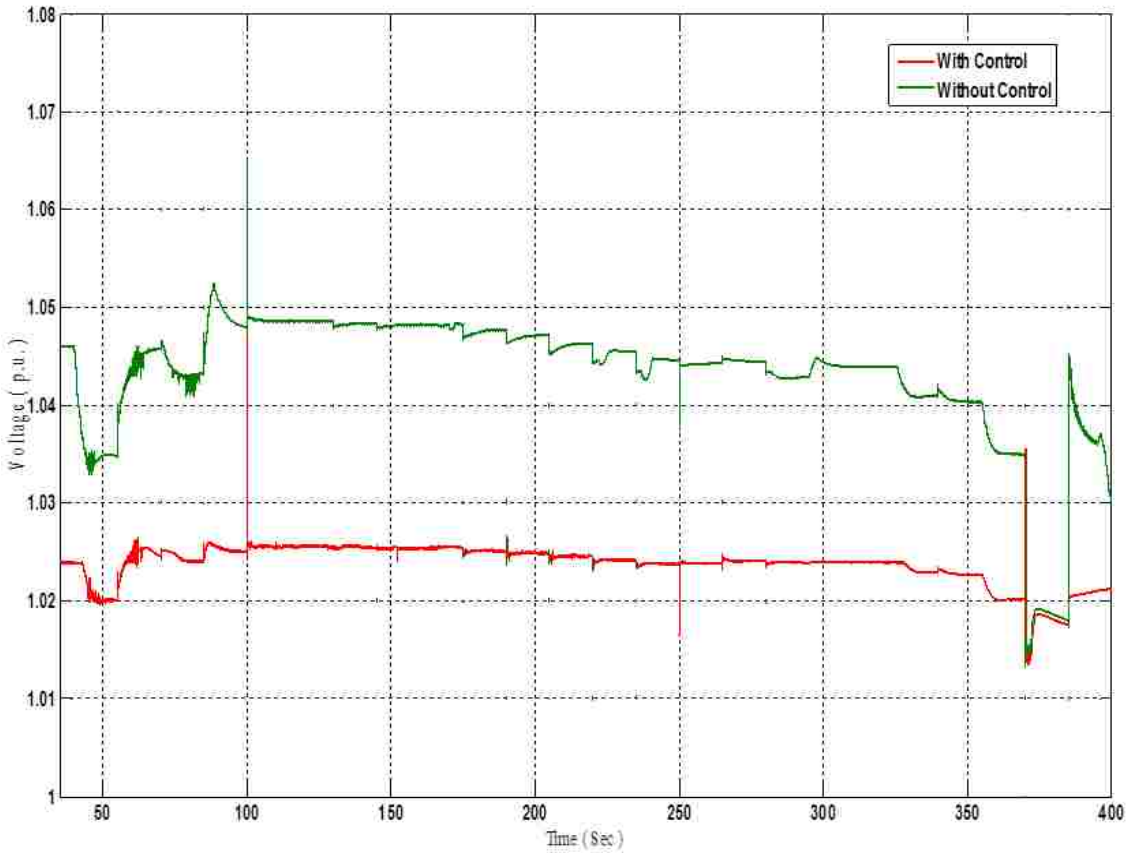

Figure 5.21: Voltage profile- Floydada, Texas July 60-40 WC & NC.

From Figure 5.21, it is evident that having wind power plants to support the microgrid keeps the voltage in check. The amount of reactive power contributed to support voltage profile is displayed in Figure 5.22. The controller commands the wind power plant to maintain the terminal voltage at 1 pu and to maintain the voltage, the wind power plant starts absorbing around 1.4 MVAR of reactive power as long as adequate amount of wind is available. The wind power plant is cut off from the microgrid on account of low wind speeds. At 11 PM (370 sec mark in Figure 5.22), the wind speed suddenly drops forcing the wind power plant to trip and stop absorbing reactive power from the grid. The active power production is also reduced to zero.

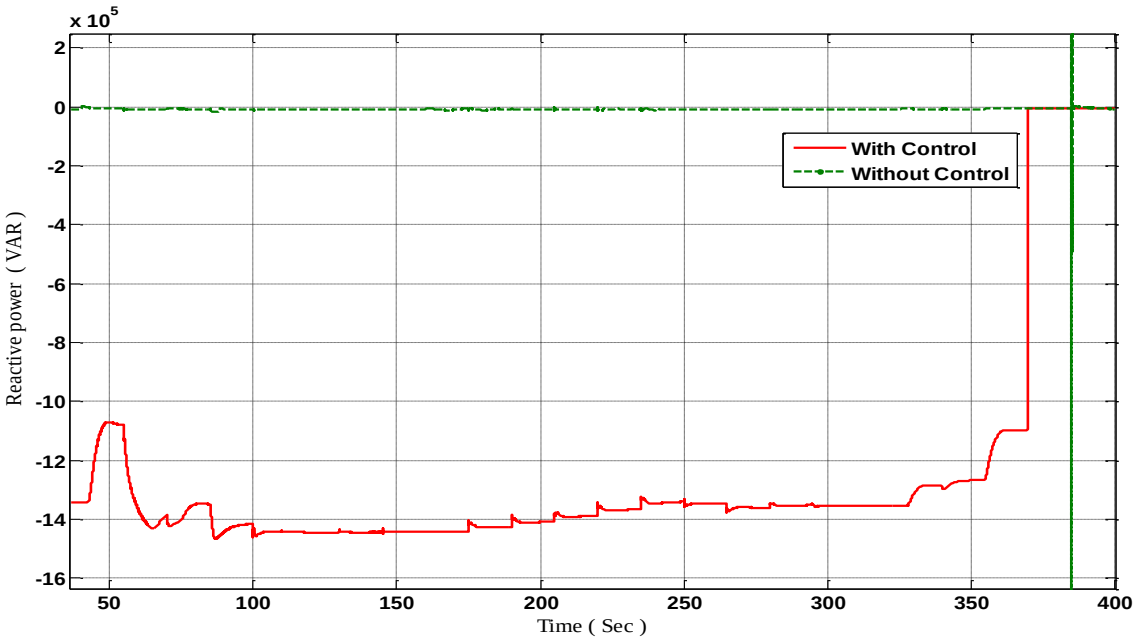

Figure 5.22: Wind reactive power contribution- Floydada, July 60-40 WC & NC.

Similar example for Fortuna, California is noted in Figure 5.23 and Figure 5.24.

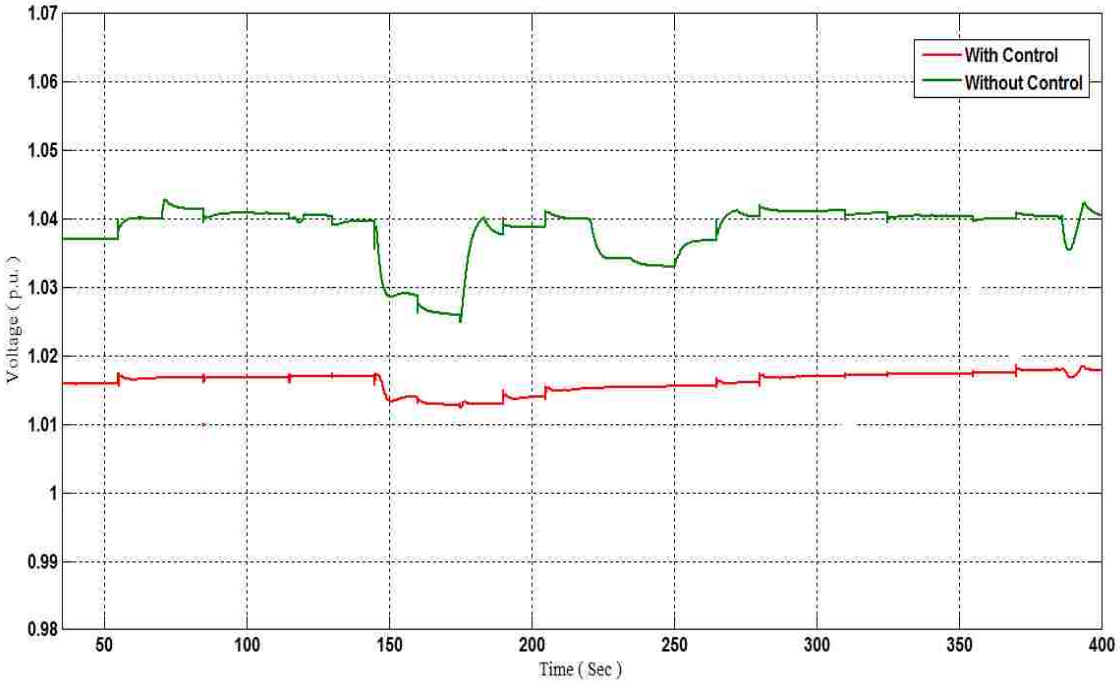

Figure 5.23: Voltage profile- Fortuna, California June 70-30 WC & NC.

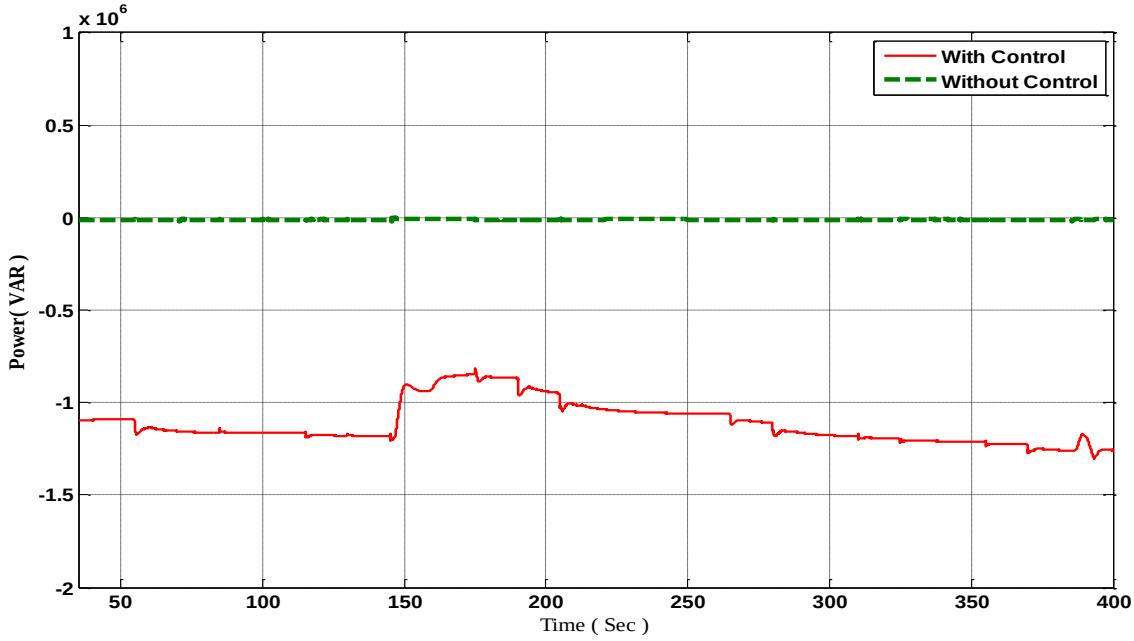

Figure 5.24: Wind reactive power contribution –Fortuna, California June 70-30.

Figure 5.23 also displays similar operation of wind power plant as Figure 5.21. By absorbing reactive power from the system the wind power plant tries to reduce the voltage to its set value of 1 p.u.. To maintain the voltage the wind power plant absorbs almost 1.3 MVAR of reactive power. The reduction of voltage to almost 1.015 p.u. from 1.04 p.u.in Figure 5.21 confirms the effectiveness of the controller.

5.3.5.4 Loss of wind power due to regulation. Regulation support has its perks but it comes at a cost. For providing regulation, wind power is intentionally operated at a point lower than the maximum power point to achieve more power in time of need. For this study, the data specifying the amount of wind power spilled due to regulation is also captured and the variation of this loss with increasing wind speed is displayed in Figure 5.25. Floydada, Texas faces a wind power spillage of around 15 % in lieu of providing regulation when the wind penetration is 50% of the rated system. This is due to high availability of wind in this region which is good for producing power, but at the same time increases the spillage. Fortuna, California loses only 9% of wind power in lieu of regulation at 50 % penetration. This is due to highly intermittent nature of wind in this region.

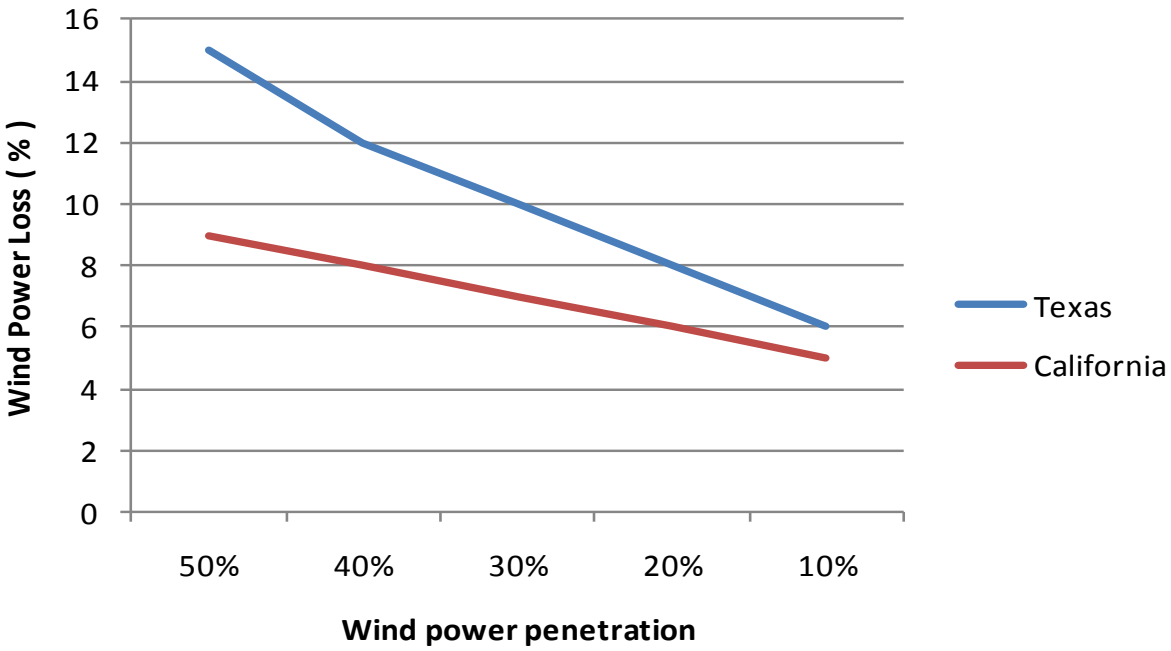

Figure 5.25: Wind power spillage due to regulation.

6. CONCLUSION AND FUTURE WORK

A novel control scheme for frequency control in wind power plants connected in a microgrid environment is proposed. This control scheme enables wind power plants to participate in frequency regulation, utilizing its untapped potential/capability to provide variable active power assuming there is adequate amount of wind speed available. This control scheme eliminates the gap between using droop control for synchronous generators and the droop controller for wind power plants. To test this control methodology for implementation in the real world, a test system was modeled in MATLAB and Simulink. This test system resembled a small autonomous grid, isolated from the legacy grid. The generation mix for the microgrid model consisted of three conventional synchronous generators and two wind power plants, adding up to a total capacity of 15 MW. The three loads connected to this system were modeled to accommodate hourly load changes for a day. The total amount of time set for the simulation of the whole test system was based on accommodating around 15 seconds of response time for each load change. To accommodate the resolution of hourly load data, the system was setup to use hourly wind data for the wind turbines.

This microgrid system was then subjected to 12 days worth of load and wind speed data from two cities - one located in Texas and the other in California. The data for each day was selected so as to represent each month of a year. The simulation study was done for numerous scenarios which included variation of the generation mix configuration from 10% to 50 % wind power to identify the effects of high penetration of wind power in a microgrid. These scenarios also included testing of the microgrid system with and without the proposed control strategy for comparison. Observations made from this study revealed the effectiveness of the control methodology to smooth out the frequency and voltage fluctuations appearing in the isolated system. A reliable generation mix configuration of conventional and wind power generation for the two cities was also deduced which was found to be relative to the overall wind capacity in that location throughout the year.

This control methodology and the system can be easily modified and scaled to specific requirements and can be used to study integration effects of other renewable or

non-conventional energy sources. The next step can be the development of a methodology for assessing and controlling a microgrid equipped with all kinds of non-conventional energy sources like rooftop or community solar photovoltaic plants, fuel cells, internal combustion engine generators, micro-turbines, battery energy storage systems, and plug-in hybrid electric vehicles. These non-conventional energy sources have the potential to support a microgrid in need of active and reactive power sources. Inclusion of these energy sources into the microgrid would definitely help to strengthen its reliability. Lastly, this structure can be used as a building block for an interconnected pool of microgrids to study its effect on the reliability and flexibility of grid operations.

APPENDIX A
EQUATION DERIVATION

Derivation of Two-port Matrices for the DFIG [7]. This section briefly shows the derivation of the two-port parameters which are used to derive the limits. As a basis for the derivations, the Z matrix is used. The Z matrix has been constructed by inspection from the equivalent circuit in Figure 2.3. The first column corresponds to the stator and rotor voltage when a stator current of 1 pu is injected and the rotor current is zero. The second column is derived by injecting a rotor current of 1 pu. with an open stator:

$$\begin{bmatrix} \mathbf{V}_s \\ V_r/s \end{bmatrix} = Z * \begin{bmatrix} \mathbf{I}_s \\ I_r \end{bmatrix} \tag{A.1}$$

$$Z = \begin{bmatrix} \mathbf{Z}_s + \mathbf{Z}_m & \mathbf{Z}_m \\ \mathbf{Z}_m & \mathbf{Z}_r + \mathbf{Z}_m \end{bmatrix} \tag{A.2}$$

$$Z_r = \frac{R_r}{s} + jX_r \tag{A.3}$$

$$Z_s = R_s + jX_r \tag{A.4}$$

$$Z_m = jX_m \tag{A.5}$$

The remaining derivations are made by inserting the Z matrix in the transformation equations where:

$$Y = Z^{-1} \tag{A.6}$$

$$G = \frac{1}{Z_{11}} \begin{bmatrix} \mathbf{1} & -Z_{12} \\ Z_{21} & \mathbf{det}\,(Z) \end{bmatrix} \tag{A.7}$$

$$B = \frac{1}{Z_{12}} \begin{bmatrix} Z_{22} & -\mathbf{det}\,(Z) \\ -\mathbf{1} & Z_{11} \end{bmatrix} \tag{A.8}$$

APPENDIX B

GOVERNOR AND EXCITATION SYSTEM MODELLING

Excitation system modeling[45].

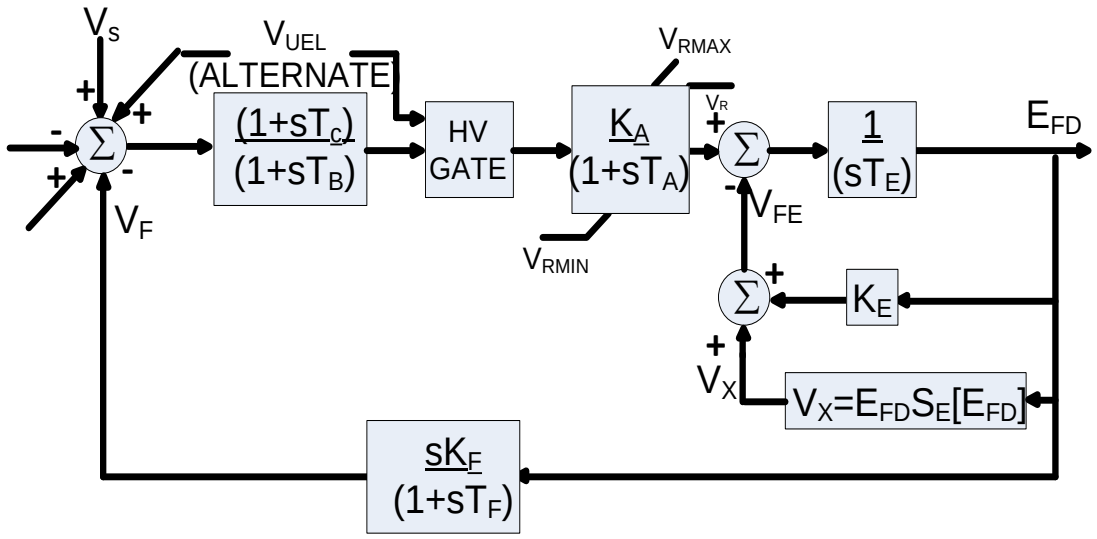

Figure B.1. Type DC1A –DC Commutator excitation system

Figure B.1. displays the control architecture of Type DC1A- DC Commutator. The time constant, T_E, associated with the integrator is the main exciter time constant derived from the ac machine d-axis time-constant; the linear feedback gain, K_E, makes this a simple low-pass filter, while the saturation included in the feedback reduces the time constant as the operating voltage and current increase.

The signal, E_{FD}, is proportional to exciter field current, which is normally used as the stabilizing feedback input signal. The structure of the feedback transfer function, and the forward AVR blocks and compensation are the same as the dc and static exciter model. This excitation system model is the most common type of excitation system model used in the industry.

The parameters for the model are given in TABLE C.1.

Governor model[46]

The Hydraulic Turbine and the Governor adopted for this thesis use a nonlinear hydraulic turbine model, a PID governor system, and a servomotor. The model used is shown below.

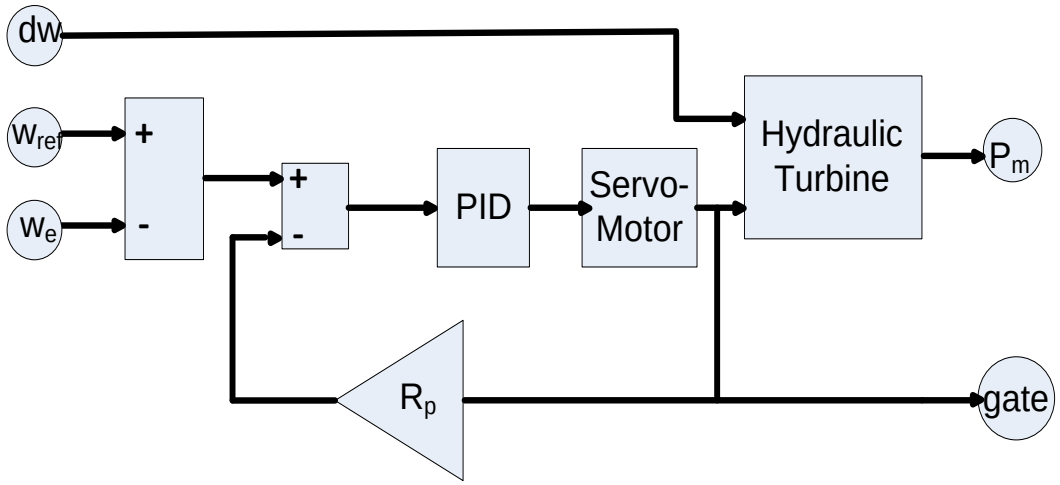

Figure B.2: PID governor system

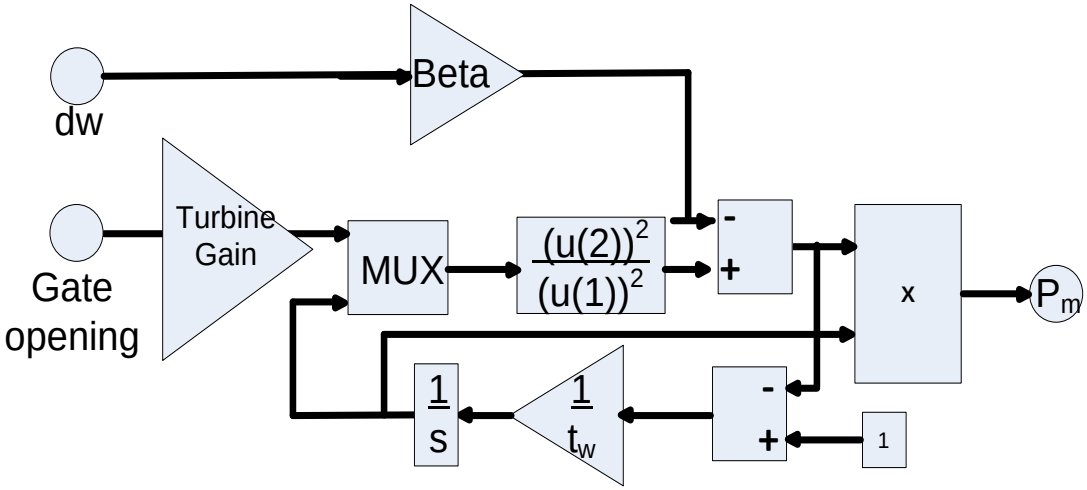

Figure B.3.: Nonlinear hydraulic turbine model

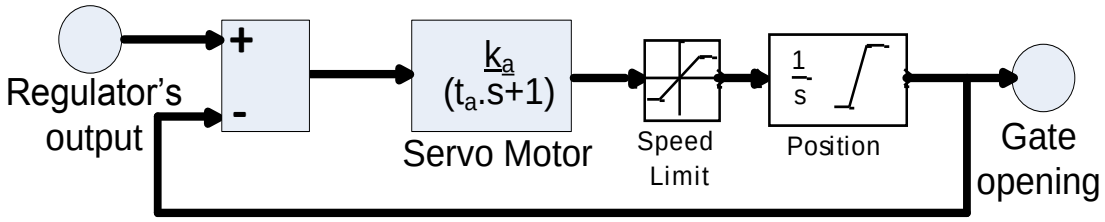

Figure B.4. Servomotor second order system

The parameters used for the governor are mentioned in Table C.2.

APPENDIX C
PARAMETER TABLES

TABLE C.1 EXCITER MODEL PARAMETERS

Parameter	Value
T_r (sec)	0.2
K_a	20
T_a (sec)	0.005
K_e	1
T_e (sec)	0
T_b (sec)	0
T_c (sec)	0
K_f	0.001
T_f (sec)	0.1
Voltage Limits (V)	[-11.5, 11.5]
K_p	0

TABLE C.2 GOVERNOR MODEL PARAMETERS.

Parameter	Value
K_a	5
T_a	0.07 sec
Gate opening limits	[0.01, 0.97518]
Gate speed limits	[-0.1, 0.1]
Permanent Droop	0.01
K_p	3.5
K_i	0.5424
K_d	1.0667
T_d(sec)	0.01
β	0
T_w(sec)	1

TABLE C.3 SYNCHRONOUS MACHINE PARAMETERS.

Machine Parameter	Value
MVA Capacity	4.5 / 4 / 3.5 / 3 / 2.5 MVA
Line to Line Voltage	4160 V
Frequency	60 Hz
X_d	1.305 pu (4.5 MVA)
X_d'	0.296 pu (4.5 MVA)
X_d''	0.252 pu (4.5 MVA)
X_q	0.474 pu (4.5 MVA)
X_q''	0.243 pu (4.5 MVA)
X_l	0.18 pu (4.5 MVA)
T_d'	1.01 sec
T_d''	0.053 sec
T_{qo}''	0.1 sec
Stator Resistance (R_s)	0.0028544 pu(4.5 MVA)
Inertia Coefficient	5 sec
Friction Factor	0
Pole pairs	2

TABLE C.4 LINE DATA

Bus	Distance(Km)	Total Impedance (Ohms)
1 - 2	2	0.2306 + j0.0565
1 - 4	2	0.2306 + j0.0565
2 - 4	2	0.2306 + j0.0565
3 - 4	5	0.5765 + j0.1412
5 - 4	5	0.5765 + j0.1412
3 - 7	7	0.8071 + j0.1977
3 - 6	0	0
7 - 8	3	0.3459 + j0.0847
7 - 9	2	0.2306 + j0.0565
8 - 9	7	0.8071 + j0.1977

TABLE C.5 TRANSFORMER DATA

Parameter	**Value**
Nominal MVA	2.1/ 2.35/ 3/ 3.2/ 3.5/ 3.7/ 4/ 4.2/4.7
Frequency	60 Hz
RMS Voltage at Terminal 1	[4160, 575] V
Resistance of Winding 1	0 pu (4.7 MVA)
Inductance of Winding 1	0.00039 pu (4.7 MVA)
RMS Voltage at Terminal 2	13.2 kV (4.7 MVA)
Resistance of Winding 2	0 pu (4.7 MVA)
Inductance of Winding 2	0.00039 pu (4.7 MVA)
Magnetizing resistance R_m	500 pu (4.7 MVA)
Magnetizing inductance L_m	500 pu (4.7 MVA)

TABLE C.6. BUS DATA

	P_{gen}- MW	Q_{gen}- MVAR	P_{load}- MW	Q_{load} – MVAR	Voltage- p.u.
Bus 1	1.31	0.885	0	0	1.0278
Bus 2	2.14	-1.55	0	0	1.026
Bus 3	1.31	1.152	0	0	1.0225
Bus 4	0	0	0	0	1.0257
Bus 5	0	0	2.3	0	--
Bus 6	0	0	3.2	0	--
Bus 7	1.31	1.05	0	0	1.0255
Bus 8	0	0	2.4	0	--
Bus 9	2.14	-1.4	0	0	1.024

TABLE C.7 Load data with full wind support

Interval	Time (Sec)	LOAD (MW)
0	40	8.1
1	55	7.8
2	70	7.7
3	85	7.7
4	100	7.7
5	115	7.8
6	130	8.1
7	145	8.6
8	160	8.7
9	175	8.6
10	190	8.6
11	205	8.5
12	220	8.6
13	235	8.5
14	250	8.5
15	265	8.4
16	280	8.4
17	295	8.4
18	310	8.5
19	325	8.9
20	340	9
21	355	9
22	370	8.9
23	385	8.6

APPENDIX D
TEST LOCATIONS ON MAP

FLOYDADA, TEXAS

Figure D.1. Location A displays Floydada, Texas.

FORTUNA, CALIFORNIA

Figure D.2. Location A displays Fortuna, California.

BIBLIOGRAPHY

[1] S. Lindenberg, B. Smith, K. O'Dell, and E. DeMeo, "20% Wind Energy by 2030 : Increasing Wind Energy's Contribution to U.S. ," Office of Scientific and Technical Information;U.S. Dept. of Energy; National Renewable Energy Laboratory (U.S.); United States. Dept. of Energy,2008.

[2] H. Li and Z. Chen, "Overview of different wind generator systems and their comparisons," *IET Renewable Power Generation*, 2008, vol. 2, pp. 123-138.

[3] B. Parsons, M. Milligan, B. Zavadi, "Grid impacts of wind power: a summary of recent studies in the United States," *Wind Energy*, 2004, vol. 7, pp. 87-108.

[4] J. C. Smith, M. R. Milligan, E. A. DeMeo, and B. Parsons, "Utility Wind Integration and Operating Impact State of the Art," *IEEE Transactions on Power Systems*, 2007, vol. 22, pp. 900-908.

[5] E. A. DeMeo, W. Grant, M. R. Milligan, and M. J. Schuerger, "Wind plant integration [wind power plants]," *IEEE Power and Energy Magazine*, 2005, vol. 3, pp. 38-46.

[6] L. M. Fernandez, C. A. Garcia, and F. Jurado, "Operating capability as a PQ/PV node of a direct-drive wind turbine based on a permanent magnet synchronous generator," *Renewable Energy*, 2010, vol. 35, pp. 1308-1318.

[7] L. Shuhui and T. A. Haskew, "Characteristic study of vector-controlled direct driven permanent magnet synchronous generator in wind power generation," in *Proc. IEEE Power and Energy Society General Meeting* 2008, pp. 1-9.

[8] T. Lund, P. Sørensen, and J. Eek, "Reactive power capability of a wind turbine with doubly fed induction generator," *Wind Energy*, 2007, vol. 10, pp. 379-394.

[9] N. R. Ullah, K. Bhattacharya, and T. Thiringer, "Reactive Power Ancillary Service from Wind Farms," in *Proc. IEEE Canada Electrical Power Conference*, 2007, pp. 562-567.

[10] N. R. Ullah, K. Bhattacharya, and T. Thiringer, "Wind Farms as Reactive Power Ancillary Service Providers;Technical and Economic Issues," *IEEE Transactions on Energy Conversion*, 2009, vol. 24, pp. 661-672.

[11] N. W. Miller and K. Clark, "Advanced controls enable wind plants to provide ancillary services," in *Proc. IEEE Power and Energy Society General Meeting, ,* 2010, pp. 1-6.

[12] S. N. Singh, J. stergaard, and B. Singh, "Reactive power capability of unified DFIG for wind power generation," in *Proc. IEEE Power and Energy Society General Meeting* 2010, pp. 1-7.

[13] K. W. E. Cheng, J. K. Lin, Y. J. Bao, and X. D. Xue, "Review of the wind energy generating system," in *Proc. 8th International Conference on Advances in Power System Control, Operation and Management , ,* 2009, pp. 1-7.

[14] G. Brauner, M. Heidl, D. Tiefgraber, M. Weniger, and H. Haidvogl, "Voltage collapse phenomena in wind parks," in *Proc. 18th International Conference and Exhibition on Electricity Distribution*, 2005, pp. 1-5.

[15] C. Marnay, "Integrated Assessment of Dispersed Energy Resources Deployment," *Consortium for Electric Reliability Technology Solutions,*2000.

[16] L. C. J.J. Iannucci, J.M. Eyer, R.L. Pupp, "DER Benefits Analysis Studies: Final Report," NREL, 2003.

[17] D. Divan and W. E. Brumsickle, "Powering the next millennium with power electronics," in *Proc. Proceedings of the IEEE International Conference on Power Electronics and Drive Systems*, 1999, vol. 1, pp. 7-10 vol.1.

[18] F. Blaabjerg, C. Zhe, and S. B. Kjaer, "Power electronics as efficient interface in dispersed power generation systems," *IEEE Transactions on Power Electronics*, 2004, vol. 19, pp. 1184-1194.

[19] M. N. Marwali and A. Keyhani, "Control of distributed generation systems-Part I: Voltages and currents control," *IEEE Transactions on Power Electronics*, 2004, vol. 19, pp. 1541-1550.

[20] M. N. Marwali, J. Jin-Woo, and A. Keyhani, "Control of distributed generation systems - Part II: Load sharing control," *IEEE Transactions on Power Electronics*, 2004, vol. 19, pp. 1551-1561.

[21] N. W. A. Lidula and A. D. Rajapakse, "Microgrids research: A review of experimental microgrids and test systems," *Renewable and Sustainable Energy Reviews*, 2011, vol. 15, pp. 186-202.

[22] C. Marnay, H. Asano, S. Papathanassiou, and G. Strbac, "Policymaking for microgrids," *IEEE Power and Energy Magazine*, 2008, vol. 6, pp. 66-77.

[23] N. D. Hatziargyriou and A. P. Sakis Meliopoulos, "Distributed energy sources: technical challenges," in *Proc. IEEE Power Engineering Society Winter Meeting*, , 2002, vol. 2, pp. 1017-1022 vol.2.

[24] M. Barnes, J. Kondoh, H. Asano, "Real-World MicroGrids-An Overview," in *Proc. IEEE International Conference on System of Systems Engineering* 2007, pp. 1-8.

[25] J. M. Guerrero, L. Hang, and J. Uceda, "Control of Distributed Uninterruptible Power Supply Systems," *IEEE Transactions on Industrial Electronics*, , 2008, vol. 55, pp. 2845-2859.

[26] F. Katiraei and M. R. Iravani, "Power Management Strategies for a Microgrid With Multiple Distributed Generation Units," *IEEE Transactions on Power Systems* , 2006, vol. 21, pp. 1821-1831.

[27] R. H. Lasseter, "MicroGrids," in *Proc. IEEE Power Engineering Society Winter Meeting*, , 2002, vol. 1, pp. 305-308 vol.1.

[28] C. K. Sao and P. W. Lehn, "Control and Power Management of Converter Fed Microgrids," *IEEE Transactions on Power Systems*, 2008 vol. 23, pp. 1088-1098.

[29] G. Diaz, C. Gonzalez-Moran, J. Gomez-Aleixandre, and A. Diez, "Scheduling of Droop Coefficients for Frequency and Voltage Regulation in Isolated Microgrids," *IEEE Transactions on Power Systems*, 2010 vol. 25, pp. 489-496.

[30] D. Menniti, A. Pinnarelli, and N. Sorrentino, "A method to improve microgrid reliability by optimal sizing PV/Wind plants and storage systems," in *Proc. 20th International Conference and Exhibition on Electricity Distribution - Part 1* , 2009, pp. 1-4.

[31] B. H. Chowdhury, H. T. Ma, and N. Ardeshna, "The challenge of operating wind power plants within a microgrid framework," in *Proc. Power and Energy Conference at Illinois (PECI)* , 2010, pp. 93-98.

[32] N. K. Ardeshna and B. H. Chowdhury, "Supporting islanded microgrid operations in the presence of intermittent wind generation," in *Proc. IEEE Power and Energy Society General Meeting*, 2010, pp. 1-8.

[33] M. Shahabi, M. R. Haghifam, M. Mohamadian, and S. A. Nabavi-Niaki, "Microgrid Dynamic Performance Improvement Using a Doubly Fed Induction Wind Generator," *IEEE Transactions on Energy Conversion*, 2009, vol. 24, pp. 137-145.

[34] S. Muller, M. Deicke, and R. W. De Doncker, "Doubly fed induction generator systems for wind turbines," *IEEE Industry Applications Magazine*, 2002, vol. 8, pp. 26-33.

[35] T. S. Basso and R. DeBlasio, "IEEE 1547 series of standards: interconnection issues," *IEEE Transactions on Power Electronics*, 2004, vol. 19, pp. 1159-1162.

[36] Associated Press, "Mass blackout hits California, Arizona and Mexico," accessed on 01 December, 2011, http://www.guardian.co.uk/world/2011/sep/09/blackout-california-arizona-mexico-san-diego.

[37] R. Pena, J. C. Clare, and G. M. Asher, "Doubly fed induction generator using back-to-back PWM converters and its application to variable-speed wind-energy generation," *IEE Proceedings -Electric Power Applications*, 1996, vol. 143, pp. 231-241.

[38] G. S. R. Gagnon, S. Bernard, D. Paré, S. Casoria, C. Larose, "Modeling and Real-Time Simulation of a Doubly-Fed Induction Generator Driven by a Wind Turbine," *Power SystemsTransients*,2005.

[39] B. J. Kirby, "Frequency Control Concerns in the North American Electric Power System," Oak Ridge National Laboratory, Technical Report, March 26, 2003.

[40] Y. Tai-Her and W. Li, "A Study on Generator Capacity for Wind Turbines Under Various Tower Heights and Rated Wind Speeds Using Weibull Distribution," *IEEE Transactions on Energy Conversion*, 2008, vol. 23, pp. 592-602.

[41] "Hourly Load Data Archives," accessed on 01 December, 2011, http://www.ercot.com/gridinfo/load/load_hist/.

[42] NREL, "Wind Integration Datasets," accessed on 01 December, 2011, http://www.nrel.gov/wind/integrationdatasets/.

[43] South California Edison, "Regulatory Information - SCE Load Profiles," accessed on 01 December, 2011, http://www.sce.com/AboutSCE/Regulatory/loadprofiles/2011loadprofiles.htm.

[44] M. Bollen, Z. Jin, O. Samuelsson, and J. Bjornstedt, "Performance indicators for microgrids during grid-connected and island operation," in *Proc. IEEE Bucharest PowerTech* , 2009, pp. 1-6.

[45] "IEEE Recommended Practice for Excitation System Models for Power System Stability Studies," *IEEE Std 421.5-1992*, pp. 0_1.

[46] "Hydraulic turbine and turbine control models for system dynamic studies," *IEEE Transactions on Power Systems*, 1992 vol. 7, pp. 167-179.

VITA

Anshuman Shrikant Vaidya obtained his B.E. degree in Electrical Engineering from Bhilai Institute of Technology, India in October 2008. From December 2008 to August 2009 he worked in ZS Associates as a Business Operations Associate. He received his Master of Science degree in Electrical Engineering from Missouri University of Science and Technology in May 2012. His research interests include power systems analysis, power electronics applications in power systems, renewable energy systems and power system operations.